

A Scalable Real-time Processing Chain for Radar Exploiting Illuminators of Opportunity



Craig Andrew Tong
BSc(Eng) UCT

Thesis Presented for the Degree of
DOCTOR OF PHILOSOPHY
in the Department of Electrical Engineering
UNIVERSITY OF CAPE TOWN

December 2014

The copyright of this thesis vests in the author. No quotation from it or information derived from it is to be published without full acknowledgement of the source. The thesis is to be used for private study or non-commercial research purposes only.

Published by the University of Cape Town (UCT) in terms of the non-exclusive license granted to UCT by the author.

“All models are wrong, but some are useful.”

-George Box

Declaration

I declare that this thesis is my own, unaided work. It is being submitted for the degree of Doctor of Philosophy in Engineering in the University of Cape Town. It has not been submitted before for any degree or examination in any other university.

Signature of Author

Cape Town
December 18, 2014

Abstract

This thesis details the design of a processing chain and system software for a commensal radar system, that is, a radar that makes use of illuminators of opportunity to provide the transmitted waveform. The stages of data acquisition from receiver back-end, direct path interference and clutter suppression, range/Doppler processing and target detection are described and targeted to general purpose commercial off-the-shelf computing hardware. A detailed low level design of such a processing chain for commensal radar which includes both processing stages and processing stage interactions has, to date, not been presented in the Literature. Furthermore, a novel deployment configuration for a networked multi-site FM broadcast band commensal radar system is presented in which the reference and surveillance channels are record at separate locations.

The processing chain design reviews existing methods for each stage of the processing chain and proposes new approaches where appropriate. The algorithm implementation and greater processing chain integration is then presented for each respective stage to maximise processing and memory transport efficiency and in turn, the total throughput of the processing chain. Optimal signal processing techniques are targeted as far as possible to maximise signal to noise ratio and signal to interference ratios. Graphics processing units are exploited to accelerate highly parallel linear algebra operations which facilitates real-time throughput. The processing chain also provides automatic scaling to multiple graphics processing units when available to hinge maximum performance out of the available system hardware. Interfacing to subsequent stages of radar processing such as tracking are also provided along with testing of an implementation

for non-coherent amplitude/range/Doppler map combination for when multiple frequency channels are exploited in the same bistatic geometry. It is shown that with a single high-end Fermi-generation NVIDIA graphics card (Geforce GTX480) and a quad core CPU (AMD Phenom II X4 955) that real-time processing can be achieved for a single FM channel and bistatic pair and, furthermore, that this processing of 100% duty cycle of sample data occupies less than 25% of the available processing resources. Results are presented for multiple high-end gaming graphics processor units, a low cost, mid range unit, several cluster computing type units and an embedded graphics processor using to present a broad scope of performance of the processing chain on different hardware. It is also shown that the presented processing chain can be ported to a central processing unit only implementation albeit with a performance knock when compared to the graphics processor unit implementations.

Typical commensal systems make use of a pair of phase-synchronous receiver channels at every receiver site. One channel is fed from an antenna surveying a region of interest to receive target reflections while the second records a line of sight reference signal from the transmitter which is being exploited. The 2 signals are then cross correlated to resolve targets from the clutter. An analysis is presented of the performance and viability of digitising the reference signal(s) at a different location to that of the surveillance signal, recording only a single version of each channel to be exploited. The channel data is then distributed via data network to a processing node (or nodes) for the processing stage. This method removes the need to digitise a copy of the reference signal at each receiver node. As a result, receiver complexity will be reduced as well as the amount of front end equipment required at each receiver site. Furthermore, given that the surveillance and reference antennas are no longer connected to a common device it will allow the surveillance antenna to be placed at a location where direct path interference from the transmitter is minimised as a result of terrain screening. The extra suppression in interference is possible because a line of site reference signal is no longer required at the surveillance antenna site. By using the developed real-time processing chain it is shown that performance improvement can be achieved using this *separated reference* configuration by reducing the multipath in the

reference channel by means of optimal antenna placement. This performance improvement can be achieved without any significant loss in coherency despite a 4 second integration time.

Acknowledgements

I wish to express my gratitude to the following individuals and organisations for assistance and support during my research.

My parents who unquestionably and seemingly indefinitely supported my adventures in tertiary education, which spanned a decade. Through highs and low they were always encouraging and supportive of my endeavours and for this I cannot even begin to express my gratitude.

My supervisor, Professor Michael Inggs whose expert knowledge, guidance and his passion for the field of radar has inspired a wealth of research projects over the years and I am proud to be able to contribute to one. My co-supervisor Dr Amit Mishra who provided valuable input especially in the context of academic procedure. Associate Professor Daniel O'Hagan who also provided helpful input into the corrections to this document.

Dr Andrew van der Byl for assistance in the investigation and implementation of the recursive discrete Fourier transform applied to range/Doppler processing as well as for many useful pointers for thesis writing and the PhD process.

All the members of the Radar Remote Sensing Group at the University of Cape Town, past and present who provided support, motivation, inspiration and company during my studies. Notably those who first got me interested in commensal radar, Dr Yoann Paichard, Mr Sebastiaan Heunis, Mr Gunther Lange and Mr Justin Coetser.

The South African National Defence Force has contributed strongly to this

project through Project Ledger bursary funding for myself.

The Radar and Electronic Warfare branch of the Defence Peace Safety and Security unit at the Council for Scientific and Industrial Research, who funded and facilitated the majority of field tests carried out during my research. Notably Mr Francois Maasdorp and Mr Christo Cloete who assisted in the field testing and provided invaluable insight into both deployment strategy and interpreting results.

Peralex Electronics who provided excellent receiver hardware and took on the role of industry partner for the commensal radar project at the University of Cape Town. Their practices have inspired an expert level of software engineering that has been central to the successful performance of the radar system described in this thesis. Notably Mr Francois Louw and Mr Alex Bassios as well as Mr Jean-Paul da Conceicao, Mr Robert Fowler, Mr Jean Wessels who assisted in field testing at various times. Also Mr Michal Kotze from GEW Technologies.

Dr James Palmer of Defence Science Technology Organisation, Australia whose recommendation of conjugate gradient methods for filter weight training for the cancellation stage of processing chain was critical to achieving real-time throughput of the system.

The University of Cape Town's ICTS High Performance Computing team for providing access for testing on machines with multiple Tesla GPUs [1].

The various authors of all the great free and open source libraries and software tools that I made use of during the course of my research.

Contents

Declaration	ii
Abstract	iii
Acknowledgements	vi
List of Figures	xii
List of Tables	xvi
List of Algorithms	xvii
List of Abbreviations	xviii
List of Symbols	xxv
1 Introduction	1
1.1 Overview of Commensal Radar	4
1.1.1 Detection	6
1.1.2 Target Location	8
1.1.3 Illuminating Signals	10
1.1.4 Overview of the Separated Reference Configuration	15
1.1.5 Motivation	16
1.1.6 Limitations	19
1.2 Problem Description	21
1.2.1 Research Hypothesis	22
1.3 Proposed Solution	23

CONTENTS

1.4	Research Objectives	25
1.4.1	Statement of Originality	26
1.4.2	Publications	27
1.4.3	Scope of Research	28
1.5	Thesis Outline	29
1.5.1	Literature Review	30
1.5.2	Processing Design	31
1.5.3	The Separated Reference Configuration	35
1.5.4	Conclusions	36
2	Literature Review	40
2.1	Research by Universities, Research Institutions and Companies	40
2.1.1	University College London	41
2.1.2	University of Birmingham	44
2.1.3	University of Rome “La Sapienza”	45
2.1.4	University of Pisa	52
2.1.5	Warsaw University of Technology	54
2.1.6	University of Cape Town	57
2.1.7	SONDRA Supelec	58
2.1.8	SELEX	58
2.1.9	Fraunhofer FHR	58
2.1.10	Airbus (formerly known as Cassidian)	59
2.1.11	Defence Science and Technology Organisation (DSTO), Australia	60
2.1.12	Nanyang Technological University, Singapore	61
2.2	Commercially Available Systems	62
2.3	Conclusions	63
3	Processing Chain Implementation	64
3.1	Introduction	64
3.1.1	Radar System Overview	68
3.2	Background and Computational Challenges of the Processing Chain	72
3.2.1	Direct Path Interference and Clutter Supression	72

CONTENTS

3.2.2	Range Doppler Processing	78
3.2.3	Detection	81
3.3	Processing Design	81
3.3.1	Direct Path Interference and Clutter Supression	82
3.3.2	Range Doppler Processing	94
3.3.3	Detection	108
3.3.4	Pipelining the design	110
3.4	A Minimalistic Solution	114
3.4.1	CPU only solution	114
3.4.2	NVIDIA Jetson TK1	115
3.5	Non-coherent ARD Fusion	116
3.5.1	Algorithm	119
3.5.2	Timing and Test Results	121
3.6	Summary of Timing Results	124
3.6.1	DPI and Clutter Suppression	124
3.6.2	CAF Processing	127
3.6.3	CFAR Filtering	131
3.6.4	Non-coherent ARD Fusion	132
3.6.5	Maximum Throughput	134
3.6.6	Comparison of Computation	138
3.7	Conclusions	138
3.7.1	Future Work	140
4	The Separated Reference Configuration	142
4.1	Introduction	142
4.2	Field Tests and Results	144
4.2.1	Deployment	145
4.2.2	Reduction of Multipath	145
4.2.3	Detection Performance	150
4.3	Oscillators Performance Considerations	153
4.4	Frequency Offset Correction	155
4.5	Further Considerations	158
4.5.1	Combating In-Band Interference	159

CONTENTS

4.5.2	Network Infrastructure	160
4.6	Conclusions	162
4.6.1	Future Work	163
5	Conclusions	166
5.1	Processing Design	166
5.1.1	Future Work	168
5.2	Separated Reference Configuration	169
5.2.1	Future Work	170
	Bibliography	172

List of Figures

1.1	A bistatic commensal radar configuration.	5
1.2	An example of an ARD map.	8
1.3	Comparison of the CAFs of FM broadcast channel and DVB-T channel.	13
1.4	Comparison of the spectral content of a FM broadcast channel and DVB-T channel.	14
1.5	Optimal placement of the reference antenna.	16
1.6	Optimal placement of the surveillance antenna.	17
3.1	Flow diagram showing the stages included in the processing chain.	68
3.2	Comparison of integration times for FM based target detection.	70
3.3	An illustration of the the separated reference configuration.	71
3.4	The effects of multiple clutter sources occurring at the same bistatic range.	75
3.5	Illustration of DPI and clutter masking targets of interest.	77
3.6	Demonstration of the least mean squares estimator as a clutter suppression algorithm.	83

LIST OF FIGURES

3.7	A graph showing the residual performance for different cancellation schemes.	86
3.8	Effect of cancellation done independently on separate sub-blocks of the CPI on magnitude and phase of the surveillance signal at a low clutter receiver site.	90
3.9	Effect of cancellation done independently on separate sub-blocks of the CPI on magnitude and phase of the surveillance signal at a high clutter deployment site.	91
3.10	Effect of inserting random sample values into simulated time data to simulate the effect of stitching points created by running cancellation on separate sub-blocks of the CAF CPI.	93
3.11	Comparison of the ARD maps produced from the XF CAF algorithm vs the Batches CAF algorithm for different batch lengths. .	100
3.12	Comparison of the CFAR maps produced from the XF CAF algorithm vs the Batches CAF algorithm for different batch lengths. .	101
3.13	Data flow through the Processing Server.	111
3.14	Screenshot of ARDView, the data visualisation GUI application. .	113
3.15	NVIDIA Jetson TK1 development kit.	116
3.16	Photo and block diagram of the ComRad3 receiver developed by Peralex Electronics.	118
3.17	Comparison of CFAR outputs generated from a single FM channel versus multiple FM channels.	123
3.18	Comparison of execution time of various stages of the processing chain executed on a single thread of a CPU.	138
4.1	The separated reference configuration allows optimal placement of both the reference and surveillance antennas.	143

LIST OF FIGURES

4.2	Flow diagram of a complete commensal radar system making use of the the separated reference configuration.	144
4.3	Locations of the radar nodes during a deployment.	146
4.4	The interference environment at the Tygerberg receiver site. . . .	147
4.5	CFAR detections with the co-located configuration show target ghosting due to multipath.	148
4.6	Modelling of signal strength at ground level for transmissions from the 1.3 kW 88.2 MHz FM broadcast channel on the Tygerberg transmitter.	149
4.7	Comparison of ARD maps of the AAFs of the reference signals for different receiver sites.	150
4.8	Removal of the target ghosting effect with the separated reference configuration.	151
4.9	Detections of a target at its furthest detectable range using the co-located configuration.	152
4.10	Detection ranges with the separated reference.	152
4.11	ARD map of separated reference data where receivers with lower quality oscillators were used.	154
4.12	Comparison of phase drift between channels on the same receiver, on separate OCXO equipped receivers and on separate TCXOs equipped receivers.	155
4.13	Fitting a curve to phase advance between the reference and surveillance channels.	157
4.14	ARD map of separated reference data where receivers with lower quality oscillators where the frequency offset has been corrected for in signal processing.	159

LIST OF FIGURES

4.15 Comparison of target signal to noise ration after frequency offset
correction. 165

List of Tables

3.1	Timing of DPI and clutter suppression on different GPU hardware	125
3.2	Timing of DPI and clutter suppression on different hardware . . .	126
3.3	Timing of CAF calculation on different hardware	128
3.4	Timing of CAF calculation on different CPU only hardware using the XF CAF algorithm	129
3.5	Timing of CAF calculation on different CPU only hardware using the batches CAF algorithm	130
3.6	Timing of CFAR calculation of the GOCA-CFAR on different hardware	131
3.7	Timing of CFAR calculation of the OS-CFAR on different hardware	132
3.8	Timing of non-coherent ARD fusion on different hardware	133
3.9	Maximum throughput for off-line processing of complete process- ing chain on different GPU hardware	135
3.10	Maximum throughput for off-line processing of complete process- ing chain on different CPU hardware using the XF CAF algorithm	136
3.11	Maximum throughput for off-line processing of complete process- ing chain on different CPU hardware using the batches CAF al- gorithm	137

List of Algorithms

1	The CGLS Algorithm for minimising $\ A\mathbf{x} - \mathbf{b}\ $	87
2	The XF CAF algorithm on GP-GPU	107
3	Data access algorithm for each processing thread and corresponding GPU device in the processing server application	111

List of Abbreviations

- 4G** 4th Generation (cellular phone network infrastructure). [17](#), [18](#)
- AAF** Auto Ambiguity Function, sometimes also referred to as self ambiguity function or simply ambiguity function in other texts. [xiv](#), [42](#), [98](#), [148](#), [150](#)
- ADC** Analogue to Digital Converter. [2](#), [6](#), [7](#), [19](#), [41](#), [46](#), [72](#), [73](#), [116](#)
- ADSL** Asymmetric Digital Subscriber Line. [161](#)
- AoA** Angle of Arrival. [9](#), [37](#), [51](#), [52](#), [57](#), [97](#), [114](#), [121](#), [140](#), [168](#)
- AP** Access Point. Typically [WiFi](#) equipment. [48](#), [50](#)
- API** Application Programming Interface. [105](#)
- ARD** Amplitude/Range/Doppler. A means of displaying a [CAF](#) on a 2D map with the amplitude dimension indicated by colour. [xii–xiv](#), [xvi](#), [2](#), [7](#), [8](#), [26](#), [34](#), [38](#), [46–48](#), [52](#), [68](#), [71](#), [75](#), [79–81](#), [83](#), [92](#), [93](#), [97](#), [98](#), [100](#), [101](#), [103–106](#), [108](#), [109](#), [112](#), [113](#), [119–122](#), [127–137](#), [139](#), [148](#), [150](#), [152–154](#), [156–159](#), [167](#), [168](#)
- ASIC** Application Specific Integrated Circuit. [2](#), [65](#)
- ATC** Air Traffic Control. [3](#), [18](#), [28](#), [43](#), [52](#), [161](#)
- BLAS** Basic Linear Algebra Subprograms. A set of kernel subroutines which perform linear algebra. Many optimised and hardware specific implementations exist with a standardised calling interface. [33](#), [67](#), [86](#), [88](#), [114](#)

- CA-CFAR** Cell Averaging **CFAR**. 60, 61
- CAF** Cross Ambiguity Function. xii, xiii, xvi, xviii, 6, 7, 11, 13, 42, 43, 47, 48, 54, 55, 70, 75, 78–80, 89, 92–100, 103, 105, 106, 109, 110, 113, 120, 127–130, 132, 134–137, 139, 148, 149, 166
- CCA-CFAR** Censored Cell Averaging **CFAR**. 61
- CFAR** Constant False Alarm Rate. xiii, xiv, xvi, xix, xxi, xxii, 7, 28, 32–34, 42, 47, 52, 55, 60, 61, 68, 70, 81, 101, 108, 109, 112, 113, 122, 123, 131, 132, 134–138, 148, 149, 151, 152, 166
- CGLS** Conjugate Gradient Least Squares. An iterative refinement approach to solving $A\mathbf{x} = \mathbf{b}$. An alternative to the least squares estimator. xvii, 33, 37, 85–89, 112, 125, 126, 138, 146, 166, 168
- CIC** Cascaded Integrator-Comb, referring to the filter type. 97
- COTS** Commercial, Off The Shelf. 2, 22–24, 36, 48, 64
- CPI** Coherent Processing Interval. xiii, xxvi, 3, 22, 24, 26, 31, 32, 45, 50, 55, 60, 65, 68–70, 73, 76, 79, 80, 83, 84, 86, 87, 89, 92, 93, 95, 96, 98–101, 104–106, 108, 110, 112–114, 120, 124–130, 134–137, 152, 156–158
- CPU** Central Processing Unit. xiii, xvi, 2, 22, 23, 29, 33, 35, 37, 55, 64–68, 86, 88, 98, 105, 106, 110, 113–115, 124–139, 167, 168
- CUDA** Compute Unified Device Architecture. NVIDIA’s framework for programming their **GPUs**. 33, 36, 67–69, 88, 105, 106, 108, 115, 124, 125, 127, 128, 135, 139, 166
- CUT** Cell Under Test. 81, 108, 109, 113, 131, 132, 135–137
- DAB** Digital Audio Broadcast. 1, 10, 12, 41, 42, 58, 59, 78
- DDC** Digital Down Converter. 37, 113, 116, 117, 168
- DFT** Discrete Fourier Transform. xxii, xxvii, 34, 94–96, 99, 102

- DoA** Direction of Arrival. [44](#), [45](#), [50](#)
- DPI** Direct path interference. The illuminating signal from a transmitter as captured in the surveillance channel and therefore interfering with the detection of target skin echoes. Also referred to as direct signal interference (DSI) in some texts. [xii](#), [xvi](#), [xx](#), [xxvi](#), [2](#), [6](#), [15–17](#), [21–25](#), [31](#), [33](#), [35](#), [36](#), [38](#), [42–48](#), [54](#), [55](#), [57](#), [59](#), [61](#), [67](#), [71–77](#), [82–85](#), [87](#), [92](#), [98](#), [99](#), [106](#), [124–127](#), [132](#), [135–138](#), [142](#), [146](#), [147](#), [149](#), [156](#), [158](#), [159](#), [163](#), [166](#), [168](#), [170](#)
- DSP** Digital Signal Processing. [2](#), [21](#), [24](#), [65](#), [72](#)
- DSSS** Direct-Sequence Spread Spectrum. [49](#)
- DTV** Digital Television. Any television standard broadcast with digital modulation. Variations of DVB, ISDB and ATSC all fall into this category. [45](#)
- DVB-S** Digital Video Broadcast - Spaceborne. [10](#)
- DVB-T** Digital Video Broadcast - Terrestrial. [xii](#), [1](#), [4](#), [10–14](#), [18](#), [19](#), [26](#), [31](#), [34](#), [44](#), [47](#), [48](#), [52–54](#), [56](#), [59–61](#), [80](#), [104](#), [121](#), [161](#)
- ECA** Extensive Cancellation Algorithm. A multi-stage [DPI](#) and clutter cancellation algorithm proposed by Colone et al. [[2](#)]. The algorithm makes use of the least squares estimator to minimise the filter residual. [46–48](#), [50](#), [57](#)
- ECC** Error Correcting Code. [84](#)
- EM** Electromagnetic. [17](#), [19](#), [72](#)
- FERS** Flexible Extensible Radar Simulator. A sample level coherent radar simulator developed at [UCT](#) by Brooker [[3](#), [4](#), [5](#)]. [57](#), [92](#), [93](#)
- FFT** Fast Fourier Transform. [xxii](#), [33](#), [55](#), [67](#), [81](#), [94–98](#), [102](#), [105](#), [106](#), [114](#), [120](#), [127](#), [139](#), [156](#), [166](#)
- FIR** Finite Impulse Response, referring to a type of filter. [97](#)

- FM** Frequency Modulation. [xii](#), [xiii](#), [xxii](#), [1](#), [3](#), [4](#), [9–15](#), [18](#), [21–23](#), [28](#), [29](#), [31](#), [32](#), [34](#), [36](#), [37](#), [41–46](#), [48](#), [50–52](#), [54–59](#), [62](#), [68–70](#), [78](#), [80](#), [83](#), [85](#), [86](#), [92](#), [96](#), [99](#), [100](#), [103–106](#), [108](#), [109](#), [112–114](#), [116](#), [117](#), [119](#), [121–123](#), [125](#), [126](#), [128–137](#), [139–141](#), [144](#), [156](#), [161](#), [168](#), [169](#)
- FMCW** Frequency Modulated Continuous Wave. [24](#), [34](#), [54](#), [98](#)
- FPGA** Field Programmable Gate Array. [2](#), [65](#), [103](#), [116](#)
- FX** Fourier transform - Cross multiply, referring to the order of these 2 operations as opposed to [XF](#). [xxiv](#), [34](#), [94](#), [97](#), [103](#), [104](#)
- GDOP** Geometric Dilution Of Precision. [58](#)
- GNSS** Global Navigation Satellite System. Encompasses systems such as [GPS](#) and Galileo. [3](#), [10](#), [15](#), [25](#), [26](#), [35](#), [38](#), [71](#), [78](#), [142](#), [162–164](#), [169–171](#)
- GO-CFAR** Greater Of (cell averaging) [CFAR](#) also known as [GOCA-CFAR](#). [60](#), [61](#)
- GOCA-CFAR** Greater Of Cell Averaging [CFAR](#). [xvi](#), [xxi](#), [34](#), [101](#), [108](#), [109](#), [113](#), [131](#), [135–137](#), [139](#), [166](#)
- GP-GPU** General Purpose [GPU](#). [2](#), [22](#), [24](#), [29](#), [64](#), [67](#), [84](#), [88](#), [110](#), [138](#), [139](#), [166](#), [167](#)
- GPS** Global Positioning System. [xxi](#), [36](#), [153](#), [156](#)
- GPSDO** [GPS](#) Disciplined Oscillator. [57](#), [145](#)
- GPU** Graphics Processor Unit. [vii](#), [xvi](#), [xix](#), [xxi](#), [2](#), [3](#), [22](#), [24](#), [27](#), [29](#), [33–37](#), [55](#), [64](#), [66–69](#), [82](#), [84](#), [86](#), [88](#), [103](#), [106](#), [110](#), [113–115](#), [120](#), [124](#), [125](#), [127](#), [128](#), [132](#), [134](#), [135](#), [138](#), [139](#), [166–168](#)
- GSM** Global System for Mobile communications. [10](#), [42](#), [55](#), [56](#), [61](#), [62](#), [78](#)
- GUI** Graphical User Interface. [xiii](#), [109](#), [112](#), [113](#), [131](#), [139](#), [140](#), [166](#), [169](#)
- HSDPA** High Speed Downlink Protocol Access. [161](#)

- IFFT** Inverse [FFT](#). [97](#), [98](#)
- IO** Input/Output. [88](#)
- IQ** In phase/Quadrature. A sample which contains both of these components is therefore complex. [22](#), [67](#), [110](#), [156](#)
- ISAR** Inverse [SAR](#). [49–51](#), [53](#), [54](#)
- LAN** Local Area Network. [65](#), [115](#)
- LoS** Line of Site. [4](#), [15–17](#), [21](#), [50](#), [72](#), [142](#), [151](#)
- MFN** Multi-frequency Network. A transmitting scheme where multiple transmitters serving an overlapping coverage area use separate frequencies from one another for broadcasting such as is done in the [FM](#) broadcast band. [11](#), [43](#)
- MIMD** Multiple Instruction, Multiple Data. [24](#)
- MTI** Moving Target Indicator/Indication. [41](#), [78](#)
- OCXO** Oven Controlled Crystal Oscillator. [xiv](#), [153–155](#)
- OFDM** Orthogonal Frequency Division Multiplexing. [31](#), [48](#), [49](#), [53](#)
- OS-CFAR** Ordered Statistic [CFAR](#). [xvi](#), [60](#), [61](#), [132](#)
- PBR** Passive Bistatic Radar. An alternative name for commensal radar. [1](#)
- PCL** Passive Coherent Location. An alternative name for commensal radar. [1](#)
- PSLR** Peak to Side Lobe Ratio. [14](#), [44](#), [47](#), [48](#)
- RCS** Radar Cross Section. [20](#), [45](#), [58](#), [74](#)
- RDFT** Recursive [DFT](#). [27](#), [38](#), [94](#), [99](#), [103](#), [163](#), [170](#)
- RF** Radio Frequency. [21](#)

- SAR** Synthetic Aperture Radar. [xxii](#), [10](#), [41](#)
- SDR** Software Defined Radio. [40](#), [45](#), [156](#)
- SFDR** Spurious Free Dynamic Range. [19](#)
- SFN** Single Frequency Network. [11](#)
- SIMD** Single Instruction, Multiple Data. [24](#)
- SINR** Signal to Interference plus Noise Ratio. [4](#), [6](#), [29](#), [30](#), [92](#), [150](#), [152](#), [158](#)
- SIR** Signal to Interference Ratio. [3](#), [6](#), [23](#), [29](#), [47](#), [60](#), [92](#), [160](#), [161](#)
- SNR** Signal to Noise Ratio. [3](#), [60](#), [120](#), [150](#), [151](#), [163](#), [170](#)
- STAP** Space Time Adaptive Processing. [56](#)
- STL** Standard Template Library. Library of the C++ programming language which provide tools such as containers e.g `std::vector`. [121](#)
- TCXO** Temperature Compensated Crystal Oscillator. [xiv](#), [153–156](#)
- TV** Television. [13](#), [57](#), [156](#)
- UCT** University of Cape Town (South Africa). [xx](#), [8](#), [57](#), [58](#), [67](#), [69](#), [70](#), [77](#), [78](#), [83](#), [84](#), [86](#), [89](#), [92](#), [96](#), [103](#), [123](#), [154](#)
- UHF** Ultra High Frequency. [104](#), [161](#)
- UMTS** Universal Mobile Telecommunications System. [52](#), [53](#)
- USRP** Universal Software Radio Peripheral. A range of low cost software defined radio boards developed by Ettus Research.. [11](#), [53](#), [57](#), [156](#)
- VHF** Very High Frequency. [161](#)
- WiFi** Wireless local area network, typically variations of the IEEE802.11 standard. [xviii](#), [1](#), [10](#), [19](#), [42](#), [45](#), [47–52](#), [115](#), [160](#)

List of Abbreviations

- WiMAX** Worldwide Interoperability for Microwave Access. [10](#), [19](#), [43](#), [48](#)
- WRAN** Wireless Regional Area Network. [161](#)
- x86** A family of backward compatible instruction set architectures[a] based on the Intel 8086 CPU. [2](#), [24](#), [65–68](#), [115](#)
- XF** Cross multiply - Fourier transform, referring to the order of these 2 operations as opposed to **FX**. [xiii](#), [xvi](#), [xxi](#), [33](#), [34](#), [37](#), [92](#), [94](#), [96](#), [97](#), [100–105](#), [109](#), [127–129](#), [134–136](#), [139](#), [166](#), [168](#)

List of Symbols

- A The “A” matrix. The A matrix makes up a model of the interference in a given section of a discrete surveillance signal. The columns are synthetically delayed (range shifted) versions of the reference signal and optionally also synthetically Doppler shifted versions of the range shifted columns. The arrangement of data in the A matrix is used as a basis for removing interference from the section of the surveillance signal. [xxvi](#), [32](#), [73](#), [74](#), [76](#), [78](#), [82–84](#), [146](#)
- Bw Bandwidth in Hertz. [120](#)
- B Bistatic baseline. The distance from the transmitter to the receiver in meters. [10](#)
- C Cross ambiguity function in discrete time. The level of correlation between the surveillance and (some Doppler shifted version of) the reference signal. [79](#), [95](#), [96](#)
- F Discrete Fourier transform or fast Fourier transform output. [94](#), [102](#)
- G_{int} Integration gain. [120](#)
- I The identity matrix. [82](#), [83](#)
- N_D Number of Doppler bins. [95](#), [96](#)
- N_s Number of samples. [79](#), [94–96](#), [98](#), [102](#)
- P_d Probability of detection. [81](#)

List of Symbols

- P_{fa} Probability of false alarm. 81, 101, 113, 123, 131, 132, 135–137
- R_{IntTx} Range to interfering transmitter. 160
- $R_{Target-Rx}$ Range from target to receiver. 160
- $R_{Tx-Target}$ Range from transmitter to target. 160
- T_{CPI} CPI duration in seconds. 80, 96, 120
- ΔR_{bin} Range bin resolution in meters (derived from sample rate). 79
- ΔR_{res} Range resolution in meters (derived from signal bandwidth). 10
- Δf_{d-bin} Doppler bin resolution in Hertz. 80
- Ψ Cross ambiguity function in continuous time. The level of correlation between the surveillance and (some Doppler shifted version of) the reference signal. 7, 79
- β Bistatic angle. The angle made by the transmitter-to-target and target-to-receiver line segments in radians. 10
- τ Correlation or matched filter delay in seconds. 7, 79
- \mathbf{b} \mathbf{b} in $\mathbf{Ax} = \mathbf{b}$, set to equal \mathbf{s}_s for adaptive filtering during cancellation. 32, 76
- \mathbf{s}_e The echo signal. The desired part of the surveillance signal. I.e. skin echoes from targets of interest. 73
- \mathbf{s}_i The interference signal. The unwanted part of the surveillance signal. 73, 76
- \mathbf{s}_r The reference signal as received by the reference antenna. 7, 79, 95
- \mathbf{s}_s The surveillance signal as received by the surveillance antenna. xxvi, 7, 73, 76, 79, 82, 95
- \mathbf{s}_{cs} The cancelled surveillance signal. The output of DPI and clutter suppression run on \mathbf{s}_s . 82, 83

List of Symbols

- s_{im} An estimate of the interference signal and therefore an estimation of the unwanted part of the surveillance signal. 73, 74, 76
- s An arbitrary signal. 94, 95, 99, 102
- \mathbf{x} Filter weights applied to the a matrix to create a vector of interference estimation to be subtracted from the surveillance signal. xxvi, 32, 73, 74, 76, 82, 83, 86
- c Speed of light in meters per second. 10, 79
- f_d Bistatic Doppler shift in Hertz. 7, 79
- f_s Sample rate in Hertz or samples per second. 79, 96, 104
- k Discrete bistatic Doppler shift in an integer number of bistatic Doppler bins or a frequency bin number in a DFT. 79, 94–96, 102
- m Discrete correlation or matched filter delay in an integer number of sample periods. 79, 95, 96
- n Sample number as an independent parameter of a function. 73, 74, 76, 79, 94, 95, 102
- s An arbitrary sample. 99, 102
- t Continuous time as an independent parameter of a function. 7, 79

Chapter 1

Introduction

Commensal¹ radar, often referred to as Passive Coherent Location (PCL) Radar, Passive Bistatic Radar (PBR) amongst other names [6] exploits illuminators of opportunity, that is, illuminators that are often intended for purposes other than radio detection and ranging. The type of emission might include transmissions from a variety of possible sources. Examples include cellular towers, WiFi access points along with associated clients, digital audio broadcasts (DAB), terrestrial digital video broadcasts (DVB-T), analogue television broadcasts or as in the case of the system presented in this thesis, frequency modulation (FM) broadcast band broadcasts in the 88 to 108 MHz band. Transmissions from existing radars can also be exploited in a non-operative manor which has the potential advantage of waveforms which are specifically designed for radar use.

Radars that make commensal use of illuminators of opportunity to detect targets of interest, have seen limited uptake in industry due to several inherent challenges such as waveform suitability, complications of bistatic geometry, and most commonly, the interfering effects of the direct signal from the illuminator directly impinging on the surveillance antenna, that is, the antenna which is intended to detect skin echoes from targets of interest. These skin echoes are

¹ The term Commensal is used to describe a sensor system that utilises the emissions of existing radiating systems to sense, but without affecting in any way the functioning of these systems. The Commensal system can be bistatic or multistatic in geometry.

typically small when compared to the direct signal from the illuminator which is referred to in this context as direct path interference (DPI) as it is an unwanted signal in the surveillance channel of the commensal radar system, that is the receiver channel intended to receive the skin echoes from the targets of interest. Multipath versions of the direct signal can also be very large when reflected from large and nearby objects such as terrain. Multipath interference, i.e. any signal reflected from an object or objects that are not targets of interest is typically referred to as clutter. In severe cases detection of the smaller target skin echoes amidst the relatively large DPI and clutter can result in a prohibitively large dynamic range requirement for the receiver front end and analogue to digital converters (ADCs) [7, 8, 9] in which case target detection might not be possible. Fortunately given the natural evolution of receiver design, antenna design and ADC technology, systems are becoming more sensitive. Assuming the dynamic range condition is met, a large amount of processing gain is, however, still required to raise the targets of interest above noise and more critically interference caused mainly by (although not limited to) the illuminating signal which is being exploited. Establishing a processing chain to create this processing gain serves as the main focus of this thesis.

This thesis presents the design of a real-time processing chain for detecting targets in a bistatic commensal radar system which includes stages of data acquisition, DPI and clutter suppression, range/Doppler processing and finally target detection. Additional details on the processing for fusion of multiple frequencies for a common bistatic geometry in the amplitude/range/Doppler ARD space are also presented. The processing chain is targeted at a COTS desktop computing platform which consists of a typical high-end x86 derivative multicore central processing unit (CPU) and 1 or more graphics processing units (GPUs) on which general purpose GPU (GP-GPU) processing can be performed. This typical “gaming” style computer platform is likely to be far more cost effective than ASICs, FPGAs or DSPs or even large server class multicore (12 or more cores) CPUs and cluster implementations. The commercial, off the shelf (COTS) desktop and GPU platform also allows for easier development and interfacing as well as mobile deployment. The processing chain is designed to maximise signal

to noise ratio (SNR), signal to interference ratio (SIR) and dynamic range. The design also aims to make the most efficient use of the available hardware with minimal operator intervention.

It is shown that real-time throughput can be achieved with what is previous generation hardware at the time of writing. The presentation of this design is novel in that it presents a complete and holistic design that includes stages of data acquisition, up to target detection as well as considerations for how to efficiently pass data between these stages and thereby reducing latency and in turn increase throughput. Provision for distributing the processed output information to subsequent processing stages such as tracking is also provided. The software is automatically scalable to multiple GPU devices with the only limitation being that they have similar memory capacities. The processing chain operates in a continuous streaming manner for 100% duty cycle of a single bistatic pair exploiting a single FM broadcast band channel which is the fundamental component of larger FM broadcast band based radar system which might be multi-frequency, multi-transmitter or multi-site or any combination of these configurations. The need to operate at 100% duty cycle is created by the exploitation of long coherent processing intervals (CPIs), typically 4 seconds in the case of the system described in this thesis. The consequence is that a duty cycle of less than 100% would result in a prohibitively slow update rate in the context of applications such as air traffic control (ATC).

To date, existing literature has shown limited presentation on this topic in its entirety and only subsections of such a processing chain such as timings of various algorithms [10, 11] or review of algorithms [12, 13, 14, 2, 15].

Additionally, a novel configuration for a networked commensal radar system for aircraft detection is proposed in which a single reference channel is recorded by a receiver node, termed the *reference receiver* node. A network of surveillance receiver nodes are then set up at several sites to survey the coverage region of interest. Channel data is transferred via a data network to a central processing node which does the radar processing. Receiver coherency is maintained by making use of global navigation satellite system (GNSS) disciplined oscillators.

This allows the reference channel to be recorded at a separate site to those at which the surveillance channels are recorded and therefore allows receiver site selection to be done purely for the function of the channel to be recorded. This configuration of receivers is termed the *separated reference configuration* [16]. The performance of this configuration is tested and evaluated in the context of detecting large commercial airliner aircraft. Some initial but limited investigations are done into the stability requirements of the the oscillators. Thorough investigation into this topic is considered to be beyond the scope of this research. The aim is to provide a means for improving the system SINR thereby relieving the dynamic range requirement on the receiver and reducing the computational requirements of the processing chain. A demonstration of performance improvements that can be obtained using this configuration is presented based on a real radar deployment the processing was performed offline due to the lack of a suitable data network.

1.1 Overview of Commensal Radar

Commensal radars, in their simplest form, operate by recording a channel from an antenna which has a line of site (LoS) to a suitable illuminator of opportunity. At least 1 additional channel is then recorded from a respective antenna which surveys a region of interest where targets are to be detected. These channels are termed the *reference channel* and *surveillance channel* respectively and the signals which these channels transport are referred to as the *reference signal* and *surveillance signal* respectively. If one considers that exploited signals for commensal radar are most typically either broadcast or communication types and that the transmitted content is therefore either continuous or intermittent in a non-deterministic manner, the time-interleaved transmit/receive operation of a conventional pulsed radar is then, as a result, not realisable as means of preventing receiver saturation during transmission which is likely be occurring for 100% of the time anyway (e.g. broadcast services such as FM broadcasts [17, 18, 7, 19, 20, 21, 22], DVB-T [23, 24, 25, 22] etc.). Commensal radar systems are, therefore, more often than not bistatic i.e. the receiving antennas

1.1. OVERVIEW OF COMMENSAL RADAR

are placed at some distance away from the transmitting antenna. This reduces the illuminating signal level on the surveillance antenna and in turn the dynamic range of the surveillance receiver channel as it is required to be highly sensitive to detect skin echoes from targets of interest.

The straight line between the transmitting antenna and the receiver antennas (which are traditionally co-located) is referred to as the *bistatic baseline* as shown in Figure 1.1. Figure 1.1 also presents terminology for the different paths of signals that occur in commensal radar bistatic configuration. Jackson [26] provides a useful overview of the features and characteristics of bistatic radar (not limited to commensal versions thereof). The paper also discusses the aspects of the geometry as well as providing general terminology for bistatic systems.

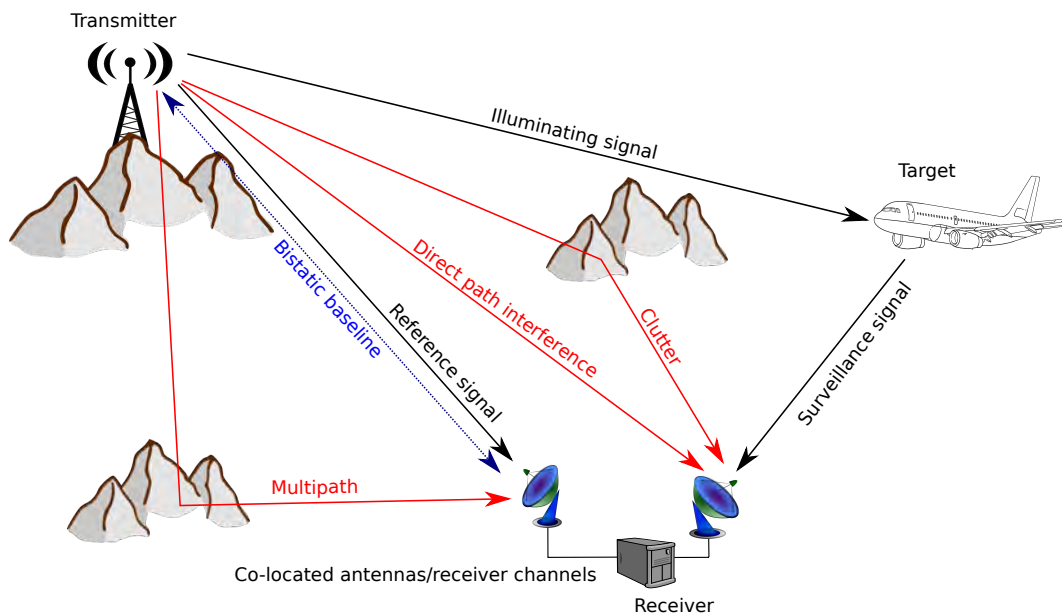


Figure 1.1: A bistatic commensal radar configuration showing the co-located receiving antennas, signals of interest (black) and unwanted interfering signals (red). The bistatic baseline is shown in blue.

1.1.1 Detection

Targets that have produced skin echoes of sufficient magnitude are detected in bistatic range and bistatic Doppler shift (often referred to simply as *Doppler*) by cross-correlating a snapshot of the surveillance signal with several synthetically Doppler shifted versions of the time-corresponding snapshot of the reference signal. These synthetically Doppler shifted versions of the reference signal are created by mixing the recorded reference signal snapshot with a complex exponential which has a frequency equal to that of the required Doppler shift. In radar terminology this correlation is often referred to as matched filtering as one wishes to determine if the surveillance signal matches the reference signal at some correlation shift. In the case of altering the reference signal such as creating the synthetic Doppler shifted versions, the correlation is sometimes referred to as a mismatched filter as the reference signal is no longer in its original form.

The mismatched filtering is performed over a range of potential Doppler shifts based on a priori knowledge of the operating velocity of the target(s) of interest. The 2 antennas are each fed into a respective receiver channel which digitises the received signal. More often than not it is necessary to run [DPI](#) and clutter suppression signal processing on the surveillance channel to improve the signal to interference ratio ([SIR](#)) in the channel. The matched and mismatched filtering (hereafter collectively referred to simply as matched filtering) of the 2 channels is a linear operation and so [DPI](#) and clutter suppression can be performed either directly on the surveillance signal in the time domain or alternatively on the matched filter output in the range/Doppler domain. The prior is the method discussed in this thesis. Matched filtering is done according to Formula [1.1](#) which produces the cross ambiguity function ([CAF](#)), also referred to as the 2 dimensional cross correlation function in some texts [[27](#), Ch. 17.2]. It is critical that digitisation between the 2 channels is phase-coherent as excessive phase drift or jitter between channels could result in decorrelating effects and a subsequent loss in signal to interference plus noise ratio ([SINR](#)) at the correlation output. For this reason the [ADCs](#) of the respective receivers' channels are typically clocked

from a common oscillator. The CAF is:

$$|\Psi(\tau, f_d)|^2 = \left| \int_{-\infty}^{\infty} \mathbf{s}_s(t) \mathbf{s}_r^*(t + \tau) e^{j2\pi f_d t} dt \right|^2 \quad (1.1)$$

where $|\Psi(\tau, f_d)|^2$ is the ambiguity response at delay time τ , (that is, the delay time corresponding to the bistatic range bin of interest) and bistatic Doppler shift f_d . Furthermore \mathbf{s}_s is the surveillance signal and \mathbf{s}_r the reference signal and * denotes complex conjugation. The CAF is visualised over an interval of bistatic range and bistatic Doppler bins of interest as an amplitude/range/Doppler (ARD) map which indicates the correlation between the 2 channels at given bistatic ranges and bistatic Doppler shifts. An example of an ARD map is shown in Figure 1.2.

It should be emphasised that both the range and Doppler measures are bistatic and, as such, monostatic radar concepts such as distance to target from the radar receiver may therefore not apply. The range as it is plotted is the distance from transmitter to target to receiver. The range is offset by the length of the baseline at the 0 delay output of the correlation due to the time taken for the reference signal to travel the length of the baseline. Targets can then be observed as peaks at a given bistatic range and at a bistatic Doppler shift produced by the resultant of the respective target state vector combined with the system geometry and carrier frequency of the exploited signal. ARD maps provide the primary insight into the performance of the individual bistatic receiver nodes of a commensal radar system. Finally the peaks are extracted from the ARD surface by thresholding. Typically this is done by using a constant false alarm rate (CFAR) filter which optimistically detects peaks at the expense of a constant percentage of false alarms, assuming some noise model for the background noise. In simple cases such as those applied in this thesis this noise is assumed to be Gaussian at the ADC input. More complex noise models can also be applied and might be necessary where the clutter environment is itself complex in nature, such as in the case of sea clutter.

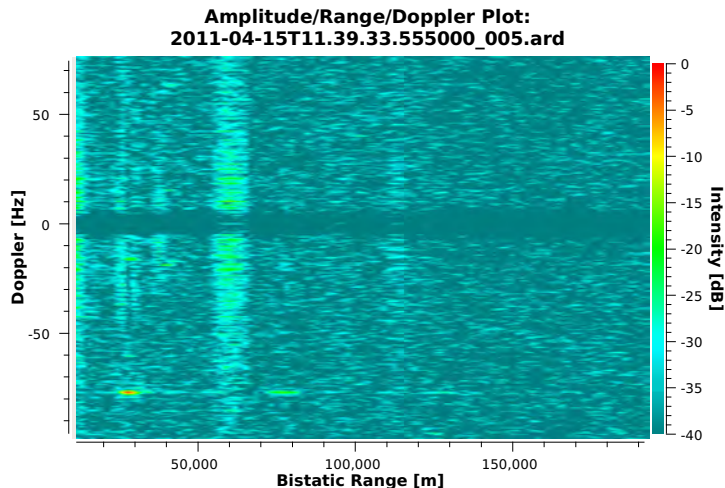


Figure 1.2: An example of an [ARD](#) map from real data recorded with the [UCT](#) prototype commensal radar system. This information serves as the primary output of a single bistatic receiver-node’s processing chain. The plot consists of the bistatic range on the horizontal axis, the bistatic Doppler shift on the vertical axis and the amplitude given by the colour. A target can be observed at 30 km, -75 Hz. The vertical strips are typically side lobes from strong clutter objects occurring at 0 Doppler.

1.1.2 Target Location

The single transmitter and receiver pair that produce detections at bistatic ranges and bistatic Doppler shifts (hereafter simply referred to as range and Doppler) are typically referred to as a *bistatic pair*. When the range from a detection is converted to Cartesian space it produces a constant bistatic range contour which is an ellipsoid with the foci being the transmitter and receiver antenna positions [28]. Multiplying by the wavelength of the carrier of the illuminating signal, one obtains the Doppler shift which in turn produces a velocity component which is the rate of change of the transmitter-target-receiver length, i.e. the bistatic range. The instantaneous direction of this velocity component is normal to the ellipsoid surface at the position of the target. The target position is, however, not derivable from information from a single bistatic pair only. The Doppler derived velocity component is referred to as (bistatic) *range rate*. Information in

this form is not very useful to a radar operator who would like a target state consisting of at least a point position and possibly a velocity vector. For this reason commensal radar systems will typically consist of a network of several of these bistatic pairs. This is achieved either by having a single receiver site exploiting multiple transmitters or multiple receivers exploiting a single transmitter or multiple receivers exploiting multiple transmitters. All of these combinations fall into the category of *multistatic radar* and allow the radar system to determine the position of targets by combining the range information from multiple bistatic pairs using a technique called *multilateration*. Similarly the range rates can be used to determine the velocity vector of the target when combined with the position. This velocity information is typically of high resolution due to relatively long integration times that commensal radars exploit. The long integration time translates into high a Doppler resolution [29].

Another method of target localisation makes use of angle of arrival (AoA) by using antenna arrays and phase interferometry. Morrison demonstrated tracking of targets of using simulated Doppler and bearing measurements along with the Gauss-Newton tracking filter [30]. This angle information can however be quite coarse at lower frequencies such as those in the FM broadcast band as noted by Howland [7]. Colone reported standard deviations of 5.75° at best when exploiting multiple concurrent FM frequencies [31]. AoA can of course, be used in conjunction with multilateration which will aid in track initialisation as a single receiver site is able to provide a position estimate which will, in turn, simplify the resolution of target ambiguities which result from combining range and Doppler information from several sites. For example 2 aircraft detected by 4 different receivers can result in a combination of up to 16 unique pairs of positions of the 2 targets of which only 1 pair is correct. Practically some of these position ambiguities maybe be unrealisable e.g. below the Earth's surface and could therefore be discarded. Nonetheless, resolution of the correct target positions is non-trivial without additional information such as angle of arrival.

1.1.3 Illuminating Signals

Exploitation of the FM broadcast band [7, 31, 19] broadcast signals is favourable due to the regular occurrence, high broadcast power, noise like structure and the relative ease of constructing receiver equipment and is as such, the main focus as an illuminating source in this thesis. Other terrestrial broadcast signals include DVB-T [23, 24, 32] which is favourable for its high bandwidth, DAB [33, 34] which is similar in structure but has narrower bandwidth and analogue television [35] which is problematic due its repetitive nature from frame to frame which results in range ambiguities and also the fact that analogue television is already largely phased out in many countries. Systems using communication signals such as GSM [36, 37], WiFi [38, 39] and WiMAX [40, 41] have also been demonstrated. Research into alternative configurations of commensal radar has included moving platform receivers e.g. receivers on aircraft [42, 43, 44, 45] along with high powered terrestrial emitters of opportunity and, alternatively, terrestrial receivers with extra-terrestrial transmitters e.g. those from GNSS [46], DVB-S [47] and SAR [48] satellites.

The range resolution of the radar, which is the minimum size to which a target can be measured, is inversely proportional to the bandwidth of the signal and can be approximated as shown in Equation 1.2 [49]. Where ΔR_{res} is the attainable bistatic range resolution in metres (which applies to the same dimension as bistatic range), c is the speed of light in metres per second, B is the instantaneous modulation bandwidth of the signal that is being exploited in Hertz and β is the bistatic angle, that is, the angle formed by the transmitter-target and target-receiver line segments in radians. The minimum distance to which 2 separate targets can be told apart will therefore be approximately twice that of the bistatic range resolution.

$$\Delta R_{res} = \frac{c}{B \cos(\beta/2)} \quad (1.2)$$

A comparison of the spectral content of a FM broadcast band channel and a DVB-T channel is presented in Figure 1.4. Applying the bandwidths of FM and

[DVB-T](#) to Equation 1.2 might suggest that the fixed width and significantly wider spectral content of the [DVB-T](#) signal would make it favourable for commensal radar use when compared to [FM](#). There are however several factors that make [FM](#) the preferable signal.

- [FM](#) requires no preprocessing before match filtering. [DVB-T](#) has inherent ambiguities which can be seen in the cross ambiguity function ([CAF](#)) which need to be mitigated e.g. pilot carrier suppression [50, 51, 52]. Figure 1.3 presents a comparison between [CAFs](#) of these 2 signal types.
- [DVB-T](#) is often broadcast in a single frequency network ([SFN](#)) which means that adjacent transmitters broadcast the same content at the same frequency. This creates range ambiguities in the matched filter stage of the radar signal processing. Adjacent [FM](#) broadcast transmitters, on the other hand, are always reported to operate on separate frequencies to one another in a multi-frequency network ([MFN](#)).
- The narrow bandwidth of the [FM](#) signal makes the construction of receiver equipment easier and low cost (e.g. Heunisch's Universal Software Radio Peripheral ([USRP](#)) based design [9]) and reduces the requirements of the signal processing subsystem. Longer integration times are also therefore possible for a given memory size which in turn translates into a higher Doppler resolution which is useful for Doppler based tracking [53].
- The lower carrier frequency of the [FM](#) broadcast band (88 - 108 MHz) makes the transmit beam pattern harder to control and as such, more energy is radiated at a positive elevation [54]. This is wasteful for the primary broadcast function but aircraft detection becomes more effective. The longer wavelength also propagates further in free space allowing for better radar coverage.
- [FM](#) broadcasting is a mature technology which has seen widespread roll out and is likely to be around for some years to come in developing countries where low cost radar is needed.

The following disadvantages are however also listed:

- As stated above the [FM](#) broadcast band channels are not wider than 200 kHz which limits the range resolution to less than 1.5 km. [DVB-T](#) has a bandwidth in the order of 7 MHz which makes for proportionally better range resolution.
- The bandwidth of the frequency modulated signal is dependant on the spectral content of the modulating signal. This implies that when audio with a low spectral content is being broadcast such as speech or audio containing periods of silence, then the bandwidth of the modulated signal will also be lower which affects the range resolution performance of the radar. [DVB-T](#) on the other hand, maintains a fixed modulation bandwidth independent of the programme content and therefore does not suffer from this problem.
- The nature of [FM](#) modulation typically results in more Doppler spread when compared to digital variations of modulation. This often requires cancellation of non-zero Doppler contributions in the lower Doppler bins.
- [FM](#) broadcasts may be discontinued in certain parts of the developed world in the near future. Replacements such as digital audio broadcast ([DAB](#)), satellite based audio services or internet based audio services are already in existence.

Despite the above disadvantages, the advantages still promote a preference towards [FM](#) based systems in an African context. Tracking filters that make predominant use of the Doppler information are proposed to be a possible technique for overcoming the low bandwidth limitations [53]. Exploiting multiple frequencies in the same bistatic triangle has also shown to be a useful method for creating robustness against bandwidth fluctuations. This technique also has further advantages such as providing robustness against multipath. Results of this are presented in Section 3.5. Suitable clutter suppression techniques can overcome Doppler spread [2].

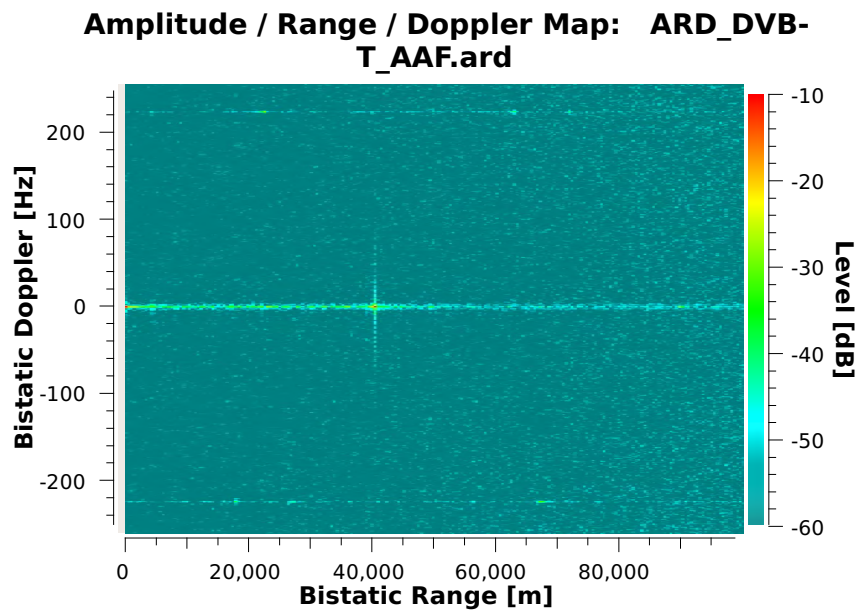
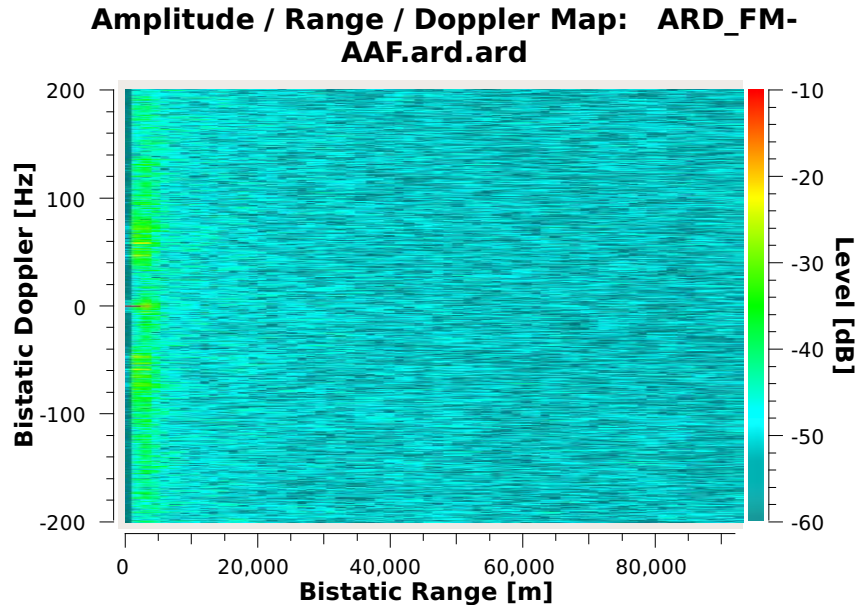


Figure 1.3: Comparison of the CAFs of a FM broadcast channel (a) and DVB-T (b). The FM channel has a peak on 0 m, 0 Hz and some slight sidelobes. With DVB-T on the other hand, several ambiguous components exist all around the the CAF surface due to guard intervals and pilot carriers. Note 0 dB occurs at 0 m, 0 Hz of both maps. This is however clamped to -10 dB for better colour contrast. These maps are generated from real data recorded at the University of Cape Town from the nearby Tygerberg transmitter which transmits FM, analogue TV and DVB-T.

1.1. OVERVIEW OF COMMENSAL RADAR

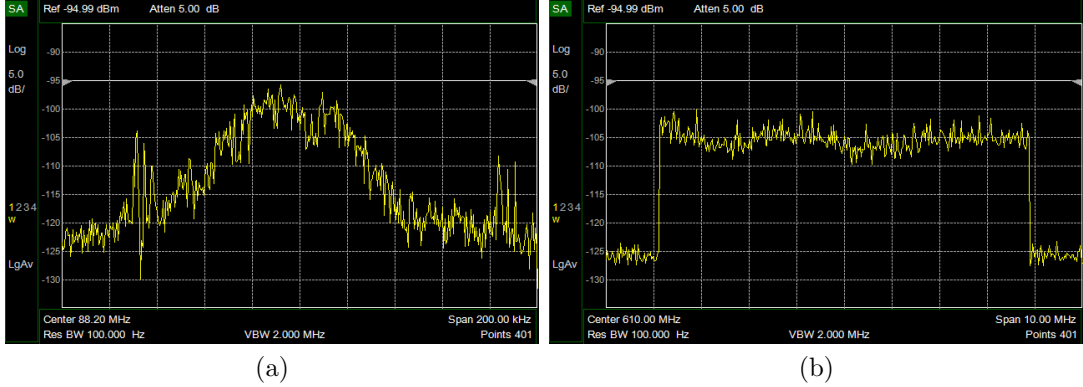


Figure 1.4: Comparison of the spectral content of a **FM** broadcast channel (a) and **DVB-T** (b). **FM** broadcast channels have a relatively low signal bandwidth which typically fluctuates between 20 and 100 kHz. The channel width is allocated at 160 kHz while instantaneous bandwidth is dependant on the modulating content which varies as a function of time. **DVB-T** (b) has a fixed bandwidth of 7.6 MHz which is independent of the modulating content. The **DVB-T** spectrum produces a characteristic rectangular pedestal shape. Note the full span of the plot in (a) is 200 kHz while (b) spans 10 MHz. These plots are generated from real data as described for Figure 1.3

Reviewing the **FM** ambiguity function, several notable characteristics are apparent. The peak-to-sidelobe ratio (**PSLR**) is typically around 25 dBm [55, 56]. This is confirmed in Figure 4.7(a), however, the **PSLR** is also dependant on the modulation content and suffers a deterioration under low modulation bandwidth. The most significant sidelobes appear offset in both range and Doppler [56]. This is visible when reviewing the zero Doppler in Figure 4.7(a), where strong clutter is present as shown in Figure 3.4(b) and also where strong targets are present such as in Figure 1.2. In all of these figures the sidelobes in Doppler sit slightly offset, both leading and trailing the peak return in range. For the zero Doppler (Figure 4.7(a)) case only the leading sidelobe peak is visible as the trailing sidelobe is beyond the lower edge of the range scale.

1.1.4 Overview of the Separated Reference Configuration

Radars which make commensal use of illuminators of opportunity have traditionally employed a single receiver device with multiple receiver channels to digitise surveillance and reference signals. The use of a single device means that a common oscillator clock can be distributed between the receiver channels which ensures coherency between the digitised signals that the receiver outputs. This configuration of receivers is referred to as the *co-located* configuration. The disadvantage of this co-located configuration is that the reference and surveillance antennas which are connected to this common multichannel receiver can only be separated by the practical lengths of the transmission cables used to connect the antennas to the receiver. The reference and surveillance antennas require different signal environments for optimal radar performance and these environments are, in fact, quite opposite. The reference antenna requires a clean LoS reference signal to the transmitting antenna. A surveillance antenna in close proximity to the reference antenna will therefore suffer large levels of DPI as it will also be subject to a LoS signal from the transmitting antenna as shown in Figure 1.5. To reduce the DPI impingent on the surveillance antenna the receiver node can be moved to a site where terrain shielding reduces the amount of DPI. Given that the reference antenna must also be moved it will then not be able to get a clean LoS to the transmitting antenna as shown in Figure 1.6.

The result of this limited spacing between the 2 antennas of the co-located receiver results in deployment planners seeking out sharp ridges such as the site of the Manastash Ridge Radar [57][6, Ch. 7], or by making use of the sharp edges of buildings [8] so that some separation can be achieved between the reference and surveillance antennas for the level of the reference signal. This separation will, however, not be very large due to fringing effects especially at low frequencies such as that of the FM broadcast band.

A possible solution to this problem is what is termed the *separated reference* [16] where the reference and surveillance channels are split into separate receivers so that each antenna can be placed optimally purely for its own function. Coherency is maintained by means of GNSS disciplined oscillators and data is transported

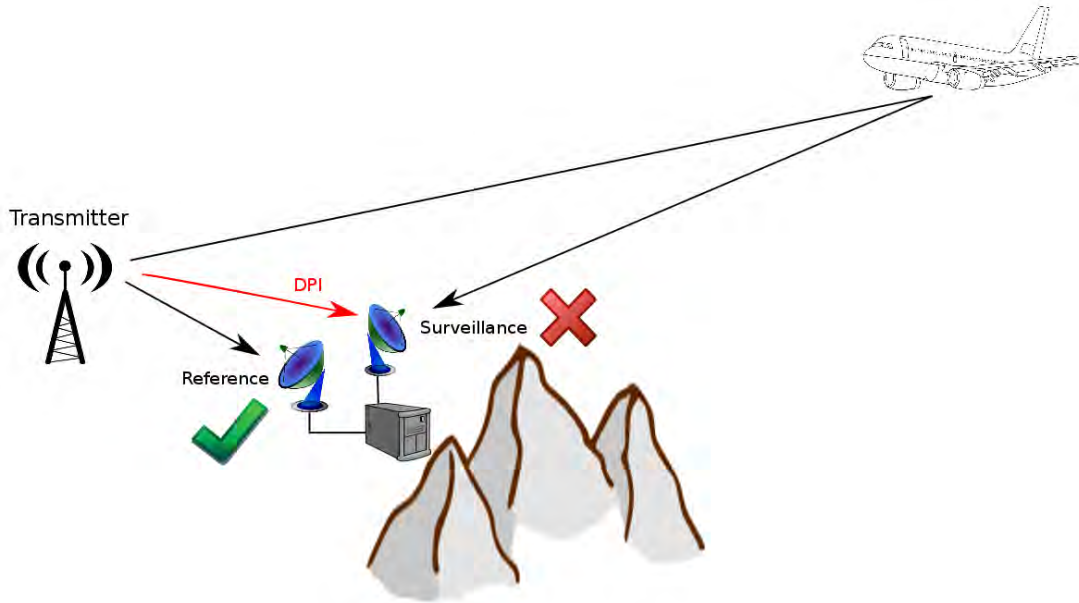


Figure 1.5: Optimal placement of the reference antenna to achieve a clear LoS signal from the transmitting antenna results in high DPI levels impinging on the surveillance antenna for the co-located configuration.

to central location for processing by means of a data network. This allows the surveillance antennas to be better screened from the transmitter and the reference antenna can be placed where there is clear LoS to the transmitter and preferably minimal multipath. The Manastash Ridge Radar was actually the first to make use of the separated reference idea to split the antennas of the reference and surveillance channels of a bistatic system to separate receivers at different sites and thereby maximise the effect of the mountain ridge for interference shielding. The system is bistatic and intended for atmospheric monitoring. In this thesis the separated reference configuration is applied to a multistatic system with 3 or more nodes for the purpose of air traffic control.

1.1.5 Motivation

While it must be conceded that commensal radar technology currently is not yet mature enough to replace conventional active radar despite large advances

1.1. OVERVIEW OF COMMENSAL RADAR

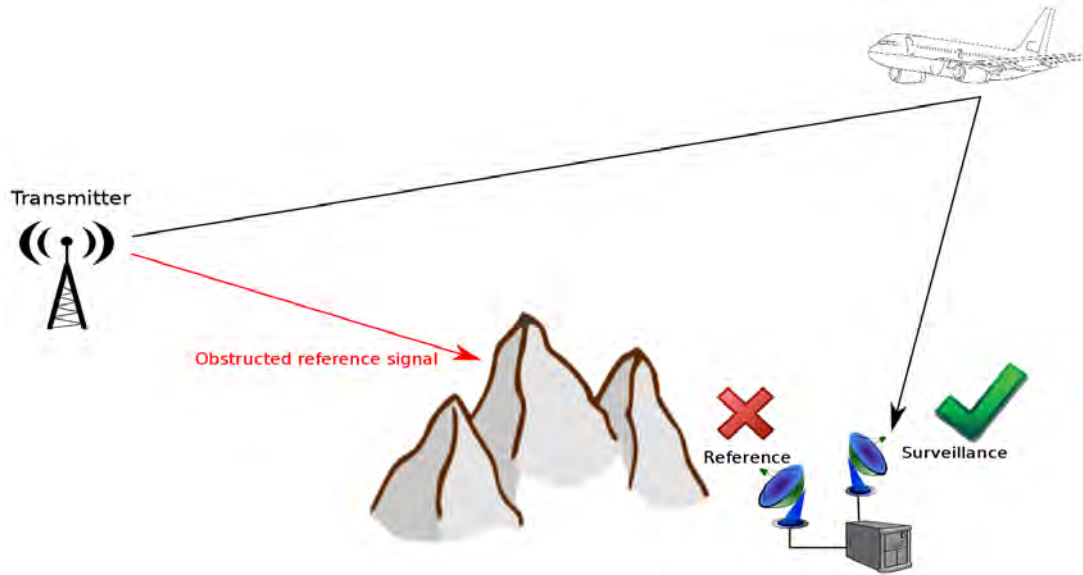


Figure 1.6: Optimal placement of the surveillance antenna to achieve minimal DPI results in an obstructed LoS reference signal for the reference antenna for the co-located configuration.

in recent years, the following benefits are presented for consideration.

Currently the most pertinent motivation for commensal radar is the growing demand for electro-magnetic (EM) spectrum. This demand for spectrum, driven primarily by the telecommunications industry is placing pressure on active radar systems which occupy bands that are suitable for telecommunications use such as the 3.4-3.7 GHz where 4G cellular services are intended to be deployed [58]. Furthermore, given that typical active radars do not occupy these respective bands for a majority of the time given their low duty cycle pulsed nature and only a fraction of the coverage area is illuminated at any time due to narrow beam scanning, this use cannot be considered to be efficient. It is therefore likely that governments start charging radar operators for the rent of EM spectrum for radar operation in future.

Commensal radar requires no transmitter and therefore requires no dedicated spectrum. Mature technology of this nature could hypothetically serve as a means to free up spectrum reserved for radar operation which can be auctioned

1.1. OVERVIEW OF COMMENSAL RADAR

off to telecommunications operators. Griffiths provides a table of the auction values of spectrum for 3 and 4G [58] which shows figures running into billions of dollars. Furthermore, from a radar operator's point of view the radar requires less power to operate and equipment costs are lower given that there is no transmitter subsystem. Of course no spectrum licensing is necessary.

Broadcast services such as FM or DVB-T provide continuous high powered transmit powers which can be effective for long range aircraft detection. For example Malanowski's results on long range aircraft detections with FM broadcasts [19]. The commensal radar systems are often envisioned to be in a networked multi-receiver/multi-site (multistatic) configuration and can therefore expect the typical advantages of such multi-site radar such as enhanced detection capability due to diversity of target aspect and multipath diversity (which includes diversity against effects such as clutter) as well as inherent system redundancy [59, Ch. 1.2].

In an African and 3rd world context commensal radar could prove to be an effective low cost alternate to traditional active air traffic control (ATC) radar which is often not affordable by governments. The technology might then also be able to offer affordable radar capability to smaller airfields and landing strips all across the world where the cost of conventional active radar is not justifiable even though the safety and practical benefits are clear.

Commensal radar systems are often said to have counter stealth capability. This is motivated by 2 considerations, firstly due to the inherent bistatic nature, where a stealth aircraft reflects energy away from the monostatic radar receiver to avoid detection, a bistatic receiver could theoretically detect this energy. The probability of detection could be increased with several bistatic receivers places at various sites. Secondly, given that stealth aircraft are likely to be optimised to have low observability either by shaping or absorbing materials at typical military radar frequencies such as X-band, these optimisation are unlikely to work at the relatively low frequencies that many commensal radar systems operate at such as the FM broadcast band. This is, as is to be expected, a sensitive topic and so there is limited literature on the concept. Kuschel [60], for example, presents

some investigation into this theory by means of simulation and use of a scale model of a stealth aircraft in an anechoic chamber.

A further benefit in a military context is that a commensal radar system emits no EM energy and therefore operates covertly.

1.1.6 Limitations

Arguably one of the biggest challenges of realising an operational commensal radar system is overcoming the effects of the direct path interference which is a problem that the research presented in this document intends to begin to address. As the future brings even faster computing technology at lower prices and high speed ADCs which are able to provide 16 bits or higher of quantisation level and analogue components with larger linear regions of spurious free dynamic range (SFDR). This challenge will in all likelihood diminish over time. The associated risk is, however, that large high powered transmitters may also be replaced by multiple lower powered transmitters but this could potentially be overcome with more short range radar receivers. This trend appears to be unlikely, at least in the immediate future, and especially in the third world.

The fundamental and unavoidable limitation of commensal radar is that the radar designer and/or operator does not have control over the transmitter which could then, hypothetically, be shut down at any point and will in turn terminate the radar functionality. Another implication of using an illuminator of opportunity is that the radar waveforms are not necessarily optimal for commensal radar operation. There is a large amount of literature that deals with how to improve performance when exploiting signals that are not obviously suitable for radar operation. Many of these are reviewed in the Literature Review chapter (Chapter 2). It is often shown that by using suitable techniques, improvements can be made as in the case of WiFi [39, 61], WiMAX [41] and DVB-T [62, 63, 52, 64]. With regard to transmitter shut down, it might be argued that in this modern, communication and media-centric age that services such as radio broadcasts and television broadcasts in their various formats and cellular based communications

have become so ingrained in everyday life that the maintenance of such services has become of the highest priority simply by public demand. A radar system exploiting any of these services for illumination, at least for normal civilian applications is extremely unlikely to suffer transmitter failure. Of course in the case of military applications or a war-time scenario these assumptions cannot be made.

If it is established that commensal radar is in fact an important addition for air traffic control or a similar service, which seems inevitable given the spectrum usage implications of active radar, then the illuminating service, what ever it might be, could be deemed an essential service and necessary backup precautions implemented to ensure redundant transmitter operation. Furthermore the waveform might be modified to be optimal for commensal radar in addition to providing the primary transmission service [58]. When the time comes for such system integration the discussion will without doubt be a political one.

Another challenging point is that commensal radar systems will provide best performance when operating as a network of receivers located across several sites and this requires complex planning and interconnecting infrastructure. A multi-receiver site configuration provides a diversity of target aspects and several degrees of redundancy in the system making it robust against effects such as clutter, multipath, in band interference from other sources in specific directions, target radar cross section (RCS) fluctuations which propagate in specific directions and so forth. Furthermore, multilateration is still possible when there are a limited number of transmitters available (as is often the case in South Africa for example). Often it is not practical to deploy a network of receivers especially in a military context. Early products such as the Silent Sentry and the Home Land Alerter 100 [65] were therefore single site systems that exploited multiple transmitters by means of digital beam steering. This system configuration is a trade off between deployment ease and performance.

1.2 Problem Description

As described in Section 1.1 the receiving antennas are placed a distance away from the transmitter in a bistatic configuration so that the surveillance channel is not saturated by the high power transmitter which often transmits continuously and therefore results in a quasi-continuous wave radar operation. Moving the surveillance antenna away from the transmitter can prevent saturation but a large direct signal is still likely to be impinging on the surveillance antenna which results in a large dynamic range requirement in the receiver so that the relatively small skin echoes from targets of interest can be detected in the presence of the large interfering direct signal (and possibly clutter). Figure 1.5 depicts a typical single site bistatic configuration where the surveillance antenna is subject to **DPI**. The effects of **DPI** and clutter can be reduced by careful selection of receiver sites [66], however, additional digital signal processing (**DSP**) is always necessary to raise the targets above noise and interference levels which might as be much as 90 dB above the target echoes [67] [68, Ch 7.5.4, 7.3.2.3].

As described in Section 1.1.4, the technique to reduce the direct path interference using terrain or man-made structures to shield the surveillance antenna from the energy emitted from the transmitter has a limitation in that the surveillance and reference antennas require converse environments. The reference antenna requires a clear **LoS** to the transmitter while the surveillance channels require as little of transmitted signal as possible. Given that the antennas are connected to the same receiver device to ensure coherence between the digitised channels, the antennas can then only be separated by the practical length of the transmission cables connecting them to the receiver. This distance limitation is typically not enough to create an effective signal level separation between the channels within the short distance separation due to the fringing effects of the **RF** propagation which is especially apparent at low carrier frequencies such as that of the **FM** broadcast band.

The majority of the gain which is required to raise targets above the noise level and more critically the interference level, needs to be provided by digital signal processing (**DSP**). This is especially the case when working at low carrier fre-

quencies such the 88 - 108 MHz band of FM broadcasts where spatial gains by means of antennas require prohibitively large antenna structures and shielding by means of large buildings or terrain structures is limited given the diffraction that occurs at these low frequencies. The amount of signal processing required tends to be very large and is often too much for a single desktop computer. Howland, for example used a cluster of Pentium 4 computers [7] to achieve real-time throughput. Specifically the processing chain of such a system would require, for each illuminating channel exploited by the bistatic receiver node, data acquisition from the receiver, DPI and clutter suppression, range/Doppler processing and finally detection. The DPI and clutter suppression and range/Doppler processing stages require large amounts of computational throughput and memory as is discussed in Sections 3.2.1 and 3.2.2. The problem is then to design a processing chain that still runs on COTS desktop computing hardware such as to keep the hardware costs to a minimum, however, the processing chain needs to be capable of processing the stated stages of the processing chain in real-time.

1.2.1 Research Hypothesis

The research hypothesis for this thesis is therefore:

It is possible to design and implement a real-time processing chain for a FM broadcast band commensal radar, including stages from baseband IQ data acquisition up to target detection, that can achieve real-time or better performance on a single desktop personal computer equipped with a multicore CPU and GP-GPU capable GPU.

Where “real-time” is as described in Section 1.4 within the time required to digitise the subsequent CPI of data, thereby allowing a 100% duty cycle. I.e. sample data for all time is processed. CPIs are typically (but not limited to) 4 seconds for the prototype system. The processing to be done by the single desktop computer is for data from a single bistatic pair exploiting a single FM broadcast frequency.

The research questions associated with this hypothesis are as follows:

- What is the optimal algorithm for each stage of the processing chain?
- How can the data flow and overall processing chain be designed to allow for efficient data flow through the chain?
- What specification of [COTS](#) general purpose computing hardware is required to perform the radar signal processing in real time?
- What is the scope for further processing, i.e. processing channel data for multiple [FM](#) channels or multiple bistatic pairs?

A further hypothesis based on the separated reference configuration is as follows:

It is possible to detect aircraft in a [FM](#) broadcast band radar system concurrently from multiple surveillance sites using a single reference signal recording for matched filtering.

The research questions associated with this hypothesis are as follows:

- Can a single reference signal recording from a single site be used for matched filtering with multiple surveillance signal recordings at multiple sites?
- Can optimal positioning of the reference antenna be used to effectively suppress artefacts such as target ghosting caused by multipath?

1.3 Proposed Solution

Counteracting the effects of direct path interference, multipath, and clutter that plague commensal radar operation is essentially a task of improving the signal to interference ratio ([SIR](#)). This is solved on 2 fronts.

Recent advances in computational hardware, notably general purpose computing hardware, have made the suppression of [DPI](#) and clutter as well as subsequent processing stages possible in real-time with minimal hardware costs. Emerging architectures such as multi-core central processing units ([CPUs](#)) and graphics

1.3. PROPOSED SOLUTION

processor units (GPUs) capable of general purpose GPU (GP-GPU) processing allow the commensal radar software designer to exploit large amounts of processing parallelism and concurrency in order to achieve the required real-time throughput. More specifically, the processing chain is made up of stages which consist of mathematical operations on arrays and matrices of data that can be processed using single instruction, multiple data (SIMD) techniques i.e. processing parallelism. On the other hand, the individual stages of the chain can be pipelined and therefore executed in a multiple instruction, multiple data (MIMD) nature, i.e. using processing concurrency. The result of using these parallel and concurrent methods on this general purpose COTS type of hardware is a likely reduction in hardware cost when compared to typical active radar systems [6, Ch 6.3.1.4].

In the digital signal processing (DSP) domain, an optimised, real-time signal processing chain is developed using COTS x86 computing hardware and GPU hardware. This processing solution encapsulates all stages from data acquisition from the receiver's digital back-end to output after target detection. The processing chain is pipelined and employs minimal memory copies to minimise latency and increase throughput. The processing chain includes an adaptive cancellation filter which reduces in band DPI and clutter interference and also a complete matched filter stage. I.e. not an approximation such as the "FMCW-Like" algorithm [68, chap. 7.5.8] and therefore requires no extra parametrisation other than coherent processing interval (CPI) length and maximum bistatic range to process to. The matched filter also then suffers no approximation loss as discussed in Section 3.3.2.3 as the processing chain aims to provide detection even of the weakest target returns in the digitised channel data. This processing chain is intended to be deployed on general purpose computing hardware in the form of a common desktop x86 derivative personal computer also exploiting GP-GPU techniques on a GPU device. This also aids in keeping the processing subsystem costs to a minimum which is in line with the concept of developing a low cost radar capability.

Digital signal processing can only work up to a point and is limited by the dynamic range available in the receiver. With the phrase "prevention is better than

cure” being ever applicable, the second approach involves reducing the level of the interfering signals impinging on the antennas by means of optimal site selection. This way the interference is not digitised in the first place. To make antenna placement more effective the reference and surveillance antennas are moved to separate receivers which removes the trade off condition describe in Section 1.2 and the antennas can therefore be place optimally for solely their own function whether it be capturing a reference signal or surveying a region of interest for targets. Coherency and timing is maintained by using GNSS disciplined oscillator equipped receivers at each site. It is shown that the Manastash Ridge Radar design using the separated reference configuration can be further extended to a multistatic case for air target detection. By using this *separated reference configuration*, a single reference signal can be recorded and used for matched filtering with each surveillance channel from a network of surveillance channels and provide detections of commercial airliners. Furthermore, the reference antenna can be placed where there is good line of site to the illuminator and also minimal multipath. The surveillance antenna can be placed where there is minimal DPI and clutter. Both antennas can then also be more easily placed to avoid in-band interference from third party transmitters.

1.4 Research Objectives

The research objectives are therefore as follows:

For the real-time processing chain:

- Describe the challenges in designing a real-time processing chain for com-mensal radar.
- Provide suitable algorithm, implementation and greater system integration to, in turn, provide solutions to identified challenges.
- Develop and implement a pipelined, real-time processing chain capable of accepting data from a receiver’s digital backend, perform DPI and clutter suppression to raise targets above the interference level, do matched

1.4. RESEARCH OBJECTIVES

filtering to produce [ARD](#) maps and finally target detection by means of constant false alarm rate filter.

Real-time in this instance implies that for a given [CPI](#) length of samples recorded, those samples are processed completely by the time the following [CPI](#) length of samples is finished recording. [CPIs](#) are typically 4 seconds in duration for this system. All samples for all time from the start of operation are therefore processed. Note that this 100% duty cycle is specific to the narrow bandwidth of a single channel FM broadcast band data from a single bistatic node. For wider bandwidth signals such as [DVB-T](#) a duty cycle of less than 100% might be employed due to throughput limitations. I.e. blocks of samples are discarded between [CPIs](#) (or not output by the receiver).

For the separated reference configuration:

- Show that the separated reference configuration can be applied in a simple basic bistatic configuration similar to the Manastash Ridge Radar for the purpose of detecting commercial airliners, using receivers equipped with [GNSS](#) disciplined oscillators.
- Show that a single reference channel can be used with a network of surveillance receivers to create multiple bistatic pairs.
- Demonstrate that by being able to choose a dedicated site for the reference signal antenna that a better reference signal can be obtained which in turn improves system performance.

1.4.1 Statement of Originality

The candidate believes that the following parts of this work constitute original contributions to the field of commensal radar:

- The presentation of a detailed design and implementation of a real-time commensal radar processing chain including all stages from data acquisition

to detection. As well as details of how the data flows through the processing chain.

- The implementation of a real-time [RDFT](#) based method for range Doppler processing on [GPU](#). [69].
- The use of a single reference recording in a multistatic multi-site commensal radar system. [16, 70].

1.4.2 Publications

The research detailed in this thesis has contributed partially or entirely to the following publications:

C Tong, M Inggs, G Lange, *Processing design of a networked passive coherent location system*, Radar Conference (RADAR), 2011 IEEE, pp. 692-697. [17]

C Tong, M Inggs, A Mishra, *Towards a MIMO radar based on commensal use of FM Broadcast transmitters of opportunity*, Synthetic Aperture Radar, 2012. EUSAR. 9th European Conference on, pp. 283-286. [18]

M Inggs, C Tong, *Commensal radar using separated reference and surveillance channel configuration*, Electronics letters 48 (18), 1158-1160. [16]

M Inggs, C Tong, A Mishra, F Maasdorp, *Modelling and simulation in commensal radar system design*, Radar Systems (Radar 2012), IET International Conference on, pp. 1-5. [66]

C Tong, M Inggs, F Maasdorp, *Performance improvements using the separated reference configuration for a multi-static FM broadcast band radar system*, Radar (Radar), 2013 International Conference on, pp. 224-229. [70]

M Inggs, A van der Byl, C Tong, *Commensal radar: Range-Doppler processing using a recursive DFT*, Radar (Radar), 2013 International Conference on, pp. 292-297. [69]

F Maasdorp, J Cilliers, M Inggs, C Tong, *Simulation and measurement of pro-*

pler modulation using FM broadcast band commensal radar, Electronics Letters 49 (23), pp. 1481-1482. [71]

C Tong, M Inggs, C van Dyk, *ComRad3, a Multichannel Direct Conversion Receiver for FM Broadcast Band Radar*, Radar Conference (RADAR), 2014 IEEE. [72]

M Inggs, C Tong, R Nadjiasngar, G Lange, A Mishra, and F Maasdorp, *Planning and design phases of a commensal radar system in the FM broadcast band*, Aerospace and Electronic Systems Magazine, IEEE, vol. 29, pp. 5063, July 2014. [73]

1.4.3 Scope of Research

The intended application of the research described in this thesis is to form an air traffic control (ATC) radar which utilises FM broadcast band radio broadcasts as the signal of opportunity. Commensal radar is not envisioned to replace existing conventional ATC radar, at least for the immediate future. This is not a realistic goal as a commensal radar cannot guarantee performance simply because the transmitter infrastructure is not under the control of the radar designer or operator. The system would therefore better serve as a backup to, or augmentation of existing radar systems to perform tasks such as gap filling or as low cost “better than nothing alternative” for where conventional ATC radar is simply not economically viable.

As the demand for spectrum grows, however, the paradigm will shift more and more towards considering commensal systems as a primary and permanent means of skin echo detection. University based research such as that outlined in this document will hopefully form a useful precursor to that inevitability. Nonetheless, the safety implications of all these applications would need to be thoroughly investigated before any operation system is commissioned.

The signal processing of the radar system is dealt with up to the stage of target detection, in this case performed by CFAR filters. Details on tracking are alluded to on occasion where relevant but target tracking is considered to be beyond the

scope of this document. The tracking stage is however critical to the performance of the radar system and will require innovative design to solve due the inherent non-linearities associated with bistatic radar geometry [53]. It is therefore likely to be a large focus in the future work of this research.

The separated reference configuration is presented as a means of improving the SINR and primarily SIR impinging on the antenna. The primary focus of this thesis is the design implementation and testing of a real-time processing chain from data acquisition to detection and so the subject of the separated reference is only investigated briefly with a presentation of proof of concept in the bistatic configuration and then extension to a multistatic configuration where a single reference channel is shared amongst all surveillance channels for matched filtering. Aspects that will need to be more thoroughly investigated in the future are presented in the Future Work section (Section 4.6).

1.5 Thesis Outline

This introductory chapter is followed by a review of the literature in Chapter 2 to provide insight to both the background and current development of commensal radar systems.

The report chapters of this thesis are broken down into 2 main sections. Firstly the design of a processing chain and related system software which is the primary focus of this thesis (Chapter 3). The chapter describes in detail a system where the flow of data is optimised by means of pipelining and efficient memory usage which in conjunction with the use of GP-GPU techniques for the arithmetic, allows for real-time operation of a commensal radar bistatic node up to the detection stage. This bistatic node is, in turn, the fundamental building block for the larger multistatic commensal radar system. It is demonstrated that for a single FM channel from a bistatic node, real-time throughput can be adequately achieved on previous generation GPU and CPU hardware leaving remaining capacity for additional processing.

Secondly as an additional concept the *separated reference* configuration is briefly described, investigated and some results presented in Chapter 4. This configuration splits reference and surveillance antennas on to separate receivers thereby facilitating an improvement in the commensal radar system's SINR by allowing more optimal antenna placement because the different antenna types are no longer tied to a common device and therefore a common site. This improvement in SINR at the receiver input reduces the demands on the receiver's dynamic range and the processing chains interference suppression capability. Some remarks are made on the performance requirements of the oscillators in the separate receivers and it is demonstrated that signal processing can be used to correct for the poor performance of oscillators in certain deterministic cases, however, a detailed analyses into this is considered to be beyond the scope of this research.

More detailed summaries of the each chapter are presented below.

1.5.1 Literature Review

The literature review in Chapter 2 covers notable contributions from various research institutions, academic institutions and organisations. The content in this section is organised by institution or organisation as the work often spans generations of researchers especially in an university environment.

The contributors include:

- University of Birmingham
- University of Cape Town
- University College London
- Nanyang Technological University, Singapore
- University of Pisa
- University of Rome "La Sapienza"

- Warsaw University of Technology
- Airbus (formerly known as Cassidian)
- Defence Science and Technology Organisation (DSTO), Australia
- Fraunhofer FHR
- SELEX
- SONDRRA Supelec

Further texts are also cited throughout the thesis where relevant.

1.5.2 Processing Design

Chapter 3 presents a detailed design of a real-time processing scheme for the detection of aircraft in the bistatic node(s) of commensal radar system. The design focusses on FM broadcast band signals but is largely applicable to most types of commensal radar although additional processing may be required for certain signal types where there are inherent ambiguities in the signal such as the OFDM based DVB-T standard [64].

The chapter begins by giving an overview of the prototype commensal radar system developed at the University of Cape Town. It is established that the data dimensions are derived from an integration time of 4 seconds of sample data, collection for both the reference and surveillance channels, both sampled at 204.8 kSps. The 4 second data dimension translates into 819200 samples per channel for each CPI. CPI and clutter suppression is done on smaller sub-blocks of 1042800 samples to alleviate memory requirements and create a slight generalisation of filter response in the Doppler dimension.

Following on in Section 3.2 are the computational challenges that are identified in the processing chain of a commensal radar processing scheme. The challenges arising in the various stage processing chain include:

Packetisation of data from the receiver over Ethernet

This first stage is important for organisation of the subsequent data flow throughout the processing chain, ensuring that all receiver data is correctly accounted for and also ensuring that the data that the receiver is providing is correct. I.e. continuous over time, or correctly batched in blocks, in the correct order.

DPI and clutter suppression

Also referred to simply as *cancellation*, and is typically the most computationally demanding stage of the processing chain. It is shown that typically this task involves solving the matrix equation $\mathbf{Ax} = \mathbf{b}$ where the A matrix dimensions are the cancellation CPI size (i.e. 102400) by the number of range bins to be cancelled (typically a few hundred). This stage therefore requires both a large amount of memory space and arithmetic throughput.

Range/Doppler processing

It is shown, as with the cancellation stage, that both a large amount of memory is necessary with matrix dimensions of the CPI size (i.e. 819200) by the number of range bins to visualise (typically several hundred). As a result a large amount of arithmetic throughput and memory space is required.

Target detection

Detection is performed by means of CFAR filters. The computational requirements of CFAR filters are shown to be negligible in comparison to the previous processing stages. Nonetheless the implementation is presented for completeness. Requirements are discussed also in the context of user interaction and data flow to subsequent stages of the greater radar system.

The additional processing requirements for combination of FM channel data from multiple frequencies (when use of these frequencies forms the same bistatic tri-

angle) is also presented. It is shown, as in the case of the [CFAR](#) filters to be relatively negligible when compared to cancellation and range/Doppler processing and can be implemented in a single [CPU](#) thread.

Proposed solutions to the challenges presented in Section [3.2](#) are then discussed in Section [3.3](#). The section details which algorithms were used to implement the respective stages of processing chain and how they fit into the greater system. It is demonstrated that both the cancellation and range/Doppler processing stages are well suited to be implemented on [CUDA](#) capable [GPU](#) hardware. Use of highly optimised [CUDA](#) libraries such as implementations of [BLAS](#) and batch [FFTs](#) allow for highly efficient use of the hardware. Specifically Geforce GTX480s were primarily available for testing and development and therefore serve as the base hardware for the design of this system.

For each single FM channel received by a single bistatic pair, the following design is proposed and implemented:

A packetisation scheme that continuously receives data from a network socket or from hard disk in a streaming manner. Using circular buffering and a “zero copy” ideology when handling data allows for a 100% duty cycle of data for all time to be reliably handled by this stage or optionally in a block mode when the duty cycle is less than 100%.

[DPI](#) and clutter suppression is achieved by making use of the conjugate gradient - least squares ([CGLS](#)) algorithm implemented on the [GPU](#). [CGLS](#) is an iterative refinement type algorithm and the ability to vary the amount of cancellation performed by limiting the number of refining iterations allows the algorithm’s execution time to be optimised by performing only the minimum required amount of cancellation. This is typically when the zero Doppler and surrounding region is reduced to the level of the background noise floor.

For range/Doppler processing several methods all suitable for [GPU](#) implementation are reviewed. It is shown that cross multiplying before Fourier Transforming ([XF](#)) is preferable for FM broadcast band signals due to the associated long integration times and low sample rates. Fourier Transforming before cross mul-

tiplying (FX) can be suitable for wider bandwidth signals such as DVB-T. The “FMCW-like” or batches algorithm is also evaluated and is shown to be orders of magnitude lighter in computation but comes with the expense of losses at high Doppler when parametrised incorrectly. Given the sufficiently fast implementation of the XF algorithm in the context of an FM broadcast band radar, the XF algorithm is deemed to be preferable over the batches algorithm. A novel method using the recursive DFT is also presented which has the benefit of arbitrarily high update rates and therefore high temporal resolution. This streaming algorithm is however not currently suitable for the commensal radar processing chain due to the block nature of the prior cancellation stage as well as a compounding error in floating point calculations. Its potential applications are, however, suggested in the chapter.

The target detection stage by means of CFAR has negligible computational requirements in comparison to the cancellation and range/Doppler processing and is even less intensive than the interpolation algorithm required to draw ARD or CFAR data on a computer monitor. For this reason the CFAR filter is implemented in the plotting software so that each radar user receiving range/Doppler information from the processing server can tune the CFAR filter individually which is useful given the developmental status of the system. It is also shown that the “greater of” cell averaging CFAR algorithm (GOCA-CFAR) is optimal for a radar exploiting FM broadcast band signals due to its ability to reject clutter ridges. The CFAR filter is implemented in the Doppler domain only, so as to be robust against the target length fluctuations that occur in the range domain due to the modulation bandwidth fluctuations that are characteristic of a FM broadcast band signal.

The resulting processing timings indicate that data for a single bistatic transmitter-receiver pair, exploiting a single FM broadcast channel, sampled at 204.8 kSps can run approximately 5 times faster than real-time (the time taken to capture the data) on a high end desktop system with a NVIDIA Geforce GTX480 GPU (which is a previous generation GPU at the time of writing). The above scheme produces ARD maps with 280 range bins by 1601 Doppler bins over and integration time of 4 seconds as well as CFAR detection data for the ARD maps.

[DPI](#) and clutter suppression is performed for 220 range bins on the 0 Doppler bin in this case. Furthermore, it is shown that the processing chain scales automatically to a NVIDIA Geforce GT640 and to multiple NVIDIA Tesla M2090s and performance is better than real-time and proportionally scaled for these respective cases. Results are also presented for the NVIDIA Jetson TK1 which is an embedded [GPU](#) platform. The present processing is also ported to a [CPU](#) only version and results for several different [CPU](#) architectures are presented. A concise summary of these timings is presented in Section [3.6](#).

1.5.3 The Separated Reference Configuration

The second topic of this research, contained in Chapter [4](#) discusses an investigation into the separated reference configuration which is a term used to describe a system that records reference and surveillance channels (to be cross correlated together) with separate receivers at separate locations. This allows each antenna site to be optimised specifically for that antenna's function. The idea was first demonstrated by Sahr in the Manastash Ridge Radar [\[57\]](#)[\[6, Ch. 7\]](#) for a bistatic system. The application of this radar configuration is demonstrated for a multistatic system used to detect commercial aircraft which is believed to be novel.

The chapter begins with an overview of the concept and illustrates some of the advantages of the configuration such as each antenna being able to be positioned solely for its own signal given that the reference and surveillance antennas are no-longer attached to receiver front-ends in a common device.

Section [4.2](#) presents results from a field test where 3 co-located receiver nodes were deployed and different sites in a multistatic configuration in the Western Cape of South Africa. With the receivers operating coherently by means of [GNSS](#) disciplined oscillators, any reference channel from any of the 3 sites can then be combined with any surveillance channel of any of the 3 sites. This created several combinations in which the performance of the separated reference configuration could be tested against that of the co-located configuration. And these results

are presented.

It is shown that when using adequate stable [GPS](#) disciplined oscillators the separated reference can be applied with no measurable loss in coherency in the range/Doppler space. Furthermore, selecting a cleaner reference site is shown to remove effects of target ghosting caused by multipath interference.

It is shown in [Section 4.4](#) that where a fixed frequency offset exists between poorly performing oscillators it is possible in certain cases to correct for this effect by mixing out the frequency offset. These offsets tend to create spurs in the Doppler spectrum which result in false alarms. The mixing largely removes these spurs. The technique does, however rely on the dominating [DPI](#) in the surveillance channel to perform a comparison to the reference channel to determine the frequency offset. It is important to note then that in a case where the separated reference configuration truly removes the [DPI](#) effect this technique will probably not be applicable.

One of the challenges with reference and surveillance sample data being collected and different sites is that this data needs to be brought to common location for the radar signal processing to be done. This requires the provision of an adequate data network which will in all likelihood need to be fibre-optic to meet throughput requirements. Networking considerations are discussed in [Section 4.5.2](#).

1.5.4 Conclusions

The following summarises the conclusions and future work presented in [Chapter 5](#).

The design of a processing chain for a [FM](#) broadcast band based commensal radar system is presented that is intended to run on [COTS](#) based general purpose desktop computing hardware with 1 or more [CUDA](#) capable [GPUs](#). It is shown that previous generation equipment is capable of producing faster than real-time throughput obtainable for a single [FM](#) channel from a single bistatic node for processing stages up to the point of target detection. Furthermore, it is shown

that with this hardware, specifically, a high end desktop system equipped with 2 NVIDIA Geforce GTX480s there is estimated capacity to process 10 such streams of data whether it be from multiple FM channels for multiple bistatic nodes.

Results are also presented for other variations including both high end cluster computing hardware and mid level general purpose computing hardware. It is shown that the software automatically scales to this different hardware including capability to scale to multiple GPU devices and in all cases shows better than real-time performance suitable for 100% duty cycle streaming output for a single FM channel and single bistatic triangle and with the higher end hardware leaving capacity for processing of more data.

This capability further solidifies the low cost attribute of commensal radar. As general purpose computing hardware is fractional in cost in comparison to the purpose built processing subsystems found on typical active radars.

At the time of completion of this thesis a receiver with 3 analogue to digital channels and 16 DDCs in total was developed by an industry partner, namely Peralex Electronics, specifically for the purpose of investigation of FM broadcast band based commensal radar. This allows for both AoA and the combination of 5 separate FM channels (each digitised by the 3 analogue to digital channels coherently). The integration of this capability into the real-time processing chain is therefore the immediate focus of future work. As described in the performance results of the processing chain in Section 3.3 there is capacity on the current hardware to expand the throughput on the GPU by approximately 10 times when using the CGLS cancellation algorithm and the XF range/Doppler processing algorithm (on 2x NVIDIA Geforce GTX480 cards). It was also shown that at maximum possible GPU throughput only half the resources of a quad-core CPU are utilised. Handling the data throughput from the new receiver on the current processing hardware is likely to be borderline possible then. The new receiver is sampled at 200 kSps as opposed to 204.8 kSps which will relieve the processing overhead slightly which may be adequate to allow processing of all data from the receiver on the current processing hardware, otherwise less intensive algorithms such as the batches algorithm for range/Doppler processing

might be considered to realise the processing and also to provide [ARD](#) updates at more regular intervals than 4 seconds by means of a sliding window.

Tracking is not discussed in this thesis in any detail but in the context of a working radar system it will prove critical. Work has already been done at the University of Cape Town to investigate tracking for commensal radar systems [[30](#), [53](#)] and it is likely to require further innovation to make a sufficiently robust tracking system that can extract the most out of the measurement information that the commensal radar processing chain can provide.

Results from tests with the separated reference configuration indicated that it is a valuable technique for suppressing unwanted signals in the receiver channels. This was originally demonstrated with [DPI](#) in the case of the Manastash Ridge Radar and now with multipath in the reference channel in this thesis. The same principle should be applicable to in band interference from other illuminators and also to clutter provided there are structures to hide behind while maintaining a suitable view of the region to be surveyed. Invariably the availability of a suitable data network will determine whether such a configuration is realisable unless the system is able to run in an offline manner where data is recorded and distributed by removable storage. This is only likely to be acceptable in certain geosensing applications such as atmospheric monitoring and is unlikely to be desirable.

There is much scope for further work into the separated reference configuration and the following are presented for consideration.

- Detailed Investigation into the temporal stability requirements of and associated coherency of the receiver oscillators.
- Further experimentation with long baselines (100s of km) between receivers. Cancellation algorithms may then not be necessary at all. This will then also allow for the use of the [RDFT](#) based range/Doppler processing as presented in Section [3.3.2.4](#) with benefit of the associated high temporal resolution.
- Very long baselines may result in the exploitation of different [GNSS](#) satellites at different radar sites. The effects of this phenomenon on [GNSS](#)

1.5. THESIS OUTLINE

disciplined oscillator performance will need to be evaluated.

- Determining the degree to which frequency offsets can be corrected for and how this is affected by the front end architecture (e.g. heterodyning v.s. direct sampling).

Chapter 2

Literature Review

The concept of commensal radar is as old as radar itself [65]. Early demonstrations to detect targets of interest by means of electromagnetic energy made use of high energy emitters which were invariably not designed for radar applications. Today major advances in the field of high performance computing have sparked renewed interest in the field as this resource might serve to overcome many of the inherent obstacles by means of real-time software defined radio (SDR) techniques and signal processing.

2.1 Research by Universities, Research Institutions and Companies

The following are relevant and/or significant research efforts that have been published relating to the field of commensal radar. The literature is arranged chronologically and grouped as far as possible by University, research institution or company. These groupings have sometimes overlapped or changed as individual authors have moved between them and/or collaborated.

2.1.1 University College London

UCL has a rich heritage of radar and specifically commensal radar research with work spanning multiple generations over a variety of flavours of illuminator and application.

During the 1980's Griffiths and Long, performed an investigation into using analogue television broadcasts as a means of transmission for bi-static radar [35]. The methodology investigated the pulsed nature of the analogue television signal structure to implement a pulsed radar. ADC technology at the time was limited to 8 bits which is equivalent to 48 dB of dynamic range. This proved to be insufficient to provide effective processing gain to resolve targets. As stated by Griffiths et al. [35] "...the processing gain cannot exceed the dynamic range of the system" so with 8 bits of dynamic range in the ADC and in all likelihood a lower effective number of bits, the processing gain that could hypothetically be achieved is less than 48 dB which is unlikely to be sufficient for all but the closest and largest aircraft targets. Target detections could, however, be observed in a real-time analogue video output which was connected to a digital moving target indicator (MTI) canceller. The work highlighted many of the challenges involved in commensal radar such as dynamic range and signal processing requirements. The researchers were unable to achieve any documented results, however they maintained that illuminators of opportunity still had "substantial attractions".

In 2002 Griffiths et al. analysed some of the aspects of using a space-borne SAR satellite as an illuminator for a stationary ground receiver [48]. Griffiths et al. described some of the expected signal levels and ambiguities and expected performance. A design for a receiver was also described using a conventional heterodyning mechanism.

In 2005 Griffiths and Baker published a paper discussing performance of commensal radar systems [74], pointing out that this was a topic that had not been covered in any great detail to date. The paper analysed the theoretical performance that could be achieved using typical FM, DAB and cellular base station transmitters. The bistatic radar equation was reviewed with a commensal radar

2.1. RESEARCH BY UNIVERSITIES, RESEARCH INSTITUTIONS AND COMPANIES

context and comments on the amount of [DPI](#) suppression are provided. Part 2 of the paper then discusses waveform properties [\[55\]](#) and provides analyses of [FM](#), [GSM](#), [DAB](#) and analogue television. Resolutions are determined by means of the auto ambiguity function ([AAF](#)) and the effects that geometry have on these resolutions are discussed.

In 2007 Griffiths and Baker published a paper on the signal and interference environment [\[67\]](#) which compares the ambiguity function properties of several illuminators of opportunity. They go on to discuss different sources of interference that occur in the presence of commensal radar operation and detail some methods for cancelling these. It is emphasised that 80 dB of interference suppression is typically necessary for useful system operation.

Guo et al. published on investigations into using [WiFi](#) access points as illuminators of opportunity for short range surveillance in indoor environments. Initial work demonstrated detections in a controlled environment in an anechoic chamber where metal objects and a person was detected using the beacon transmissions from a [WiFi](#) access point over short distances (less than 4 m). A brief analysis of the [CAF](#) of the [WiFi](#) waveform was also presented [\[75\]](#). Further work presented a comparison between the [CAF](#)s of parts of the beacon packets that are encoded with differential binary phase shift keying (DBPSK) and differential quadrature phase shift keying (DQPSK) respectively. Outdoor experiment results are also presented on this analysis [\[76\]](#).

O'Hagan's PhD [\[8\]](#) submitted in 2009, provides an in depth analysis of a [FM](#) broadcast based commensal radar. The work completely characterises a system from the antennas up to the constant false alarm rate ([CFAR](#)) detection stage. Aspects include antenna placement, receiver hardware design and signal processing i.e. [DPI](#) and clutter suppression and matched filtering.

In 2009 Chetty et al. published results of experiments using [WiFi](#) as a source of illumination in an indoor environment [\[38\]](#) to determine detection capabilities in the presence of high levels of clutter. These experiments were done using the NetRad system [\[77\]](#) for data collections. The results of these experiments demonstrated that persons could be detected above the clutter at walking speed

2.1. RESEARCH BY UNIVERSITIES, RESEARCH INSTITUTIONS AND COMPANIES

albeit with certain idealistic conditions. That is, with highly directive antennas pointing at the target. This work was later extended to demonstrate detection capability through multilayer walls (with air gaps in the middle) [78].

In 2010 Chetty et al. published an analyses of [WiMAX](#) as an illumination source for maritime surveillance [40]. The simulation results suggested that large ships could be detected at ranges of up to 10 km and small to medium sized vessels in ranges of 2 to 5 km. It was noted that [DPI](#) was the main limiting factor for systems of this type which suggests that the separated reference configuration [16] could be helpful in this case.

Brown did tests with a demonstrator of an airborne [FM](#) based commensal radar system [42] near Heathrow airport in London. Using a single [FM](#) transmitter, he was able to show detections of air targets that occurred outside the moving and stationary clutter regions. Also, given the narrow variations in flight paths and velocities that large airliners observe due to mandates by [ATC](#), they were often able to postulate the velocity vectors of the detected targets.

Olsen (also affiliated with the Norwegian Defence Research Establishment) did a PhD [79] (2011) and related work on range resolution improvement of commensal radar systems by combining multiple channels from a single illuminator site. Initial work demonstrated that the range resolution could be improved in [FM](#) based commensal radar by mixing sparsely populated channels such that they lie adjacent to one another [80, 81]. This mixing is necessary because gaps between channels (as they typically occur in multi-frequency networks ([MFNs](#)), raise sidelobes and cause ambiguities in the correlation stage of [CAF](#) processing. A further challenge with the [FM](#) waveform is, given that the modulation bandwidth fluctuates with time, gaps may form between the adjacent channels when the bandwidth narrows. The suggestion by Olsen is therefore to use narrow sections of each channel (the centre 20 kHz of the possible 160 kHz is proposed) to minimise this effect. It might be argued that this requires a lot of post processing to achieve a range resolution which is not significant anyway. For example 5 20 kHz channels combined results in 100 kHz and therefore a theoretical minimum 1.5 km range bin. Furthermore, this channel combining will come with a

penalty in [PSLR](#). Olsen then extended the [FM](#) based work to cater for the fact that the different [FM](#) channels in the same bistatic triangle produce different Doppler shifts for a given target state because the exploited [FM](#) channels have different carrier frequencies. Previously this was dealt with by using low integration times and correspondingly coarse Doppler resolution such that the different Doppler shifts all end up in the same Doppler bin. It is, however, demonstrated that a phase correction term can be used to make different channels produce similar Doppler shifts and longer integrations times can therefore be exploited. This is important in [FM](#) based commensal radar as it results in a proportionally high Doppler resolution and high integration gain. The extension of the multi-channel [FM](#) work also presents a method for dealing with phase synchronicity between channels [82].

In 2012 Olsen published further work a multi-band processing scheme that combined multiple [FM](#) or [DVB-T](#) channels [83, 84]. The work was based on simulated scenarios and showed that range resolution improvement could be achieved as well as the ability to better resolve closely spaced targets.

2.1.2 University of Birmingham

During the 1990's Howland did research at DERA, Malvern, into television based bistatic radar [29, 85, 86]. He was able to track and position aircraft using a single receiver location and therefore a single bi-static pair. The technique involved tracking using direction of arrival ([DoA](#)) and Doppler information. Given the nature of the measures of Doppler and [DoA](#) Howland used a complex algorithm to perform the tracking. A Kalman filter was used to track in Doppler and [DoA](#). From there the Cartesian tracking initialisation was done using a 2 stage process. Firstly an approximate estimate of the position was found using a genetic algorithm. The approximation was then further optimised using a Levenberg-Marquardt optimisation. This position was then used as the initial condition to drive an extended Kalman filter which tracked in 2D Cartesian space.

In 2003 Saini et al. published on the design of a [DPI](#) suppression scheme for

DTV based commensal radar using a hardware canceller which comprised of a delay lock tracking loop [87]. The interesting feature of this system is that it is designed for a rotating surveillance antenna. Saini claimed a 30 - 40 dB reduction in **DPI** when using a 600 ms **CPI**. Also noteworthy was the claim that disc-on-rod antennas have far better cross polarisation rejection in their sidelobes which meant that 10 - 15 dB of **DPI** rejection could be achieved when using these types of antennas. The possible loss in target **RCS** for a cross polarised surveillance antenna is not, however, mentioned.

In 2005 Howland (although then at NATO Agency, Hague, Netherlands) along with Maksimiuk and Reitsma published a paper that detailed a commensal radar that made use of **FM** broadcasts [7]. The system that was developed holds much significance because it is one of the few detailed in literature up until recently that used **SDR** techniques and operated in real-time. The system provided range, Doppler and **DoA** information after performing clutter and (**DPI**) suppression. The research published in this paper is a milestone in the development of commensal radar.

In 2005 Saini et al. published an analyses of the **DTV** ambiguity function for the signal standard used in the UK at the time [52]. The work included a method for reducing the ambiguities cause by guard intervals and sub carriers. Saini showed that his method could suppress ambiguities by 40 dB while incurring a 1% error in filtering.

2.1.3 University of Rome “La Sapienza”

The Infocom Department at the University of Rome have produced an extensive number of publications on commensal radar systems initially concentrating on **FM** Broadcast systems and later diverting their attention to **WiFi** based systems for personnel, goods and motor vehicle monitoring for both indoor and short range outdoor security applications.

In 2006 Colone et al. published a paper detailing an algorithm for **DPI** and clutter suppression [12]. This algorithm made use of the least mean squares

estimator to determine the filter weights as well as a sequential expansion for the estimator in an attempt to reduce the computational load of the algorithm. The paper also describes a process for progressively cancelling strong returns to extract weaker targets. This processing was later described as the sequential cancellation algorithm (SCA) [14].

In 2007 Cardinali presented a review of several [DPI](#) and clutter cancellation algorithms [14] including least mean squares (LMS), normalised LMS (NLMS), recursive least squares (RLS) as well as the authors' own sequential cancellation algorithm (SCA) and extensive cancellation algorithm ([ECA](#)) both based on the least means squares estimator technique. Findings were that LMS and RLS take longer to converge while RLS and [ECA](#) are relatively computational heavy. SCA is therefore preferred.

In 2007 Lauri published an analysis of the [FM](#) signal for use with commensal radar [56]. It was shown that range resolution could be related to the standard deviation and kurtosis of the modulation signal. A method for automatic silence detection within the modulating content was presented. A simulation model of the [FM](#) signal was also constructed using 2 rays to produce direct and multipath effects.

In 2007 Lauri published the design of a “geometrically based multipath channel model for passive radar” [88] which aimed to serve as a simulation for operational commensal radar environments, particularly when multiple antennas are being used for beam forming. This model made use of single bounce propagation theory to determine the amplitude and phase of signals arriving at the receiver.

In 2008 Bongioanni presented results from a bistatic system exploiting multiple [FM](#) broadcast channels concurrently [20]. The paper presented a comparison of a super-heterodyne receiver v.s. a direct sampling design. The conclusion was that the performance was comparable but that the direct sampling receiver was slightly better as it was able to make better use of the full [ADC](#) dynamic range. The multiple [FM](#) channels were added together non-coherently in [ARD](#) space. This is done by first normalising each map to its noise level which is determined at high range and Doppler where targets are unlikely to occur. The

integration time for each channel is then varied proportionally to the carrier such that the velocity resolution of the maps are the same. The conclusion on channel combination was that obvious detection gains were observed up to 3 channels but a 4th yielded no further benefit. The 4th channel was, however, noted to be poor performing. A modified expression for the false alarm rate was also derived for the [CFAR](#) filter in the multichannel summed [ARD](#).

In 2009 Bongioanni published on [DVB-T CAF](#) analyses and a means for suppressing the ambiguities caused by pilots and sub-carriers in the [DVB-T](#) signal [63]. The new approach was claimed to be beneficial over Saini's parallel stage approach [52] in that it was a linear single stage, did not require synchronisation and did not create spurs in the presence of multiple targets. Furthermore, mismatched losses were reported to be comparable to those of Saini's method.

In 2009 Colone Proposed a revised version of the [DPI](#) and clutter suppression algorithm approach intended specifically for commensal radar applications [2]. The algorithm is an iterative process that selects and cancels the strongest amplitude disturbances in the range/Doppler plane during each iteration. It was termed the "Extensive Cancellation Algorithm" ([ECA](#)).

Colone published further work in 2009 describing techniques for cleaning the reference (direct) signal by removing multipath components [89]. This is expected to improve [SIR](#) ratios and will be an important future consideration for the proposed separated reference channel configurations. A detailed overview of the separated reference configuration is provided in Chapter 4.

In 2009 Falcone published a technique for the reduction of range sidelobes when exploiting [WiFi](#)-based signals [90]. This was achieved by means of filters targeted specifically at the sidelobes created by the Barker codes that are used in the beacon transmission of the [WiFi](#) signal. The remaining sidelobes inherent in the signal [CAF](#) are also suppressed by subtracting scaled and delayed versions of the signal autocorrelation function. It was shown that a 20 dB improvement in [PSLR](#) (from 20 to 40 dB) can be achieved using the described techniques which were shown, in a practical deployment, to be adequate to raise a target sufficiently above sidelobe level without the need for [DPI](#) and clutter suppression.

2.1. RESEARCH BY UNIVERSITIES, RESEARCH INSTITUTIONS AND COMPANIES

In 2010 Falcone followed up with experimental results for [OFDM WiFi](#)-based commensal radar [39] based on the previous sidelobe suppression work. It was shown that a running person following a moving car could be resolved in close proximity (10 m) when using both [ECA](#) for [DPI](#) and clutter suppression and the range sidelobe suppression technique [90].

Falcone demonstrated a [WiFi](#) based system [39] in 2010. Using high gain antennas typically used in point to point [WiFi](#) links and a typical [COTS D-Link WiFi](#) Access Point ([AP](#)) the researchers demonstrated that the [WiFi](#) signal contains sufficient bandwidth to detect both vehicles moving slowly in a car parking lot as well a person walking. The system was arranged in a mono-static configuration with the reference channel being fed directly from the [AP](#) to the receiver channel via a transmission line. The same [ECA](#) algorithm developed for [FM](#) was applied to this system to reduce [DPI](#) and clutter.

In 2010 Bongioanni published work on exploiting polarimetric diversity to mitigate the effect of interferences in [FM](#)-based commensal radar [91]. It was shown that by non-coherently combining [ARD](#) maps from surveillance antennas with both polarisations, better detection gains could be achieved both due to suppression of signal interference and due to the fluctuation of the polarisation of the skin echo from the target of interest. Polarisation of the reference antenna was found to have minimal effect on the radar performance.

In 2010 Colone published a method for suppressing ambiguous peaks in the [CAF](#) of the [WiMAX](#) signal [41]. The method is derived from that of the [DVB-T](#) treatment as [WiMAX](#) also makes use of [OFDM](#). The ambiguous peaks which result from the guard interval and pilot carriers could be effectively suppressed for all range bins, however, the resulting Doppler ambiguities' temporal separation between the integrated pulses resulted in a pair of non-zero Doppler peaks symmetric about zero. These peaks were however only found in the zero-delay range bin. Overall a [PSLR](#) of 35 dB could be obtained in the Doppler dimension.

In 2010 Gumiero published work on multistatic geometry optimization for target 3D positioning accuracy [92]. This work made use many transmitters in fairly close proximity (17 within a 50 km radius) and determined the best 3 bistatic

pairs formed with a single receiver site for 3D positioning. While the simulation did account for practical details such as keeping transmitters out of surveillance antenna main beams and keeping targets in the beams, the estimation of range resolution is perhaps idealistic in that it does not factor in the effect of bistatic angle (see Section 3.1.1, Equation 1.2). Furthermore, the assumed high density of transmitters is not always applicable in practice, at least in an African context. Another potential limitation of the optimisation is that it required that the chosen bistatic pairs be suitable for the entire simulation manoeuvre. While this simplifies the optimisation problem it does potentially limit the achievable performance as the optimal conditions can vary largely with target position.

In 2011 Gumiero followed up on the multistatic geometry optimisation work by running the data with actual transmitter positions and aircraft routes derived from ADS-B data [93].

In 2011 Colone published a paper investigating the feasibility of WiFi as an illumination signal of opportunity by analysing the ambiguity functions of the WiFi signals [94]. A subsequent paper presented the idea of using both DSSS and OFDM modulation of the WiFi signal for detection [61].

In 2011 Falcone published further work into sidelobe level control for WiFi, this time concentrating on suppression of sidelobes in the Doppler dimension [95]. The proposed commensal radar system makes use of the intermittent WiFi beacon as an effective pulse for a pulse-Doppler radar processing scheme. The problem with the beacons is that they are not transmitted at regular intervals which results in Doppler ambiguities. By using an “optimised Doppler weighting network” Falcone demonstrates that Doppler side lobes can be reduced by greater than 10 dB.

In 2011 Colone demonstrated ISAR based cross-range profiling with WiFi based commensal radar [96]. Targets are detected by conventional range/Doppler processing and the detection range is then used for ISAR processing. An auto-focussing algorithm is used to estimate the correct phase rotation rate before the ISAR processing is done. Results showed that dominant scatters can be distinguished down to sub-meter accuracy as was demonstrated by an experiment

with 2 cars moving $\frac{2}{3}$ of a metre apart.

In 2011 Colone published a paper that detailed the improvement in detection capability and accuracy in a **FM** based commensal radar system that exploited multiple **FM** channels concurrently [31]. The system, being an extension of Bongioanni's work in [20] produced range, Doppler and **DoA** similar to Howland's **FM** system [7], however the processing was done off-line. Using multiple channels showed notable improvements in **DoA** and detection capability. Multiple channel capability does however, require increased receiver complexity and the processing power required scales proportional to the number of channels.

In 2012 Colone published a review of the **WiFi** processing techniques developed at the University of Rome to date [97]. The paper also introduced a technique where the reference channel data could be synthesised from the surveillance channel thereby removing the necessity for a dedicated reference antenna and channel on the receiver. The synthesis was achieved by demodulating and remodulating the direct signal in the surveillance channel which reconstructs the **LoS** reference signal reasonably cleanly. A further note is that the carrier frequency offset between the receiver and the **WiFi AP** needs to be accounted for during the remodulation stage to maintain coherency during the matched filtering stage of the radar processing. This is done for both long term frequency drift but taking the average frequency difference over a full **CPI** and for shorter duration phase noise by averaging over shorter durations of data. The paper shows similar detection performance to the classic dedicated reference channel case for the presented test scenarios in the paper. Theoretically this technique should be applicable to any digitally modulated signal of opportunity that can be correctly demodulated.

In 2012 Falcone described an extension of the **ECA**-batches algorithm for application to the **WiFi** based **ISAR** processing for high resolution cross-range profiling [98]. A problem arises in the **ISAR** processing making use of cross range target motion. In the case of no down range motion, a zero Doppler shift of the target occurs. This means that the cancellation filter is likely to remove the contribution of the seemingly stationary target. The proposed solution by

Falcone is to generate the filter weights of the clutter scene when no targets are present and to re-use these weights continuously during radar operation. This means that only the contribution of the clutter will be cancelled and the target skin echoes should then be visible. The results show that the technique does in fact provide up to 15 dB of gain in the cross range profile, however it should be considered that the clutter contribution may vary with time due to effects such as temperature and variation in the illuminating signal. As a result the effectiveness of the cancellation filter may degrade with time, also potentially resulting in signal corruption. These effects are described in the [FM](#) broadcast band case in Section [3.3.1.1](#) of this document, specifically the blue curve in Figure [3.7](#) shows the divergence of the filter residual due to this phenomenon. It is however possible that the divergence could be less pronounced in the case of [WiFi](#) and this would need to be investigated.

Falcone published further work on [WiFi](#) based illumination in 2012 demonstrating the localisation of moving targets using a multistatic system. The experiment setup comprised of a 2 channel phased receiving array for [AoA](#) setup in a quasi-monostatic geometry with the transmitting antenna and another single antenna 20 m from the transmitting antenna. [99]. A vehicular target was then localised and tracked moving away from the antennas perpendicular to the baseline that they form. Using a Kalman filter Falcone reported positional standard deviations of 0.75 m for range only measurements and 0.49 m for range and [AoA](#) measurements. Falcone then went on to point out that the approach assumes that the variance of the different types of measures are the same which is not correct and so after implementation of a maximum likelihood estimator for the different measurements types, positional standard deviations of 0.49 m for range only measurements and 0.45 m for range and [AoA](#) were reported.

In 2012 Falcone published a paper “Potentialities and Challenges of WiFi-Based Passive Radar” [100] which summarises the combination of the sidelobe control techniques, [ISAR](#) processing and target tracking and localisation. The target localisation and tracking was done using 2 bistatic pairs and a Kalman filter. Targets’ motions were all in a straight line during the experiments. Complex target motion is likely to require substantial increase in complexity of the [ISAR](#)

2.1. RESEARCH BY UNIVERSITIES, RESEARCH INSTITUTIONS AND COMPANIES

processing. A description is given of the envisioned system, used in an indoor personnel and goods tracking system in a scenario such as airport security.

In 2012 Macera revisited the results of the multichannel [FM](#) band system in the context of ARGUS-3D (AiR GUiDance and Surveillance 3D) [101] which is a European Union funded project intended to improve [ATC](#) systems for civil applications. A multi-sensor system is described which incorporates existing primary surveillance radars, secondary surveillance radar, enhanced primary radars (such as being able to provide elevation), commensal radar networks, as well as other bistatic sensors. Some brief requirements are outlined before a review of the [FM](#) based commensal radar system results are described.

In 2013 Longelloti presented results of a [DVB-T](#) based system [32] which was able to show detection of aircraft as well as detection of ground based vehicular targets moving along a nearby road.

In 2013 Macera presented the design of a receiver architecture for 3 signal standards namely, [FM](#) broadcast band, [DVB-T](#) and [WiFi](#) [102]. The work discussed several front end designs and presented the optimal choice for each signal standard. The front ends are then switched into a common digital backend. The paper also presented results for [FM](#) and [WiFi](#) based deployments using the receiver.

In 2013 Colone published further results on their [FM](#) based multichannel and [AoA](#) work. 2 papers were published, the first of which addressed combination of the [ARD](#) data for obtaining better [CFAR](#) detection [103] and the second [104] presented combination of the of the [AoA](#) estimation for each [FM](#) channel to improve that measurement.

2.1.4 University of Pisa

In 2009 Petri presented an evaluation of the suitability of the universal mobile telecommunications system ([UMTS](#)) signal for commensal radar by analysing the ambiguity function [105]. It was shown that the wide bandwidth of the signal

2.1. RESEARCH BY UNIVERSITIES, RESEARCH INSTITUTIONS AND COMPANIES

yields good range resolutions however sidelobe reduction techniques will likely be needed and the typically low radiation power of cellular base stations may limit target detection ranges and sizes.

In 2010 Berizzi described the design of a multiband commensal radar system capable of exploiting both [DVB-T](#) and [UMTS](#) signals by making use of [USRP](#) boards [106]. The design proposed a configuration which allowed for control of the hardware to in turn exploit both signal types concurrently or independently and also to survey a common region or separate regions. Demonstrations of ambiguity functions of the recorded data and radar detection of a bus travelling down a road are also presented.

In 2010 Conti presented simulation work on high resolution commensal radar based on [DVB-T](#) signals [64]. Range profiles were produced with simulated data showing how 4 channels could be used to improve the range resolution of the radar when a wide band receiver is used that is capable of digitising 4 adjacent [DVB-T](#) channels. Alternatively 4 narrow band receivers can be used to digitise the channels separately. This, however, requires wideband reconstruction similar to the work of Olsen [79, 83, 84]

In 2011 Conti published results on ambiguity function sidelobe mitigation for a multichannel [DVB-T](#) based system. Some real world measurements were done and demonstrated that target detection was possible using the scheme.

In 2011 Petri (then affiliated with the RaSS National Laboratory, CNIT) demonstrated a further practical implementation of Conti's multi-[DVB-T](#) channel investigation. 3 adjacent channels were digitised with a [USRP-2](#) board. A preprocessing stage was run on the data to suppress ambiguities caused by the [OFDM](#) modulation and the target detection of a commercial airliner was demonstrated. When comparing the range/Doppler maps of single channel data to the 3 channel data it is evident that improved range resolution produced by the multiple channels creates a visible range profile of the aircraft [23].

In 2012 Olivadese demonstrated first by simulation [107] and then in practice [108] [ISAR](#) imaging of large sea targets. The technique made use of multiple

adjacent [DVB-T](#) channels again to achieve higher range resolution and a specially developed algorithm for focussing the images. The results showed that imaging was possible however the bandwidth was still a limiting factor when comparing results to purpose built active imaging radars.

In 2012 Petri presented on use of the Batches (or [FMCW](#)-like algorithm) for [CAF](#) calculation [109]. It is stated that a 96% speedup can be achieved over other [CAF](#) calculation methods which is on par with what is evaluated in this thesis as described in Section 3.3.2.3. The losses that the algorithm suffers at high Doppler shifts when the batch lengths are long are discussed and it is shown that to avoid this the batch length in seconds times the maximum Doppler shift in Hertz should be much less than unity.

In 2013 Olivadese presented a more detailed report on the [ISAR](#) work [110]. Additions including a heuristic method for mitigating the grating lobes caused by gaps between adjacent [DVB-T](#) channels that are being exploited. Further imaging results of both ships and aircraft are presented.

2.1.5 Warsaw University of Technology

The Warsaw University of Technology has produced a large amount of literature related to aircraft detection. There is a variety of work published on many aspects of commensal radars systems for this purpose exploiting mainly [DVB-T](#) and [FM](#) broadcast band signals.

In 2006 Malanowski reported on some common filtering techniques to serve as [DPI](#) and clutter suppression algorithms for commensal radar [13]. The least mean squares, recursive least squares, normalised least mean squares and least mean lattice predictor were reviewed. It was found that the least mean lattice predictor algorithm was optimal, displaying the fast convergence speed of the recursive least squares algorithm but at lower computation cost.

In 2006 Kulpa described stretch processing applied to commensal radar to allow for long integration times [111]. This allows for maximum processing gain to be

achieved without suffering from the effects of range walk.

In 2008 Malanowski presented an analysis of integration gain and its relation to integration time [112]. It was shown that integration gain can be lost due to both fast targets which can be rectified with time stretching and target manoeuvres which can be rectified by implementing an appropriate motion model in the matched filter. Some investigation into target fluctuations were also presented which might serve as an indication of how much integration time can be used.

In 2009 Szumski presented a comparison of commensal radar processing stages on CPU, GPU and the cell processor in the Playstation 3 [10]. It was shown that stages of beam steering, DPI and clutter suppression, CAF calculation, CFAR and final target extraction could be performed in real-time on all platforms. The processing dimensions were, however, not presented other than to say that the CPI is 250000 samples. It is therefore hard to gauge the significance of these results.

In 2011 Malanowski reported on a method for "Extending the integration time in DVB-T-based commensal radar while without incurring range and Doppler walk" [24]. This is achieved by applying both time stretching and an acceleration component to the CAF function. Both simulation and real world results show that by using the technique additional processing gain is achievable.

In 2011 Krysiak reported on the detection of ground moving targets with GSM signals as illumination [113]. A simple demonstrator system was set up to capture a reference signal of a GSM channel and surveillance region covering a street when a high volume of traffic is present. Given that the scenario was encapsulated in the first range bin, the Doppler processing could be done with a single FFT. The DPI and clutter cancellation was, however, performed until the 10th range bin to adequately suppress multipath.

In 2011 Kulpa described a moving platform system [43] where FM based experiments are carried out with a receiver mounted on both a car and an aircraft. A target detection was made from the car data using an adaptive filter to cancel range and Doppler sections however it was concluded that a more advanced

2.1. RESEARCH BY UNIVERSITIES, RESEARCH INSTITUTIONS AND COMPANIES

space time adaptive processing ([STAP](#)) -like algorithm would be necessary for the aircraft based receiver due to the high Doppler shift of the clutter.

In 2012 Malanowski published work on 3 dimensional target localisation in a multistatic commensal radar system [28]. Specifically two methods were dealt with namely the spherical intersection and spherical interpolation, both derived from time difference of arrival localisation techniques. It was found by Monte-Carlo simulation and real world data that the spherical intersection method is more accurate for the commensal radar application.

In 2012 Krysik published further [GSM](#) based results, showing that fast moving air targets in the form of fighter jets could be detected at distances of 10 km [114].

In 2012 Malanowski reported on the Passive Radar Demonstrator (PaRaDe) system results from a military exercise where both fast manoeuvring fighter jets and commercial civilian airlines were detected [115]. The results showed satisfactory detection capability, range and parameter estimation accuracy. A high-level overview of the real-time processing scheme is also presented.

In 2012 Malanowski presented a study into long range FM-based commensal radar [19]. It was shown that the PaRaDe demonstrator is capable of detecting large airliners at a bistatic range of 630 km with a 60 kW transmitter.

In 2012 Dawidowicz presented results on a multichannel (that is receiver channel) airborne system for detecting moving targets. [44]. [STAP](#) techniques were demonstrated in simulation with [DVB-T](#) signal and displacement phase centre antenna (DPCA) was demonstrated in practice using a 2 channel [FM](#) based system. The authors recommend the use of [DVB-T](#) in future as it allows for smaller antennas and the use of [STAP](#) processing. An overview of the DCPA technique was also published [45].

In 2013 Kulpa presented a study on wind farm interference with [DVB-T](#) based commensal radar [116]. A basic model was developed to simulate the effects and this was compared to actual measurements. A range/Doppler mask was proposed as an initial step to counter false targets, given the high Doppler resolution obtainable with commensal radar.

2.1.6 University of Cape Town

The University of Cape Town has produced an array of research into the field of commensal radar. Aside from the papers directly related to the research presented in this thesis (which are listed in Section 1.4.2) the following are also relevant to field of commensal radar.

In 2007 Morrison presented simulation work of target tracking based on [AoA](#) and Doppler measurements making use of the Gauss-Newton tracking filter [30].

In 2009 Paichard presented on the design of a multistatic commensal radar system [117].

In 2009 Lange presented on the development of a performance prediction and planning tool for networked commensal radar systems based on propagation modelling determined using the AREPS software [118, 119].

In 2010 Heunis's work at [UCT](#) [9] [120] detailed the design of a [FM](#) commensal radar using open-source tools. The work showed that detections could be made using low cost [TV](#) tuner boards on a [USRP-1](#) platform. The low dynamic range of the [TV](#) tuners coupled with oscillator drift between channels was found to degrade the sensitivity of the system. Heunis also performed an analyses of [DPI](#) and clutter suppression algorithms and found [ECA](#)[2] to yield superior results.

In 2010 Inggis presented a discussion on commensal radar as a potential form of cognitive radar [121, 122].

In 2010 Tsai presented on the design of a circular antenna array for null placement to reduce [DPI](#) in the surveillance channel [123].

In 2011 Han published work relating to the prediction of the performance of MIMO based commensal radar [124, 125, 126].

Brooker developed a netted radar simulator called [FERS](#) which is able to coherently simulate a multitude of radar scenarios at the signal level [3, 127, 128, 4].

Sandenbergh presented work on development of low cost common view [GPSDO](#) oscillators for the synchronisation of netted radar systems [129, 130].

2.1. RESEARCH BY UNIVERSITIES, RESEARCH INSTITUTIONS AND COMPANIES

Nadjiasngar presented work on tracking filter development mainly incorporating the Gauss-Newton tracking filter [131, 132, 133, 53].

2.1.7 SONDRA Supelec

Pisane (also affiliated with the University of Liège) presented target classification work based VHF Omni-range (VOR) transmitters. A system was built that was able to log target RCS responses along with the target position and aspect derived from ADS-B data. Once a large database of this data as assembled it could be used to classify targets with an average accuracy of up to $\sim 82\%$ [134, 135]

2.1.8 SELEX

In 2009 Anastasio described a procedure for optimal receiver positioning in multistatic commensal radar [136]. Assuming 2D space, with 2 transmitters and 1 receiver in the system, the process first specifies functional regions where the surveillance antenna has a target manoeuvre in its main beam, the exploited transmitters in its back lobe and target not near the bistatic baselines. The Cramer-Rao Lower Bound was then used to optimise for geometric dilution of precision (GDOP). This work is more appropriate in Europe where there is higher transmitter density. In a South African context there are likely to be few (often only 1) transmitter(s) and optimisation for multiple receiver sites needs to be performed. This has been investigated at UCT [53, 66].

In 2010 Anastasio extended the work to include a probability of detection less than unity [137]. This was done using the enumeration method. It was noted that the processing requirements for this are quite high.

2.1.9 Fraunhofer FHR

In 2011 Kuschel presented a multi-frequency system for medium range air surveillance [138]. The system composed of receiver capability for FM, DAB and

[DVB-T](#), with [FM](#) providing the long distance cover, [DVB-T](#) provided shorter distance but higher resolution coverage and the [DAB](#) provide also short range coverage but with better coverage at higher elevations. The system makes use of a track before detection scheme where the [FM](#) stage queues detection of targets for the other 2 stages. This multi-stage tracking also allows for extended integration times based on target state estimates.

In 2012 O'Hagan elaborated on the system and performance [33]. It was pointed out that there is much about the behaviour of bistatic radar that is not as fully understood as that of monostatic radar, for example clutter. Resolution and integration considerations are presented as well as points about single and multiple frequency broadcast networks. Signal processing is discussed, notably the use of reconstruction of the reference channel to remove multipath and potentially the need for [DPI](#) and clutter suppression altogether. A planning tool is also presented and finally some pointers on military utility.

2.1.10 Airbus (formerly known as Cassidian)

In 2010 Shroeder presented the concept of Cassidian's multi-band system along with some initial results [139]. As with Fraunhofer's multi-band system, the Cassidian system is able to exploit [FM](#), [DAB](#) and [DVB-T](#). Detection results for each signal type are presented against truth data. Visualisation software for the results is also described.

In 2011 Shroeder reported on upgrades to the system which included several integration steps [34]. The antennas for the different bands were integrated into a single multi-level structure. All 3 bands can be processed in real-time concurrently and the system equipment was installed into a van with a retractable arm on the roof that raises the antenna for quick mobile deployment. A mission planning tool was also added to the software. In 2012 more results were published about the system's detection performance by Schroeder [140]

Edrich presented more work with the system in 2012 [141] and 2013 [142]. New detections were included such as that of small aircraft. Schroeder also presented

more results in 2013 [143].

2.1.11 Defence Science and Technology Organisation (DSTO), Australia

In 2004 Van Cao presented a [CFAR](#) algorithm called the switching [CFAR](#) [144]. The algorithm compares the number of reference cells that are greater and smaller than the cell under test and for a certain minimum value of cells smaller than the cell under test, the thresholding is done only against the cells larger than the cell under test, thus reducing the false alarm rate. This filter is shown to outperform [CA-CFAR](#), [SO-CFAR](#), [GO-CFAR](#) and [OS-CFAR](#) in non-homogeneous environments and is no worse than [CA-CFAR](#) in homogeneous environments.

In 2008 Fabrizio (in collaboration with the University of Rome) demonstrated HF Band commensal radar [145], using an L shaped antenna array which could be steered both in elevation and azimuth. The detection of a co-operative aircraft was demonstrated. The signal processing required adaptive beam forming to locate the target with sufficient [SNR](#) and [SIR](#). This work was extended to further investigate adaptive beam steering techniques [146]. It was found that although performance improvements were obtained, the system was not necessarily able to run at an operational standard.

In 2009 Palmer presented a demonstrator that makes use of a geosynchronous satellite illuminator which provides television, audio and communications broadcasts [47]. The paper provides some theory about detection capability followed by the design details of the receiver hardware and then goes on to present detection results of a truck, a train and an aircraft using the receiver equipment. A comparison of [CPI](#) vs. [SNR](#) is also presented.

In 2010 Harms (specifically from Princeton University) presented a review of the [DVB-T](#) structure specifically the variation used in Australia [62]. An improvement over the existing 2k-subcarrier mode [DVB-T](#) conditioning filter which removes ambiguities was presented that can be applied to 8k-subcarrier modes of the signal.

In 2010 Searle (specifically from the University of Melbourne) presented on a technique for remodulating the [DVB-T](#) signal to reduce ambiguities inherent in the signal ambiguity function [50]. The technique was shown to be effective for applications such as reducing pilot carrier power. It was pointed out that a challenge that arises is to maintain coherency in the matched filter process when the signal clocks of the transmitter and receiver drift relatively. This needs to be accounted for in the remodulation.

In 2010 Van Cao published another investigation into [CFAR](#) filter performance comparing theoretical and experimental performance of [CA-CFAR](#), [SO-CFAR](#), [GO-CFAR](#), [OS-CFAR](#), [CCA-CFAR](#) and a mean-to-mean ratio (MMR) based [CFAR](#). It was shown that when using data sets from DSTO's [DVB-T](#) based experimental system, the [CA-CFAR](#) algorithm gave the most similar performance to the theoretical prediction, while the [SO-CFAR](#) produced the highest mismatch to the theoretical prediction. In conclusion Van Cao stated, "[CFAR](#) algorithms that have higher [CFAR](#) detection losses in a homogeneous environment will have larger theory-experiment false alarm mismatches, especially at smaller false alarm rates and larger [CFAR](#) window sizes."

In 2012 Palmer presented a review of algorithms for [DPI](#) and clutter suppression [15]. Specifically, the Wiener-Hopf, steepest descent, conjugate gradient (which is the algorithm selected for use in this thesis), least mean squares, recursive least squares and Euclidean direction search.

2.1.12 Nanyang Technological University, Singapore

In 2003 Tan provided an analysis into [GSM](#) signals from cellphone basestations for commensal radar [36]. It was noted that ambiguities exist in range at multiples of approximately 80 km, however, with a transmit power of less than 50 W this is further from the transmitter than detections are likely to occur. Ambiguities also exist in Doppler at multiples of 1700 Hz. Once again this translates to velocity components far greater than what is likely to be measured from targets within the radiation pattern. The ambiguities are therefore, for practical pur-

poses not a problem. The paper goes on to explain that the low bandwidth of the communication channels result in a very poor range resolution and preference is therefore to use the Doppler shift to extract target information as is the case with FM. The researchers also describe a design for a receiver for a system in [147]. Target detections are obtained with the system at low bi-static ranges. Given the range resolution of the system (approximately 1.8 km) the targets fall into the 0 range bin and only Doppler information is available.

Tan also published results on sea and air moving targets with GSM [37] in 2005 and showed target detections of 1 and 3 km respectively.

In 2007 Lu published results on a multi-channel (that is multi-receiver channel) tracking system for GSM based system [148] which had 4 antennas and produces improved detection ranges of up to 6 km for commercial airliners.

2.2 Commercially Available Systems

There is little documentation published on commercial commensal radar systems and this is typical due to military considerations. The following systems are known to be available or have been available:

Silent Sentry, originally developed by IBM and now by Lockheed Martin. In its 3rd revision the system consists of a single receive station that can make use of up to 6 spatially separated transmitters. The system can process FM radio channels in real-time to track aircraft in 2D or missile launches in 3D. The system can also use analogue television channels however due to the required throughput the processing cannot be performed in real-time. The range capability is reported as being 100-150km [6]

A joint development between Thales and French Aerospace Lab (ONERA) produce a seemingly similar system called the Home Alerter (HA) 100. The receiver site consists of a single circular array antenna. Information available about this system is minimal but a press release on Thales' website [149] states system has a detection range of 100 km for low and medium altitude aircraft.

Roke Radar, in collaboration with BAE Systems have developed a system called CELLDAR which exploits cellular base stations.

2.3 Conclusions

As is clearly evident from the vast amount of literature presented in this chapter than there is an ever growing interest in commensal radar technology especially from universities and research institutions. There is also a vast diversity of approaches and applications which is encouraging to note. Useful detection performance has been proven using a variety of illuminating signals and so it is likely that efforts in the next decade will shift towards data fusion and tracking domains. It is unfortunate that the only systems that have made it to product have been for military use and nothing as yet appeared specifically for air traffic control. This likely attributable to a fact that O'Hagan points out in that there are several factors to commensal radar systems that are still not well understood (e.g. bistatic clutter) [33] and this will need to change before the aviation industry is likely to embrace the technology.

Chapter 3

Processing Chain Implementation

This chapter details the design and implementation of a real-time processing chain for commensal radar based on commercial, off the shelf (COTS) general computing hardware consisting of multi-core central processing units (CPUs) and graphics processor units (GPUs), the latter of which should be capable of general-purpose GPU (GP-GPU) processing.

3.1 Introduction

There have been a number of works published about processing algorithms [2, 12, 15, 87] and real-time processing techniques [10, 150, 7] in the open literature, however, very few of these (e.g. the work by Howland [7], or the PaRaDe system at the Warsaw University of Technology [115]) make direct reference to a complete integrated processing chain that can accept data from a digital receiver front-end on the fly, process it appropriately and provide insightful visual output in real-time. In these cases, only a reference to the functional system is provided and specific design details are not presented.

3.1. INTRODUCTION

The most significant presentation of a real-time processing solution was that of Howland which was published some 9 years prior to the writing of this thesis, Howland used a cluster of six 2.6 GHz Pentium-4 computers that allowed for an update rate of 5 s when processing 1 s of data. It should be noted that this system used 2 surveillance channels to allow for angle of arrival estimation and therefore essentially had 2 signal processing chains in parallel. A further point that is to be noted is that processor speeds have plateaued in the last decade peaking at around 3.2 GHz and now often reverting back to around 2.2 GHz in order to reduce power consumption. Multiple cores are then included in the physical processor package to run instructions in parallel. With typical CPUs having 4 to 8 cores it is fair to assume that a Pentium 4 cluster of 6 machines will have similar computing power to a current multicore CPU but with significantly less inter-processor overhead as this does not require a local area network (LAN) connection. Comparing the required workload of Howland's processing chain to what is required at present, the current system requires that it be able to process 4 s of data in less than 4 s and ideally in much less than 4 seconds per illuminating channel as applications include angle of arrival and processing multiple illuminating channels over the same CPI [7, 31] and this may need to be done sequentially due to memory limitations. It is shown in this chapter that these memory limitations are often the limiting factor with GPU implementation. Functional ranges of commensal radar have been proven to be in excess of 600 km [19] which requires approximately double the amount of correlation to what Howland demonstrated and therefore an equivalent increase in processing throughput. A more powerful processing solution is therefore required. The solution should ideally be small and light and relatively low power to facilitate mobile deployments. As such, clusters of computers are not practical.

Radar signal processing can typically be implemented on a variety of architectures including ASICs, FPGAs, DSPs, x86 derivative CPUs or accelerator cards which are typically peripheral to x86 derivative CPUs. ASICs, FPGAs, DSPs tend to be highly costly and complicated to develop for, requiring high levels of customisation which is not easily realisable in a university environment which makes up a large contingent of the commensal radar development community,

3.1. INTRODUCTION

although a resurgence of interest in the technology has seen an ever increasing uptake by both industry and research institutions in recent years. The [x86](#) and derivative architectures as well as the accelerator cards for [x86](#) are expectedly cheaper given high market penetration of the desktop computing form factor. The [x86](#) and derivative architectures can be classified into 3 relevant categories. These are listed as follows with typical specifications at the time of writing.

- Standalone multicore desktop machines that typically have up to 8 [CPU](#) cores.
- Server computing nodes that have 16 to 32 cores often having multi-CPU-socket motherboards allowing for multiple physical [CPU](#) packages.
- Compute clusters that are a network of either of the previous 2 variations, typically the latter, along with suitable libraries to parallelise jobs across the cluster.

Standalone multicore desktop machines tend to be an order of magnitude more cost effective than server computing nodes when comparing cost per [CPU](#) core, again due to higher market penetration by being aimed at the general public but also due to extended functionality of the server platforms such as error correcting memory, hardware redundancy and vendor support. It is however, acknowledged that some of these features may be applicable to a commercial single site commensal radar or in a configuration where all data is brought together centrally for processing.

Mobile platforms, equivalent to standalone multicore desktop machines, are of course another variation but these are not well suited to high performance computing due to design for low power operation and relative high cost per unit, especially for high end variations.

With regard to accelerator cards, [GPUs](#) tend to be the most cost effective for similar reasons to that of the desktop computing platforms. Accelerator cards at present have 3 significant competitors which are as follows.

3.1. INTRODUCTION

- NVIDIA's [CUDA](#) [151] capable [GPU](#)s providing [GP-GPU](#) capability.
- AMD's APP SDK [152] capable [GPU](#)s providing [GP-GPU](#) capability.
- Intel's Xeon Phi accelerator cards [153]

At present [CUDA](#) appears to be dominating the market share. NVIDIA offers a large set of [BLAS](#) libraries and [FFT](#) libraries for use with their [CUDA](#) capable hardware. AMD's APP SDK relies on the open standard OpenCL [154] which, at present offers a less comprehensive set of tools suitable for radar signal processing. Intel's Xeon Phi cards present an interesting architecture that appears to have more [x86](#) like processing elements in contrast to the [GPU](#)s which can only do the most simple arithmetic operations per processing element. Nonetheless the the Xeon Phi's appear, to date, to have seen limited uptake in radar related literature which is likely attributed to their relatively complicated architecture and higher cost of both hardware and software. There is also a limited range of hardware variations compared to the [GPU](#) options

It is therefore interesting to note that most of the significant literature on commensal radar signal processing schemes target desktop [x86](#) and/or [CUDA](#) capable [GPU](#) platforms. The processing chain presented in this thesis will follow the same trend. Typically desktop [x86](#) derivative hardware with [GPU](#) capability is cheap, can be constructed to have relatively low power requirements as well as weight and is often already available as existing computing infrastructure at any particular institution or organisation. Furthermore, development for multicore [CPU](#) and [CUDA](#) capable [GPU](#) can be done (relative to FPGA or cluster development for example) quickly and efficiently using available C and C++ libraries.

The research presented in this chapter seeks to provide a solution to the integrated real-time processing chain. The processing chain solution is intended for a prototype commensal radar system under development at [UCT](#) in collaboration with the Council for Scientific and Industrial Research (CSIR) and Peralex Electronics. The processing chain for the system under discussion includes stages from packetising of [IQ](#) data from the receiver, [DPI](#) and clutter suppression, range/Doppler processing, detection and finally visualisation of constant false

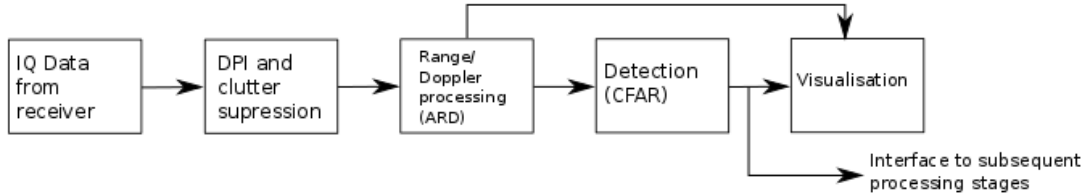


Figure 3.1: Flow diagram showing the stages included in the processing chain.

alarm rate (**CFAR**) and amplitude/range/Doppler (**ARD**) data. A flow diagram is presented in Figure 3.1. Interfacing is also provided to send **CFAR** data to subsequent processing stages i.e. tracking. Non-coherent fusion of **ARD** data from multiple **FM** broadcast channels in a common bistatic geometry is also discussed. The target hardware is any typical multi-core **x86**-derivative desktop **CPU** and 1 or more **CUDA** capable **NVIDIA GPU**s with a condition that the **GPU**s be of similar memory capacity when more than 1 is used. Similar memory sizes facilitates automatic scaling of processing across multiple **GPU** devices.

3.1.1 Radar System Overview

The prototype system [18] exploits commercial **FM** broadcast band broadcasts as an illuminating source for detecting aircraft. **FM** transmitters are typically high powered and sparsely spaced. This makes them ideal for long range detections of commercial airliners. The system is intended to make use of the Doppler information as far as possible in the tracking stage [53] given the potential high resolution of this quantity. Tracking on the Doppler information should help overcome the low bandwidth limitations with the correspondingly poor range resolution provided by the **FM** signal. Longer integration times allow for a high Doppler and equivalently velocity resolution (see Section 3.2.2 for a further description on resolutions).

The system typically makes use of a 4 s coherent processing interval (**CPI**) at a sample rate of 204.8 kSps. All data is obtained at 204.8 kSps in baseband IQ form from receiver hardware. All processing is done in single precision floating point arithmetic (32 bit floating point numbers) which are complex pairs for

3.1. INTRODUCTION

most of the arithmetic. Typical [CUDA](#) compatible [GPU](#)s can perform a single precision floating point operation in a single clock cycle per [CUDA](#) core. A floating point operation on a complex floating point number would therefore be a few sequential floating point operations with the components of the complex number.

The [CPI](#) and sample rate translate to 819200 samples in total per channel for the coherent processing. The 4 s provides a large amount integration gain and is empirically determined to be short enough to avoid problems such as maintaining coherence over the [CPI](#) and also Doppler and range walk. While longer durations are possible it might be deemed to create intolerable output latency from the system in the context of functions such as air-traffic control. It is argued that a [FM](#) based system for commercial aircraft detection should not exceed more than ~ 1.1 s of integration time due to acceleration, jerk and time stretching effects [[111](#), [112](#), [19](#), [33](#)], but these effects have rarely been seen to be detrimental to integration gain with [UCT](#)'s prototype radar, except for targets showing rapid bistatic acceleration e.g. crossing the bistatic baseline. This is likely attributed to the low bandwidth of the [FM](#) signal which is often far lower than the range cell width derived from the sample rate, and furthermore, the algorithm used for the range/Doppler processing makes use of an arithmetically optimal point-multiple/Fourier transform method as apposed to an approximate algorithm. This is discussed in more detail in Sections [3.3.2.5](#), [3.3.2.3](#) and [3.3.2.6](#). To further illustrate, Figure [3.2](#) shows a detection of a commercial airliner at long range (>400 km bistatic). A comparison between 1 and 4 s of integration time shows that 4 s provides more reliable detection and this has been shown to be consistent across many large datasets.

Furthermore, proportionally better Doppler resolution is provided which is important for the Doppler based tracking. It is noted that Figure [3.2](#) does not display the maximum possible bistatic range rate that could be observed for targets of this type, it is however quite typical. The integration time can of course be easily adapted depending on the priority of the target type to be detected and these effects would need to be investigated further in detail once a suitable tracking infrastructure is in place. The most simple solution would be to run

3.1. INTRODUCTION

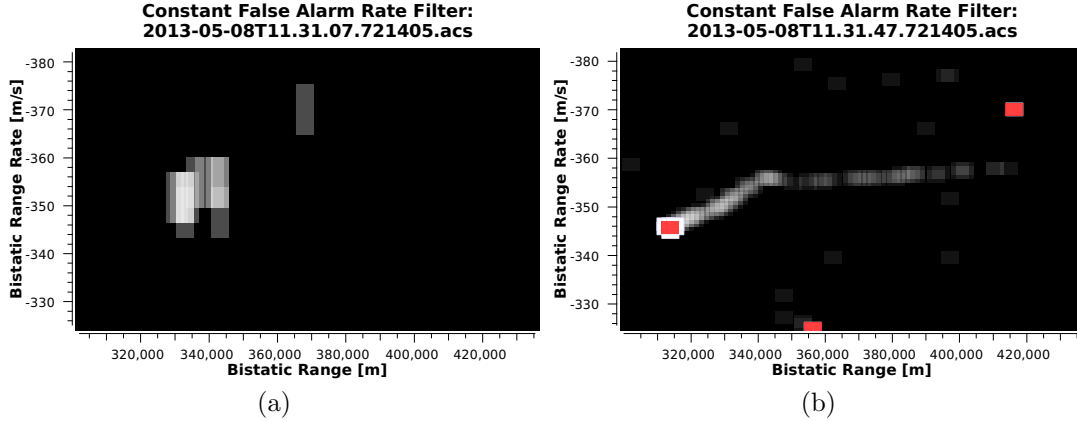


Figure 3.2: Comparison of integration times for FM based target detection using real data collected with the UCT prototype radar system. (a) shows a CFAR output over several CPIs from a 1 s integration time while (b) shows CFAR output over the same total time window using 4 s CPIs. It is clear that the longer CPI provides better integration gain and also proportionally better Doppler resolution.

The grey bins are detections of previous CPIs and therefore represent an artificial “phosphor” effect. This painting of these transparent bins is incremental so less transparent bins have had successive detections in past CPIs. Non-transparent white bins represent detected cells in the current CPI. A red cell shows the centroid of adjacent cells detected in the current CPI. This centroided cell is not bound to the resolution grid of the range Doppler plot and in the current implementation assumes that all component cells are equally weighted. This weighting for the centroid may need to be revised in the future when the system position accuracy is tested as well as how quantisation of CFAR cells will affect this accuracy. This CFAR map colour scheme is used throughout this document.

multiple CAF processors in parallel with different integration times.

Given that the FM broadcast transmitters are typically spaced far from one another (10s to 100s of km in South Africa), the system is envisioned to consist of few transmitter sites (often only 1) and a network of low cost receivers at multiple sites connected by a data network. It should be noted that each transmitter site will typically have a number of co-located transmitters operating at separate frequencies, and these can be used to mitigate against multipath due to different propagation characteristics of the different frequencies. Given a high

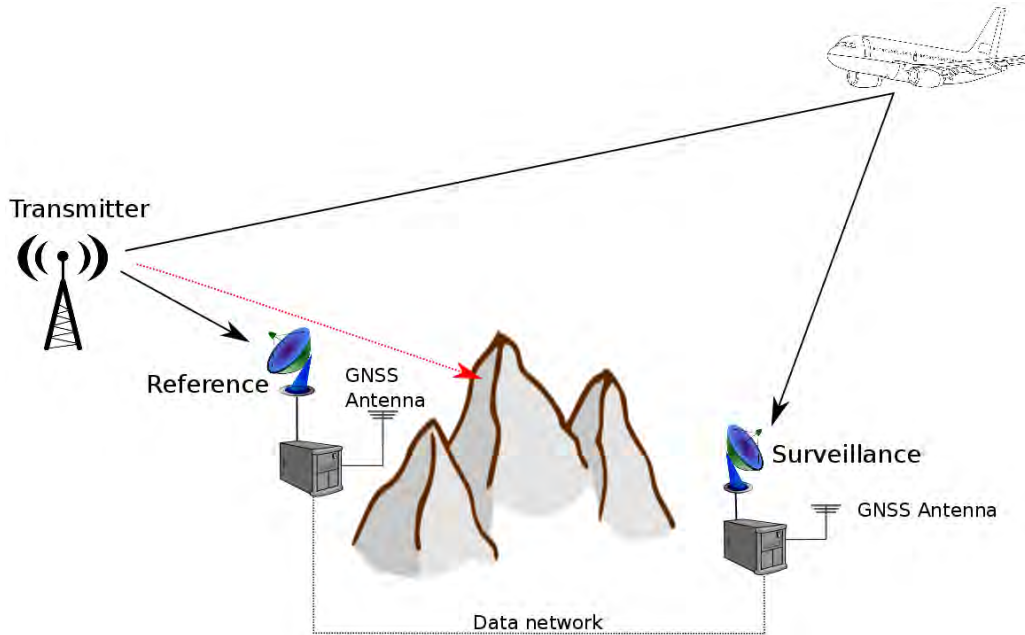


Figure 3.3: An illustration of the separated reference configuration. The reference and surveillance antennas and related digitisation hardware are located at different sites which allows the surveillance to be positioned such that DPI and clutter are at a minimum. The reference antenna is placed such that it has a direct and clean (multipath at a minimum) reference signal from the transmitter. Synchronicity is maintained by GNSS disciplined oscillators.

capacity data network capable of transporting sample data, the “separated reference” [16, 70] configuration can then also be implemented to further reduce receiver complexity and reduce DPI and multipath effects. An illustration of the separated reference configuration is depicted in Figure 3.3 and Chapter 4 presents further investigation into this concept.

This chapter is organised as follows. The computational challenges of DPI and clutter suppression, range/Doppler processing and detection stages are presented in Section 3.2. Section 3.3 presents the proposed solutions to these challenges as well as how the solutions are implemented and integrated into the larger radar system. An overview of non-coherent ARD fusion is presented when multiple frequencies are exploited in the same bistatic geometry. Finally timing results and conclusions are presented.

3.2 Background and Computational Challenges of the Processing Chain

This section provides some background and outlines the challenges faced for the 3 main signal processing stages of the system. These stages are **DPI** and clutter suppression, range/Doppler processing and finally, target detection.

3.2.1 Direct Path Interference and Clutter Supression

DPI and clutter are unwanted signals that occur in the surveillance channel of the commensal radar. **DPI** results from **LoS EM** radiation from the transmit antenna while clutter is produced by **EM** radiation reflected from objects in the surveillance scene that are not of interest. In a bistatic radar clutter can also be considered as multipath [155] of the **DPI**. Both of these phenomena typically result in much larger returns than those created by skin echoes from targets of interest which might include aircraft, spacecraft or other spacebourne bodies, land vehicles, sea or water based vessels and animals or humans. The result is that the targets of interested are masked by the larger returns or Doppler sidelobes of the returns produced by **DPI** and/or clutter and are therefore not detectable by the radar detection algorithm or the radar operator.

In order to be able to reduce **DPI** and clutter by means of **DSP** it is necessary to model the effects that these phenomena have on the signal channel in question as these effects cannot easily be measured directly. Both **DPI** and clutter can be represented in the surveillance channel as delayed, scaled versions of the reference signal added to the surveillance signal. This assumes that the reference signal undergoes only linear scaling as it travels through transmission cables, antennas and air (or free space) on its path to the **ADC** of the surveillance channel in the receiver node. This can be approximated to be true for most practical purposes where the transmitter and receiver are stationary relative to the clutter and to one another and as such the surveillance channel subject to **DPI** and clutter can

3.2. BACKGROUND AND COMPUTATIONAL CHALLENGES OF THE PROCESSING CHAIN

be described by Equation 3.1 [15].

$$\mathbf{s}_s(n) = \mathbf{s}_e(n) + \mathbf{s}_i(n) \quad (3.1)$$

$$\mathbf{s}_{im}(n) = A\mathbf{x} \quad (3.2)$$

$$\mathbf{s}_{im}(n) \approx \mathbf{s}_i(n) \quad (3.3)$$

$$n \in [0, CPI_{size}) \quad (3.4)$$

From Equation 3.1, $\mathbf{s}_s(n)$ is the surveillance signal as digitised by the ADC, $\mathbf{s}_e(n)$ is the reflection from any targets in the scene i.e. the signal(s) of interest and $\mathbf{s}_i(n)$ is the interference component caused by DPI and clutter which masks $\mathbf{s}_e(n)$. Furthermore an estimated model of this interference shown in matrix form in Equation 3.2, $\mathbf{s}_{im}(n)$, the model of the DPI and clutter component, is a sum of vectors representing the DPI and clutter energy at discrete bistatic range bins. A is a matrix which is made up of these vectors and as such contains in each column, a zero padded (from the top of the column) version of reference signal where the number of padded zeros corresponds to a number of sample delays and therefore clutter source(s) at the bistatic range bin corresponding to that total delay. Given that these are complete sample delays they are in phase with the signal that the matched filter would detect and can therefore be used to effectively modify the the matched filter surface (e.g. remove zero Doppler components). Equation 3.3 shows that this estimation approximates the actually interference contained in the digitised surveillance signal. Note that these clutter sources could hypothetically lie anywhere on the constant bistatic range contour, which is an ellipsoid in 3-space although the sources will likely occur at ground (or sea) level. Figure 3.4 demonstrates how clutter returns at a given bistatic range can come from different directions simultaneously. \mathbf{x} represents a vector in which each element scales a corresponding column of A .

3.2. BACKGROUND AND COMPUTATIONAL CHALLENGES OF THE PROCESSING CHAIN

So in summary, the product of each respective A column and the corresponding element of \mathbf{x} therefore represents interference contributions for the bistatic range bin corresponding to the delay produced by the number of zeros padding that A column. As described by Equation 3.4 n , the discrete sample index covers the length of the CPI in question.

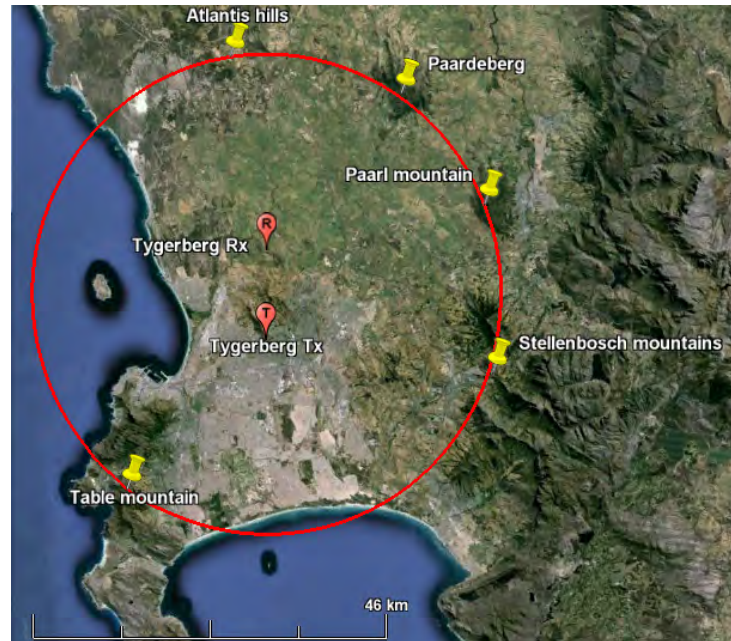
The scaling provided by \mathbf{x} , which is relative to the complex envelope of the captured reference signal, which in turn, makes up the columns of A , is the result of several physical phenomena that include the combined radar cross section (RCS) of all clutter sources occurring at the bistatic range bin of the respective column, the free space loss corresponding to that bistatic range and the effect of antenna gain patterns for that bistatic geometry.

As per matrix/vector multiplication, the columns of A are scaled and summed to form $\mathbf{s}_{im}(n)$ in Equation 3.2. All vectors (which are indicated by bold face symbols) are column vectors.

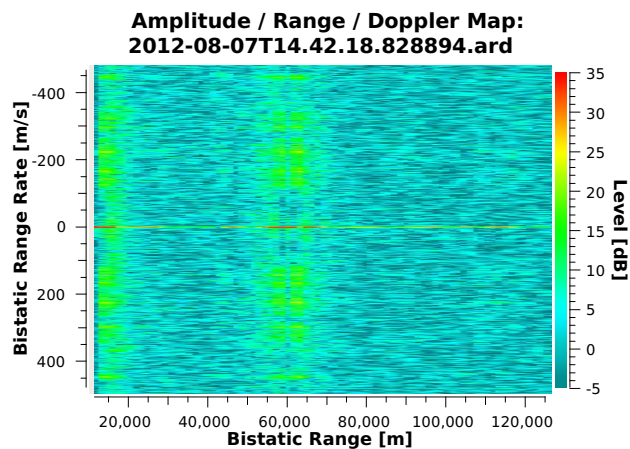
One of the columns of A will also represent the contribution of DPI which is the reference signal from the illuminator directly impinging on the surveillance antenna. For both reference and surveillance antennas located in the same position, this will be the zero delay version of the reference signal i.e. no zero padding. This is likely to be the largest contribution to the surveillance channel as it is a direct antenna to antenna path.

The matched filtering stage used to calculate the cross ambiguity function (see Section 3.2.2) can provide large processing gains. The integration gain will however also apply to clutter and DPI sources as they typically remain coherent as well. The resulting sidelobes of these typically large peaks will therefore often mask targets of interest. It is therefore necessary to remove as much of the DPI and clutter signal as possible in order to detect the relatively small skin echoes from targets of interest. Large clutter at zero Doppler creates sidelobes in the range/Doppler processing that mask even moving targets which exist at large Doppler shifts. Figure 3.5 shows how clutter sidelobes can mask targets that then become visible when the clutter is suppressed. Direct path interference and clutter suppression are the signal processing techniques that are necessary to

3.2. BACKGROUND AND COMPUTATIONAL CHALLENGES OF THE PROCESSING CHAIN



(a)



(b)

Figure 3.4: The effects of multiple clutter sources occurring at the same bistatic range. (a) Shows a constant bistatic range contour of 60 km where it intersects with the ground for a bistatic deployment in the Western Cape of South Africa. ‘T’ and ‘R’ mark the transmitter and receiver sites respectively and the thumbtacks indicate major mountain structures occurring on the 60 km contour. (b) Shows an **ARD** map of a **CAF** generated with data from this configuration where no **DPI** and clutter suppression is performed. A very strong peak can be seen at 60 km bistatic range and 0 ms^{-1} range rate. This peak is a cumulative effect of energy reflected by all the clutter occurring along the 60 km contour. Sidelobes formed by the Doppler processing are also present and are likely to mask nearby targets of interest.

3.2. BACKGROUND AND COMPUTATIONAL CHALLENGES OF THE PROCESSING CHAIN

do this. Given that both **DPI** and clutter can be represented by the model in Equation 3.2 concurrently, they can be removed by the same process.

It should be apparent that the signal processing operation necessary to remove the interference component from the surveillance channel is to subtract $\mathbf{s}_i(n)$ from the surveillance signal $\mathbf{s}_s(n)$ which (ideally) will leave only the target echoes. To produce and estimate of $\mathbf{s}_i(n)$, namely $\mathbf{s}_{im}(n)$ the matrix A can be constructed by building a matrix out of the recorded reference signal and zero padding according to each bistatic range bin for which it is desirable to suppress **DPI** or clutter. All that is required then is an estimate of \mathbf{x} . If we consider that $\mathbf{s}_i(n)$ contains the majority of energy in Equation 3.1 we can set $\mathbf{b} = \mathbf{s}_s(n)$, i.e. the recorded surveillance signal, and solve the familiar matrix equation $A\mathbf{x} = \mathbf{b}$ to obtain the correctly scaled estimate $\mathbf{s}_{im}(n)$.

The number of delays, which is equal the number of columns in the A matrix, will however, typically be less than the number of samples in the **CPI**, which is, in turn, the number of rows of A . A is, as such, not square and therefore not invertible and $A\mathbf{x} = \mathbf{b}$ is therefore not directly solvable. The solution is to minimise the residual $\|A\mathbf{x} - \mathbf{b}\|^2$ in a least squares sense [156, Ch. 21.2]. I.e.

$$\min(\|A\mathbf{x} - \mathbf{b}\|^2) \tag{3.5}$$

which will then remove as much interfering energy as possible from the surveillance channel.

It should be noted that the A matrix can also contain rows of synthetically Doppler shifted versions of the reference signal if returns at non-zero Doppler need to be suppressed. This can be used to suppress strong target returns after they have been detected that might mask weaker target returns in their side-lobes. Clutter spread into the first few Doppler bins can also be reduced in this manner [2]. Care should be taken here that targets of interest will not occur along the non-zero Doppler bins which are to be cancelled as they would be removed as well.

3.2. BACKGROUND AND COMPUTATIONAL CHALLENGES OF THE PROCESSING CHAIN

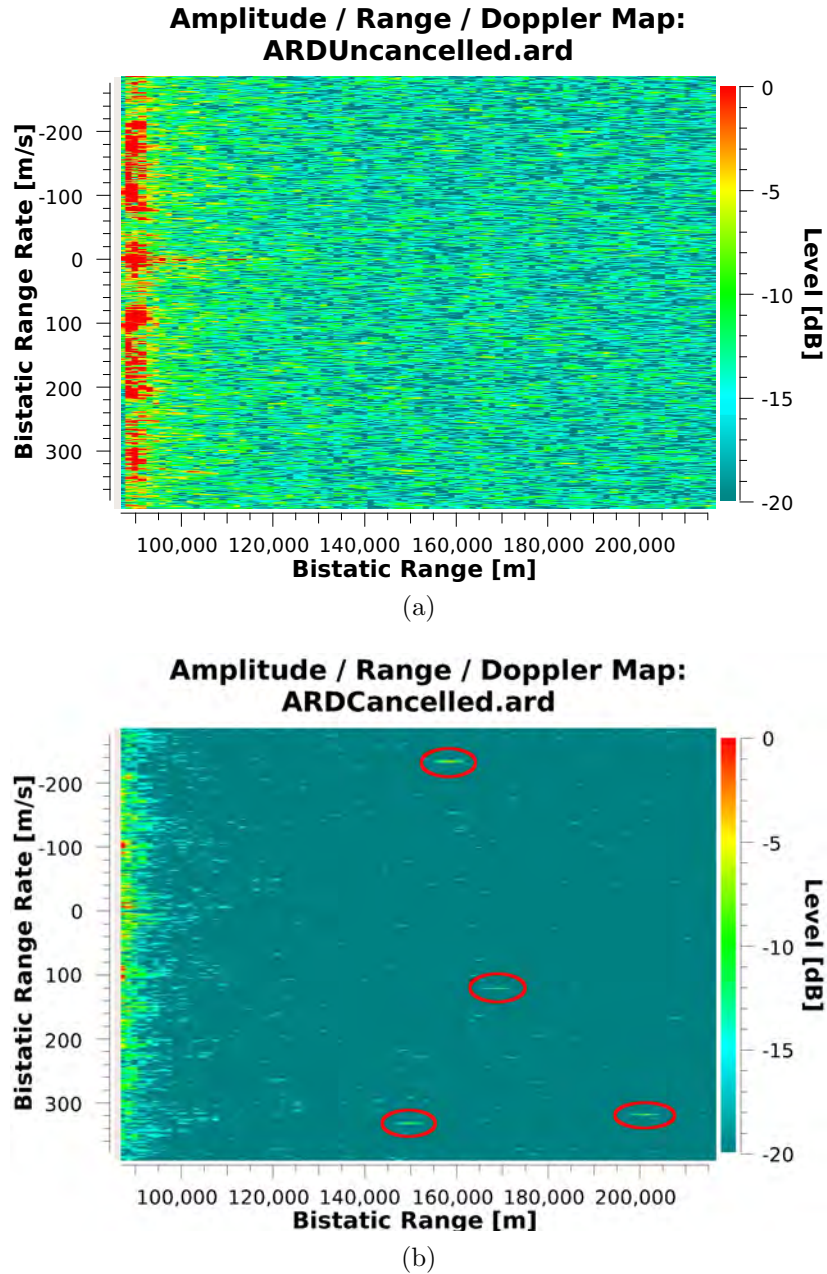


Figure 3.5: Illustration of clutter sidelobes masking a target of interest. Targets are not visible in (a) due to large **DPI** and clutter. Once clutter suppression has been run a targets becomes visible in (b) as shown by the red ellipses. Note also that the **DPI** and clutter ridge along 0 ms^{-1} in (a) is removed in (b) and replaced by a notch. The amplitude range has been reduced to clip just above the noise floor of (b) to better indicate targets but is the same for both maps. The data shown here is real data collected with the **UCT** prototype radar system.

Minimisation of the expression in Equation 3.5 can be a computationally challenging task in real-time due to the typically large size of the A matrix. Challenges therefore include both memory limitation of the processing hardware as well as arithmetic throughput.

3.2.2 Range Doppler Processing

The illuminators of opportunity that commensal radars typically exploit are invariably designed to illuminate large portions of the ground as this is where the human population and receiver equipment exist. Examples include FM broadcasts, DAB, analogue and digital variations of television from both terrestrial and space-borne transmitters, GNSS and GSM are all directed at large portions of the earth. While this will often translate to large potential coverage areas for the commensal radar it will also create large (mainly stationary) clutter returns from the terrain and man-made structures. As a result moving target indication (MTI), where moving objects are detected by projecting them into a different subspace to that of stationary clutter is essential for target detection. Aircraft, the targets of interest for UCT's prototype system, will invariably be moving targets and even helicopters which can hover and remain largely stationary have moving rotor blades which make MTI possible. Furthermore, Doppler processing can be performed which might be seen as an extension of MTI as it allows for velocity component values to be extracted along with detection of moving targets [157, Ch. 17]. Maasdorp demonstrates that the effects of rotor blade modulation are detectable and the rotation rate of the rotor measurable by commensal use of FM broadcast signals (with UCT's prototype system) on light aircraft [71].

The cross ambiguity function (CAF) provides a technique by which to perform Doppler processing [6, Ch 11.2.2.1] along with range processing. This is achieved by splitting the 2 dimensional returns of the radar signal in which amplitude varies only in time, into a 4 dimensional space where amplitude can vary in bistatic range, bistatic Doppler shift and time. This allows potential targets to be distinguishable from stationary clutter in the Doppler dimension and to be

3.2. BACKGROUND AND COMPUTATIONAL CHALLENGES OF THE PROCESSING CHAIN

positioned on a constant bistatic range contour in 3-space.

The CAF [27, Ch. 17.2] can be expressed for a given bistatic delay τ in seconds and a bistatic Doppler shift f_d in Hertz as

$$|\Psi(\tau, f_d)|^2 = \left| \int_{-\infty}^{\infty} \mathbf{s}_s(t) \mathbf{s}_r^*(t + \tau) e^{j2\pi f_d t} dt \right|^2 \quad (3.6)$$

where $\mathbf{s}_r(t)$ and $\mathbf{s}_s(t)$ are the reference and surveillance signals in continuous time respectively (* denotes complex conjugate). Note that the entire expression is squared to provide square-law detection.

More practically for a finite CPI in discrete time the CAF can be written as

$$|C(m, k)|^2 = \left| \sum_{n=0}^{N-1} \mathbf{s}_s(n) \mathbf{s}_r^*(n + m) e^{j2\pi kn/N_s} \right|^2 \quad (3.7)$$

Where m is the delay expressed as an integer number of sample periods, k is a discrete Doppler shift bin index and N_s is the length of the CPI in number of samples.

A slice of the CAF function, taken for a fixed delay (or equivalently bistatic range) is referred to as a range bin or range gate. Equivalently a slice for a fixed Doppler shift is referred to as a Doppler bin or gate. The Doppler quantity is directly proportional to the bistatic range rate (expressed in metres per second) which is often a more insightful scale for analysing bistatic radar data.

These range and Doppler bins will have a dimension determined by the resultant sample rate and coherent processing interval respectively. Specifically, the range bin size is determined by the sample rate of the data i.e $\Delta R_{bin} = \frac{c}{f_s}$ (where ΔR_{bin} is range bin size in metres, c is the speed of light in metres per second and f_s is the sample rate in Hertz). It should be noted that this is the width of discrete range bins on the ARD map surface. An actual peak in the data may span several bins depending on the signal content (see Section 1.1.3, specifically Equation 1.2

3.2. BACKGROUND AND COMPUTATIONAL CHALLENGES OF THE PROCESSING CHAIN

describing range resolution). The Doppler bin size is inversely proportional to the coherent processing interval, i.e $\Delta f_{d-bin} = \frac{1}{T_{CPI}}$ where Δf_{d-bin} is the Doppler bin size in Hertz and T_{CPI} is the coherent processing interval in seconds which will be an integer multiple of sample periods as it consists of an integer number of samples.

The discrete CAF data is plotted as an ARD map over the range and Doppler space of interest for analyse by the radar engineer. Otherwise it is fed into a detection stage to extract target range and Doppler co-ordinates before being passed to the subsequent tracking stages of the signal processing. When a single discrete range and Doppler pair are specified for the CAF, the resultant region is referred to as a *cell* of the ARD map.

For an FM broadcast based system for aircraft detection the CAF surface will consist (as an example) of approximately 280 range by 1601 Doppler bins. This translates to a bistatic range of approximately 400 km for a 204.8 KSps data rate and a bistatic range rate of -600 to 600 $m s^{-1}$ derived from the Doppler shift when the illuminating signal has a carrier frequency of 98 MHz. Note that bistatic range rate can be up to twice the target velocity which has a maximum in the order of 300 $m s^{-1}$ for commercial airliners. The reason for this doubling effect is that the range rate is the rate of change of the bistatic range. I.e. the sum of the transmitter-to-target and target-to-receiver distances. Other potential illuminating signals such as DVB-T have a similar total number of ARD cells comprised of a different range/Doppler ratio due to the wider signal bandwidth. This implies that more bins are necessary to describe the same range extent but less to describe the same Doppler extent. Practically however, DVB-T based systems are likely to have lower detection ranges due to greater propagation losses at the higher carrier frequencies, better control of the downward elevation patterns of the transmit energy and lower typical transmit powers.

Each cell of the CAF or ARD map is the output of a correlation shift producing a power level for a given delay and equivalent bistatic range bin. The correlation is performed over a full CPI length. This results in a challenging amount of arithmetic calculations which need to be done in real-time. Fortunately this

problem is highly parallelisable. Other techniques such as exploiting the fast Fourier transform (FFT) to reduce computation complexity are also exploited.

3.2.3 Detection

The detection stage involves extracting targets from the ARD map space. This is done by evaluating each cell according to some criterion and making a binary choice as to whether it is considered to be a target or not. An effective way of implementation uses the concept of CFAR filters which compare the the given cell, often referred to as the cell under test (CUT) to surrounding cells. The comparison for a positive detection is weighted optimistically such that, if the statistics of the background interference are known, a fixed percentage of false alarms (false positives) occur [158, Ch 5.7] [157, Ch 16.1]. This weighting provides a method by which the probability of detection can be tuned optimally by varying the probability of false alarm. It should be noted however, that while the probability of detection (P_d) and probability of false alarm (P_{fa}) are related they are not directly proportional so finding an optimal $P_d : P_{fa}$ ratio is not an easily tractable problem.

The computational requirements of this stage are negligible when compared to those of the prior 2 stages. Typical CFAR algorithms are highly parallelisable because each CUT can be independently evaluated.

3.3 Processing Design

This section presents solutions and implementation for the challenges outlined in Section 3.2. The aspects of designing the solution to integrate into the larger system are also discussed. In certain cases multiple solutions may exist and a comparison will be presented and the selection of the optimal solution discussed.

All stages of the processing chain are implemented in C++ making use of object orientation so that both data structures and processing algorithms can be

referred to as objects. Object orientation also allows for an inheritance hierarchy which is important for keeping different implementations of the processing chain standardised. Interpreted languages such as Matlab or Python may provide easy algorithm prototyping but are not suited for this sort of system design as they do not allow for the low level memory control that is necessary to maximise performance on the target hardware.

Data flow during online processing occurs from a socket connection to host memory to GPU device memory, back to host memory and finally out on another socket connection. One of the most important aspects of creating an effective processing pipeline is to minimise the number of memory copies during this pipeline path. It is the low level control provided by languages such as C++ that provide the means for optimising the data path.

3.3.1 Direct Path Interference and Clutter Supression

This section discusses algorithms for performing DPI and clutter suppression (a processing often referred to as *cancellation*). The selection, overview and implementation of the optimal algorithm is discussed along with how it fits into the larger software subsystem.

3.3.1.1 Algorithms

Many algorithms have been proposed for solving the DPI clutter problem outlined in Section 3.2.1 [87, 159, 7, 12, 13, 14, 2]. Most notably Palmer [15] presents a comparison of several algorithms from a computational standpoint which serves as a suitably relevant overview of suitable algorithms.

Colone [2] proposed using the least mean squares estimator [156, Ch. 21.2] to find a solution to Equation 3.5. The least mean squares estimator algorithm is shown in Equation 3.8

$$\mathbf{s}_{cs} = \mathbf{s}_s - \mathbf{Ax} = [\mathbf{I} - \mathbf{A}(\mathbf{A}^H \mathbf{A})^{-1} \mathbf{A}^H] \mathbf{s}_s \quad (3.8)$$

3.3. PROCESSING DESIGN

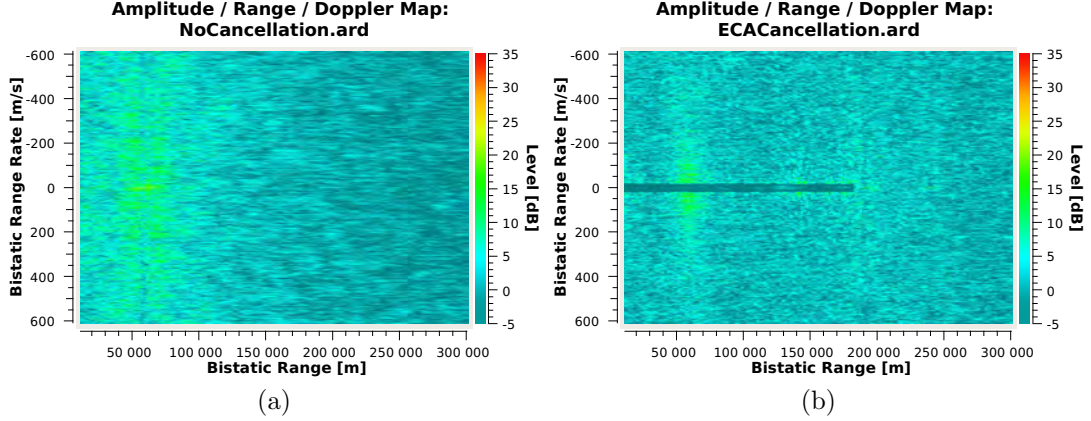


Figure 3.6: Demonstration of the least mean squares estimator as a clutter suppression algorithm. An ARD of a 4 second CPI of FM broadcast data with no DPI and clutter suppression applied is shown in (a). An ARD of the same CPI where a deep notch created by the least mean squares estimator algorithm over a specified range and Doppler region is shown in (b). Cancellation is done for several Doppler shifts about zero which can be used to reduce the effects of Doppler spread. The data shown is real data as captured with the UCT prototype commensal radar system.

where \mathbf{s}_{cs} is the cancelled surveillance signal. As in Equation 3.2, A is a model of the DPI and clutter and \mathbf{x} is the vector of filter weights. I is the identity matrix. Superscript H denotes Hermitian transpose.

This algorithm provides an effective least squares estimate to Equation 3.5 which creates a deep notch of cancellation. Figure 3.6 shows an example where the A matrix is constructed such that that the first 5 non-zero Doppler bins are also suppressed on each side of the zero-Doppler bin, thereby reducing the effects of the Doppler spread. This was found to be the favourable algorithm in an investigation by Heunis [9, 17] at UCT due to its consistent convergence capability. As O’Hagan [8] points out, this algorithm has the advantage that it requires that no parameters be tuned manually before operation.

One of the major drawbacks to the least mean squares estimator algorithm, however, is the large memory footprint required as a result of the expansion into several matrices and vectors. This can be problematic for implementation on

hardware such as a GPU. Inspecting Equation 3.8 it is clear that several matrix multiplications are necessary. To illustrate, consider that typically a 4 s CPI is used by the UCT Commensal Radar Prototype. The sample rate used for FM data is 204.8 kSps which produces a CPI of 819200 samples. For the DPI and clutter suppression stage, this 4 s is split into 8 sub-CPIs of 0.5 s to alleviate memory requirements and at the same time to provide a 2 Hz Doppler resolution. This generalisation of Doppler resolution reduces the number of discrete bins that need to be cancelled for a given notch width without creating a noticeable loss in cancellation performance. The A matrix therefore consists of columns which are 102400 samples long. DPI or clutter are typically present until the 200th range bin. Which is then, the number of columns in A matrix. For single precision complex float values A is therefore 1.28 GB big which occupies most, if not all, of the capacity of a mid to high end GPU board for typical hardware at the time of writing. Furthermore, 1.28 GB is only for the A matrix and when reviewing Equation 3.8 it is clear that addition memory space will be required for other structures.

GP-GPU specific products such as NVIDIA's Tesla [160] range offer more memory (in the order of 6 -12 GB), however, these products tend to be more costly to procure and provide reduced computation throughput per hardware thread for equivalent underlying processor hardware. This is as a result of specification for long term reliability, the lower clock speeds required for greater memory capacities and also as a result of providing extra functionality such as error correcting code (ECC) memory which is not critically necessary for this application. This is evident in the GPU stages of the processing chain where a NVIDIA Geforce GTX570 outperforms a NVIDIA Tesla M2090, the later of which has both more hardware threads and more memory. The specific timings are shown in Tables 3.6.1 and 3.6.2 of Section 3.6. It is therefore intended to develop software capable of being targeted to typical "gaming" type GP-GPU capable GPUs as far as possible to keep system costs to a minimum and maximise portability. GP-GPU software designed for gaming GPUs will typically be able to run on GP-GPU specific cards as well but not necessarily the other way around due to memory capacity differences.

A further drawback that one-shot, numerically optimal approaches such as the least mean square estimator have is that they seek to provide what will result in a maximum reduction in clutter. This generally translates into a high computation requirement. Reducing the level of clutter (after coherent integration) below that of the noise floor is not useful as targets need to exist above this noise level to be detectable anyway. These considerations make iterative refinement methods more attractive for the reduction of DPI and clutter. We seek to reduce this interference only partially, to the point that targets of interest are detectable, and thereby achieve a reduction in the computation requirements.

The conjugate gradient-least squares (**CGLS**) algorithm is an extension of the conjugate gradient technique and can be used to minimise the function in Equation 3.5 in a least squares sense. This algorithm iteratively tends towards a minimum value. Once a satisfactory residual is achieved the processing can be stopped. Alternatively the algorithm can be run for a fixed number of iterations. This will, however, not guarantee a sufficient reduction in interference but it will result in a fixed execution time. It turns out however, that for static transmitter and receiver sites the clutter and **DPI** levels are typically fairly constant over time and so a fixed number of iteration cycles can easily be estimated by trial and error to consistently provide sufficient interference suppression, which in turn, stabilises the latency of the processing chain. Using the **CGLS** algorithm therefore has the capability of providing equivalent interference suppression performance of the least squares estimator proposed by Colone but also offers the benefit of lower memory footprint and a configurable trade off between computational load and amount of interference suppression achieved.

Figure 3.7 shows residual performance comparisons between **CGLS** and the least mean squares estimator. What is notable is that running **CGLS** for only 2 iterations reduces the residual to within 3 dB of that produced by the least mean square estimator once the filter has converged. Furthermore, the blue curve shows the divergence of the residual when the filter weights are not updated. This effect is likely due to changes in the **FM** signal and the motion of antenna masts in the wind in the short term and the signal path environment and fluctuation of performance of the receiver in the longer term. It is therefore necessary to

3.3. PROCESSING DESIGN

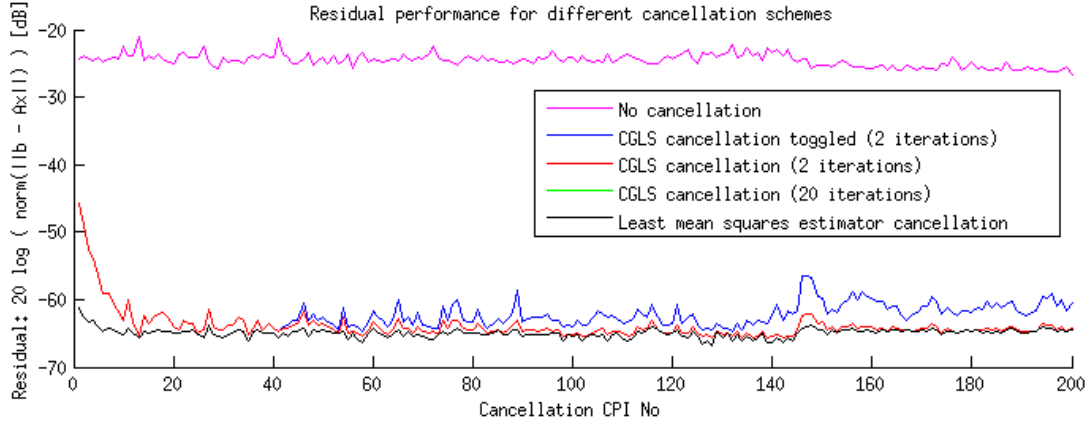


Figure 3.7: A graph showing the residual performance for different cancellation schemes. The cancellation was performed over a cancellation CPI of 0.5 seconds of 204.8 kSps FM data. The blue curve shows the residual for CGLS running for CPIs 0 to 40 and not running for the remaining time to illustrate the divergence of the filter when weights are not updated. The pink curve shows the residual for no cancellation i.e. $\mathbf{x} = 0$. The other curves show continuous filter training using CGLS or the least mean square estimator for all CPIs. Note that the difference between 2 (red curve) and 20 (green curve, hidden by black) CGLS iterations is almost negligible once the filter has converged. The results presented here are from real sample data collected in the field with the UCT prototype commensal radar system.

regularly update the filter weights. The CGLS algorithm is advantageous here as 2 iterations of CGLS take approximately $\frac{1}{10}$ of the time of the least means square estimator and the algorithm requires approximately $\frac{2}{3}$ of the memory footprint so filter weight updates can be made every CPI with minimal computation by using the weights of the previous training as a starting point.

The suitability of CGLS as a filtering technique for radar and similar signal processing fields has been identified by many as an effective method [15, 161, 162, 163]. Each step of the algorithm can be implemented using BLAS [164] operations which makes implementation on a CPU or GPU straightforward. The use of BLAS libraries will also ensure optimal use of the processing hardware and simple porting between platforms that have BLAS support as BLAS has a standardised calling interface.

3.3. PROCESSING DESIGN

The **CGLS** algorithm was therefore selected as the preferred approach for **DPI** and clutter suppression in the processing chain. The algorithm is detailed in Algorithm 1 [161].

Algorithm 1: The **CGLS** Algorithm for minimising $\|A\mathbf{x} - \mathbf{b}\|$

Data: Time domain sample data for reference and surveillance channels.

$\mathbf{x}_{prevCPI}$ the filter weight estimate from a previous **CPI** if it exists, otherwise set to $\mathbf{0}$. A and \mathbf{b} constructed from input channels as described in Section 3.2.1

```

1 . Result: Time domain sample data for surveillance channel with interference
    reduced.  $\mathbf{x}$  the new filter weight estimate to use in the subsequent
    CPI.
2 //Initialised filter:
3 if  $\mathbf{x}_{prevCPI}$  exists then
4   |  $\mathbf{x} \leftarrow \mathbf{x}_{prevCPI}$ ;
5 else
6   |  $\mathbf{x} \leftarrow \mathbf{0}$ ;
7  $\mathbf{r} \leftarrow \mathbf{b} - A\mathbf{x}$ ;
8  $\mathbf{p} \leftarrow A\mathbf{r}$ ;
9  $\mathbf{s} \leftarrow \mathbf{p}$ ;
10  $\gamma \leftarrow \|\mathbf{s}\|^2$ ;
11 //Train filter:
12 for  $i \leftarrow 0$  to  $NIterations - 1$  do
13   |  $\mathbf{q} \leftarrow A\mathbf{p}$ ;
14   |  $\alpha \leftarrow \gamma / \|\mathbf{q}\|^2$ ;
15   |  $\mathbf{x} \leftarrow \mathbf{x} + \alpha\mathbf{q}$ ;
16   |  $\mathbf{s} \leftarrow A\mathbf{r}$ ;
17   |  $\gamma_{old} \leftarrow \gamma$ ;
18   |  $\gamma \leftarrow \|\mathbf{s}\|^2$ ;
19   |  $\beta \leftarrow \gamma / \gamma_{old}$ ;
20   |  $\mathbf{p} \leftarrow \mathbf{s} + \beta\mathbf{p}$ ;
21 //Apply filter:
22  $\mathbf{s}_{sc} \leftarrow \mathbf{s}_s - A\mathbf{x}$ ;
```

3.3.1.2 Implementation

Every step of the **CGLS** algorithm can be performed using **BLAS** routines. **CUDA** provides a **BLAS** implementation called CuBLAS [165] which contains all the functionality needed to implement **CGLS** on a **CUDA** capable **GPU**. Data independent operations are split into separate **CUDA** streams which are essentially execution queues. Modern NVIDIA architectures such as “Kepler” allow concurrent kernel execution which will allow the execution of kernels contained in separate streams at the same time which will create further processing concurrency within the algorithm implementation.

Execution of the for-loop shown on Line 12 of Algorithm 1, is well suited to **GP-GPU** capable architectures as it consists of linear algebra which is can be vectorised to a fine granularity. More importantly there is no memory **IO** to or from the device during this time which would result in relatively high latencies compared to the arithmetic.

The code is organised into a worker class called “cCudacancellation_CGLS” that derives a base class “cCancellationBase”. This ensures that all implementations of cCancellationBase share a common calling interface. This will make a swap between implementations of cCancellationBase straight forward, for example there might be a version that uses Cuda, another that uses Intel’s MKL or AMD’s ACML (results from an ACML implementation are presented at the end of the chapter) or OpenCL core math libraries and another using hand coded arithmetic.

cCancellationBase then provides interfaces to operations that any cancellation algorithm implementation would have. These include inputting and storing of a CPI of sample data, setup of cancellation parameters such as the number of range and Doppler bins over which to apply the cancellation and outputting of cancelled sample data. cCudaCancellation_CGLS extends the base class implementing the **CGLS** algorithm targeted to a **CUDA** capable platform. This includes device (**GPU**) memory structures, device functions. Further functionality exists to clear all device memory, backup relevant sections to **CPU** memory (such as the most

recent [CGLS](#) filter weights) and then also to recreate the device memory and restore any backed up sections. This allows the device to be used for other operations such as [CAF](#) processing alternated with cancellation operations.

3.3.1.3 Effects of performing cancellation on sub-blocks of the matched filter CPI

As described in the previous section, it is often necessary to run cancellation on sub-blocks of the matched filtering [CPI](#) due to the memory restrictions of processing hardware and also because the Doppler generalisation can be useful against clutter spread. For both the [CGLS](#) and least squares estimator approach, this implies that the adaptive filter is trained independently on each sub-block and so the filter weightings could theoretically be different from one sub-block to the next. This in turn implies that after cancellation there could be a magnitude and phase discontinuity from 1 sub-block to the next which might negatively effect the match filtering stage.

Figures [3.8](#) and [3.9](#) show some examples of the magnitude and phase of the surveillance observed before and after cancellation in the region of some of the stitching points between the 8 sub-blocks of cancellation that are typically used in the [UCT](#) prototype radar. The data in Figure [3.8](#) was recorded at the Council for Scientific and Industrial Research's Paardefontein test range near Pretoria. The terrain in that part of South Africa has few mountains and so the clutter environment is typically quite low. Figure [3.9](#) shows data recorded at the Tygerberg site in Cape Town, which, as shown in Figure [3.4](#) has a severe clutter environment.

Inspecting these figures indicates that the cancellation can induce jumps in both magnitude and phase, for example in stitching point number 4 of Figure [3.9](#). However it is important to note that these jumps are never more severe than the typical deviation of the magnitude and phase of the signal away from the stitching point, both before or after cancellation. Another point to note is that these signals are put through a matched filter which is essentially a correlation. Correlation has an averaging effect and as such any localised discontinuity may

3.3. PROCESSING DESIGN

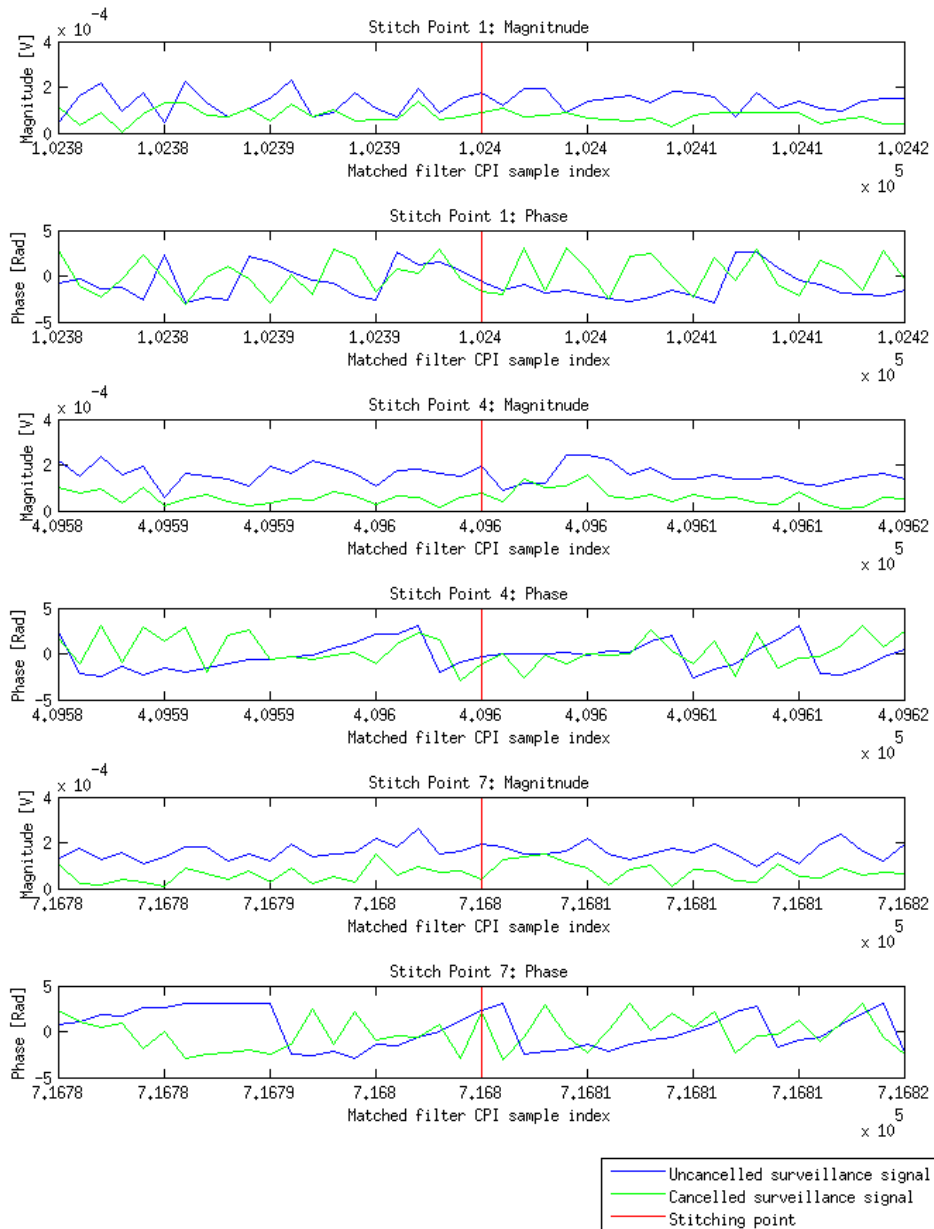


Figure 3.8: Effect of cancellation done independently on separate sub-blocks of the CPI on magnitude and phase of the surveillance signal at a low clutter receiver site.

3.3. PROCESSING DESIGN

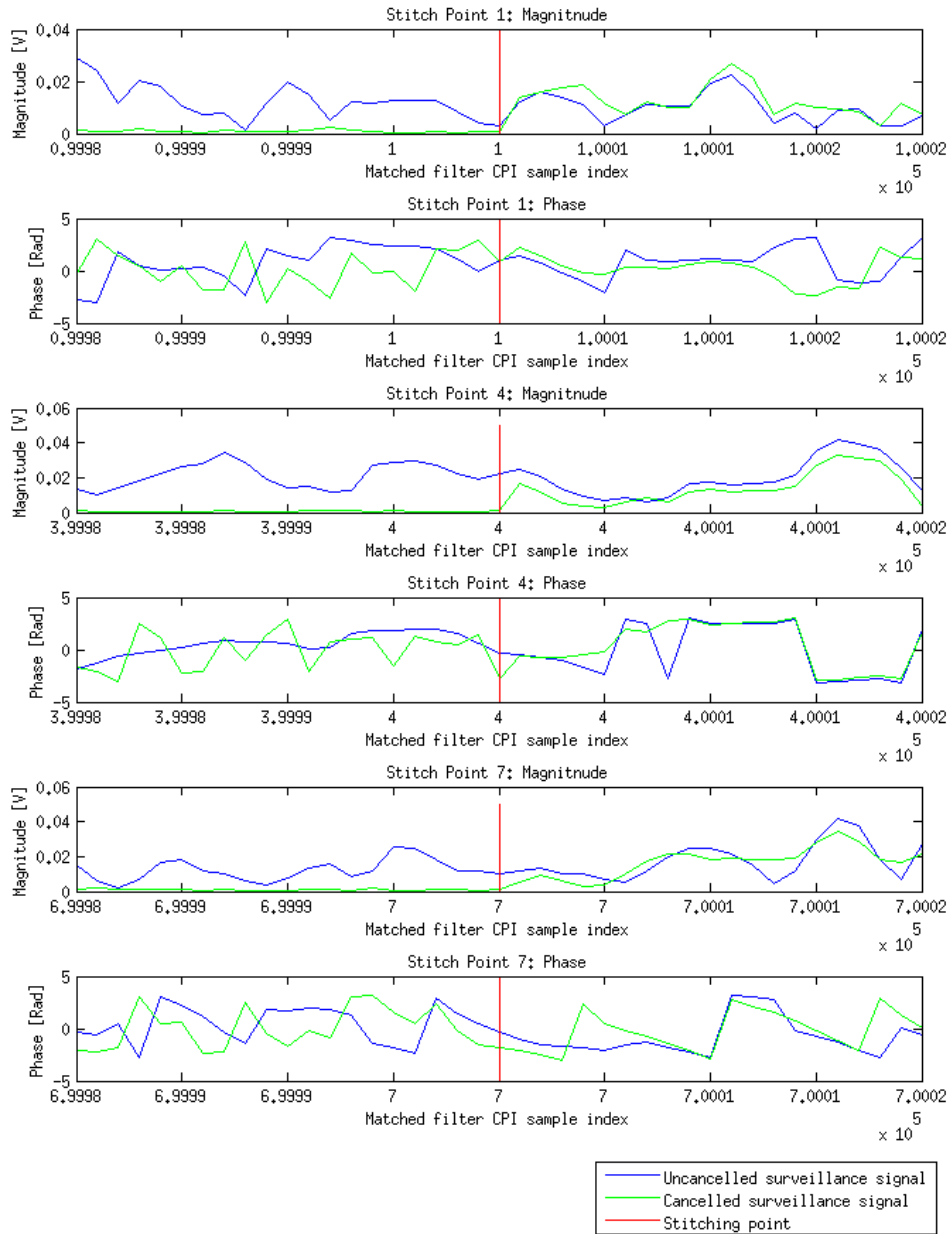


Figure 3.9: Effect of cancellation done independently on separate sub-blocks of the CPI on magnitude and phase of the surveillance signal at a high clutter deployment site.

reduce the correlation gain by some fractional amount but should not have any further detrimental effect on the **ARD** surface produced by the matched filter.

To further illustrate, a simulation is run with the Flexible Extensible Radar Simulator (**FERS**) [5]. **FERS** is a sample level simulator which uses variable delay filters to model radar scenarios where moving platforms are present. Platforms might include targets, radar nodes or clutter objects. Variable delay filters are used as opposed to the start-stop approximation and so the simulator is therefore useful for doing simulations where accurate phase approximations are necessary. A simulation is set up to match the typical processing parameters of the **UCT FM** band prototype system. A 4 s **CPI** is collected at 204.8 kSps within the simulator. real recorded **FM** data is used as the transmitted waveform. Deviating from a real world scenario however, a very large spherical target return of 90 dBsqm used to allow for a detectable **SIR** when no cancellation is applied. The target flies along the extended baseline away from the transmitter and receiver starting at a bistatic range of 90 km and with a velocity of 200 ms^{-1} . To further simplify the simulation, there is no clutter and no thermal noise. Antenna beams are set to be isotropic for simplicity and a 1.3 kW transmit power is used. The result after processing without cancellation is a target with what is a typical real world **SINR** of approximately 20 dB when cancellation is applied. It should be noted however that there is in fact no contributing noise source in this simulation.

The **XF** algorithm is then used to create an **ARD** map of the sample data as shown in Figure 3.10(a). The surveillance data is then altered by simulating the potential discontinuity of 7 stitching points that would result from using cancellation sub-blocks of 0.5 s for a 4 s **CAF CPI**. This alteration is done by randomising the samples at these stitching points. To make for a more severe effect the random values are chosen in a range of 0 to 10 times the maximum envelope level of the original surveillance signal from **FERS**.

As can be seen in the Figure 3.10(b) the effects of this corruption are negligible with the difference being only 3 thousandths of a decibel. This shows that the stitching points created by doing **DPI** and clutter suppression on sub-blocks of the matched filter **CPI** is negligible to the target **SINR**

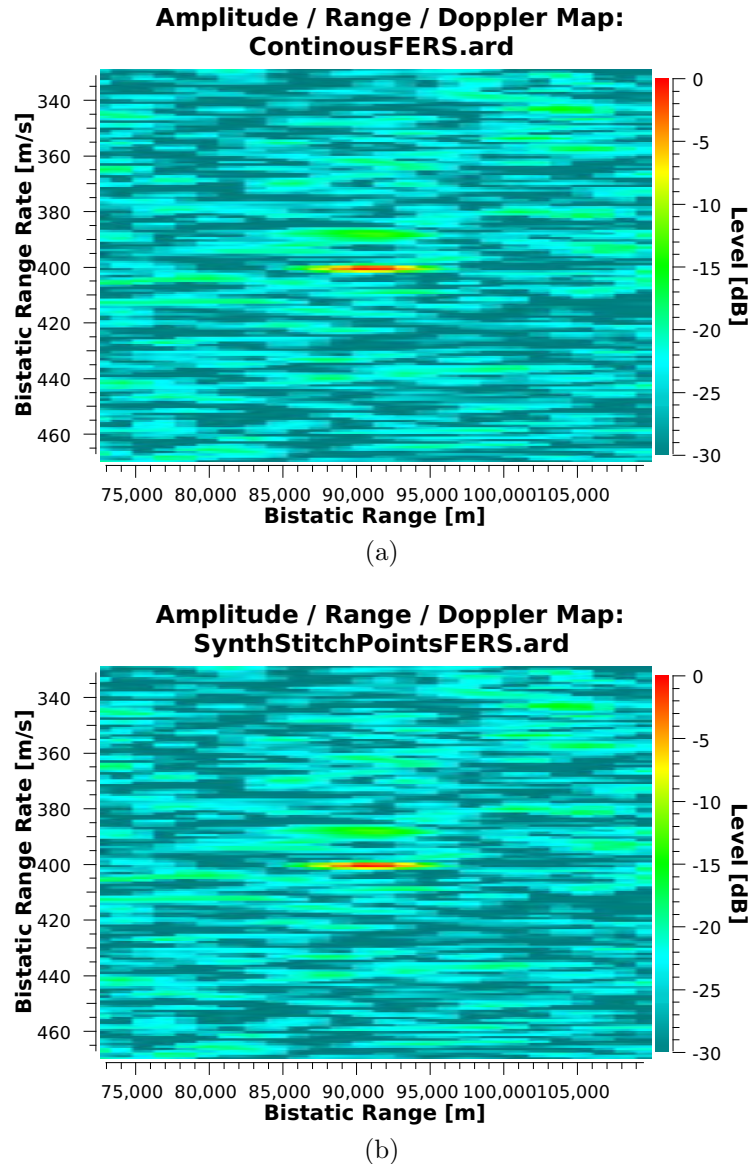


Figure 3.10: Effect of inserting random sample values into time data to simulate the effect of stitching points created by running cancellation on separate sub-blocks of the CAF CPI. The figures show data from a FERS simulation with a suitably strong target is inserted at 90 km, 400 ms^{-1} such that no cancellation is necessary. (a) shows an ARD map of the 4 s of sample data as it is output from FERS. For (b) 7 stitch points very simulated in the surveillance data by changing the samples at 0.5 s intervals to random complex numbers in the range 0 to 10 times the maximum envelope of the received signal. As can be observed, the difference is barely visible and is measured at a few thousandths of a decibel. Furthermore, 10 times the maximum envelope is likely to be a far greater discontinuity than what is created by the sub-block cancellation in reality, as is demonstrated in Figures 3.8 and 3.9.

3.3.2 Range Doppler Processing

Simply evaluating the expression as it is written in Equation 3.7 is generally not a viable option despite the calculation of each range/Doppler cell being parallelisable. This is as a result of the correlation process which is a point-wise multiplication and summation of 2 channels of an entire CPI length of samples (typically 819200) and this is required for each range/Doppler cell (typically 280 by 1601 of them) which is prohibitively large amount of arithmetic.

Methods that exploit speed-ups of the discrete fast Fourier transform (FFT) are reviewed below. There are 2 main ways of exploiting the algorithm [68], the first being to do a point-wise cross multiplication first followed by the FFT and the second involves doing the FFT first and then the point-wise cross multiplication. We borrow from radio astronomy terminology and name these 2 methods XF and FX respectively where ‘X’ represents the point-wise cross multiplication operation and ‘F’ the (discrete) Fourier transform operation (in this case the FFT) [166].

A third method called the “Batches” [109] or “FMCW-like” [68, chap. 7.5.8] method which offers further speed-ups at the expense of correlation losses in certain conditions is also reviewed.

A novel approach to the XF method, implemented using a recursive DFT (RDFT) is also briefly discussed [69]. The RDFT method allows the CAF to be updated with only a few samples at a time without using a sliding window.

3.3.2.1 XF Algorithm

On inspection, it should be apparent that the discrete CAF function defined in Equation 3.7 has a factor which is very similar to that of the discrete Fourier transform (DFT) as shown below in Equation 3.9 [156, Ch. 1.5].

$$F(k) = \sum_{n=0}^{N_s-1} \mathbf{s}(n) e^{-j2\pi kn/N_s} \quad (3.9)$$

Where \mathbf{s} is an arbitrary discrete time signal, k is the discrete frequency bin number and N_s is the number of consecutive samples that are being transformed. The continuous time Fourier transform is equivalently similar to the continuous version of the CAF show in Equation 3.6.

From Equation 3.7 we rewrite the conjugate product of the samples as a function $f(n, m)$:

$$f(n, m) = \mathbf{s}_s(n)\mathbf{s}_r^*(n + m) \quad (3.10)$$

With n the sample number and m the delay. Then Equation 3.7 becomes

$$|C(m, k)|^2 = \left| \sum_{n=0}^{N_s-1} f(n, m)e^{j2\pi kn/N_s} \right|^2 \quad (3.11)$$

Given that m is independent and can be considered constant across the expression. Equation 3.11 can also be expressed as

$$|C(m, k)|^2 = |DFT(-k, \mathbf{f}(m))|^2 \quad (3.12)$$

where $\mathbf{f}(m)$ now implicitly returns a vector of values for the full range of n i.e. the entire CPI of samples. The DFT operator performs a discrete Fourier transform on the vector that $\mathbf{f}(m)$ returns for the specified frequency bin k . Note here that k is negative in the expression because the exponential index undergoes a sign change to go from CAF to DFT expressions.

Equation 3.12 is now in a form in which we can apply a useful computing optimisation. The mathematically equivalent FFT algorithm can replace the DFT algorithm which reduces the computation complexity from $N_s \cdot N_D$ (where N_D is the number of Doppler bins of interest) to $N_s \cdot \log_2 N_s$ for each transform.

The CAF for discrete time can be written as

$$|C(m)|^2 = |FFT(\mathbf{f}(m))|^2 \quad (3.13)$$

Here the frequency bin argument k has fallen away due to the FFT algorithm implicitly calculating all discrete frequencies from $-\frac{f_s}{2}$ to $\frac{f_s}{2}$ at a resolution of $1/T_{CPI}$ Hz. Where f_s is the sample rate in Hertz and T_{CPI} is the CPI length in seconds. When visualising the CAF surface unwanted frequency bins, i.e. ones representing Doppler shifts faster than expected target velocities are simply discarded. Often more bins are discarded than what are kept, however, the reduction in complexity from $N_s \cdot N_D$ to $N_s \cdot \log_2 N_s$ will invariably justify the redundant calculations.

To illustrate, UCT's prototype system typically outputs $N_D = 1441$ Doppler bins of interest when exploiting a 88.2 MHz carrier. The CPI size is $N_s = 819200$ (i.e. the number of samples input to each FFT). The $N_s \cdot \log_2 N_s$ complexity of the FFT method equates to 1.609×10^7 while the $N_s \cdot N_D$ complexity of the DFT equates to 1.180×10^9 . I.e. there is a order of 2 magnitude improvement using the FFT despite the redundant bin calculations.

3.3.2.1.1 Reducing redundancy in the XF algorithm As described above, the XF calculation calculates all Doppler shift frequencies from $-\frac{f_s}{2}$ to $\frac{f_s}{2}$. For the 4 second CPIs preferred for the FM broadcast band based system described in this thesis the implication is that more than 99% of the bins calculated are not used when considering the maximum operating speed of typical commercial airliners. When analysing the XF algorithm it is noted that the point-wise cross multiplication stage produces a beat signal between the reference and surveillance signal segments which is also the Doppler shift in the case of moving platforms. The subsequent FFT operation then simply gives the spectral estimation of this beat signal. Given that only the lower frequencies of the beat signal (below 200 Hz for commercial airliners in the FM band) are of interest, the beat signal segment can be low-pass filtered (i.e. processed by an anti-aliasing filter) and then decimated accordingly which will require a proportionally shorter FFT to

be performed and an overall saving in the amount of computation.

Using this technique, Howland [7] showed that using a cascaded integrator-comb (CIC) filter and a subsequent finite impulse response (FIR) to decimate by a factor of 128 resulted in a reduction in complexity in the order of 15 times which makes for a most useful speed-up. The group delay effects of the filtering process on the phase of the ARD surface would, however, need to be considered if the phase information is to be used such as in the example of AoA.

3.3.2.2 FX Algorithm

An alternate algorithm exploits the cross-correlation theorem i.e. cross-correlation in the time domain is equivalent to point-wise conjugate multiplication in the Frequency domain [167, Ch 10.5]. Hence the Fourier pair:

$$Corr(f, g) \Leftrightarrow F^* \cdot G \quad (3.14)$$

Where $Corr()$ denotes the cross correlation operation of time domain sequences, \cdot denotes point-wise multiplication of the Fourier transforms of those respective time sequences and $*$ denotes complex conjugation.

Re-evaluating Equation 3.7 it is evident that the expression can be interpreted to represent cross correlations between the surveillance signal and Doppler shifted versions of the reference signal. The FX algorithm applies the correlation operations by using the FFT function as the discrete Fourier transform part of the correlation theorem.

Both the surveillance and the reference signal are therefore FFTed. The surveillance signal is conjugated. Corresponding bins are multiplied together and the resultant sequence is inverse FFTed (IFFTed) yielding the zero Doppler bin. To achieve correlation at Doppler shifted frequencies, the conjugated surveillance channel is point-wise multiplied with shifted versions of the reference signal after the initial FFTs are performed and before the IFFT operation.

Converse to the XF method the FX can generate the CAF for the specific Doppler

bins but for all range bins up to a delay of N_s-1 samples, where N_s is the number of samples in the **CPI**.

3.3.2.3 Batches Algorithm

The *Batches* algorithm is described by Griffiths et al. as *An FMCW-Like Approach* [68, chap. 7.5.8] and also in a more general form by Petri et al. [109]. This algorithm splits what would typically be the **CPI** up into smaller batches. Cross correlation between reference and surveillance is then performed on each batch and the output of the correlation is arranged such that each batch's cross correlation output forms a row of a matrix. Once again the **FFT** and **IFFT** can be used for improved correlation speeds. Columns of the matrix create a dimension similar to the "slow time" of pulsed radar. Lastly, a **FFT** is applied over the the column dimension similar to pulse-Doppler radar processing, the output produces an approximation to the **CAF**.

The advantage of the algorithm is a large computation speed up. Sequentially speed-ups in the order of 100 times are obtainable with output **ARD** maps that by visual inspection appear to be identical to that of the other methods when the Batches algorithm is appropriately tuned. This makes the batches algorithm a great tool for quick in-field analyses as **ARD** maps can be generated in real-time with a current laptop **CPU**. This is very useful for receiver site assessment. **CAFs** of the raw channel data provide an indication of the level of **DPI** and clutter returns. Calculating the **CAF** of either channel with itself produces the auto ambiguity function (**AAF**) of the respective channel. The **AAF** gives insight into the properties of the illuminating signal and and indication of the amount of multipath impinging on the antenna which is feeding the channel [55].

There is however a potential drawback to this algorithm. As discussed by Petri et al. [109] the algorithm assumes a phase shift error by correlating the non-Doppler-shifted reference signal with Doppler shifted target reflections. The longer the length of each batch the more the error of this approximation compounds and it is also as expected compounded by larger Doppler shifts. It is therefore important to keep batches short in length. An example of the effects of this Doppler error

are illustrated in Figures 3.11 and 3.12. The recommendation by Petri is that the product of batch length in seconds and the maximum target Doppler shift in Hertz be much smaller than 1. This creates a degree of freedom in the tuning of this algorithm which needs to be correctly selected.

3.3.2.4 A Recursive Algorithm for CAF calculation

The integration gain of the CAF is directly proportional to the time-bandwidth product. For low bandwidth signals such as FM broadcast a long CPI (in the order of 1 to 4 s) is therefore necessary to raise target reflection above the background noise levels and also to create suitable fine Doppler resolution. It is possible however, that an update rate of more than 4 s is required for the tracking stage of the radar system. This would require a CPI sliding window approach where the entire CAF needs to be recalculated for each update.

The idea of recursive discrete Fourier processing for radar data appears to date back many years, for example the work by Dillard [168]. Applying the recursive DFT (RDFT) to CAF processing it is possible to progressively update the CAF surface for each new reference/surveillance sample pair. This means that the update rate can be matched to prior stages such as DPI and clutter suppression. Furthermore if using the separated reference configuration [16] over long baselines it may be possible to run the processing chain without any DPI and clutter suppression which would allow for an arbitrary update rate after CAF processing.

The recursive DFT algorithm works by updating each frequency bin by adding the energy that a new single sample introduces to the respective frequency bins and then removing the energy that a previous sample added a number of samples prior.

It can be further described as follows [169]:

Let:

$$s_{out} = \mathbf{s}[0] \text{ be the outgoing sample} \quad (3.15)$$

3.3. PROCESSING DESIGN

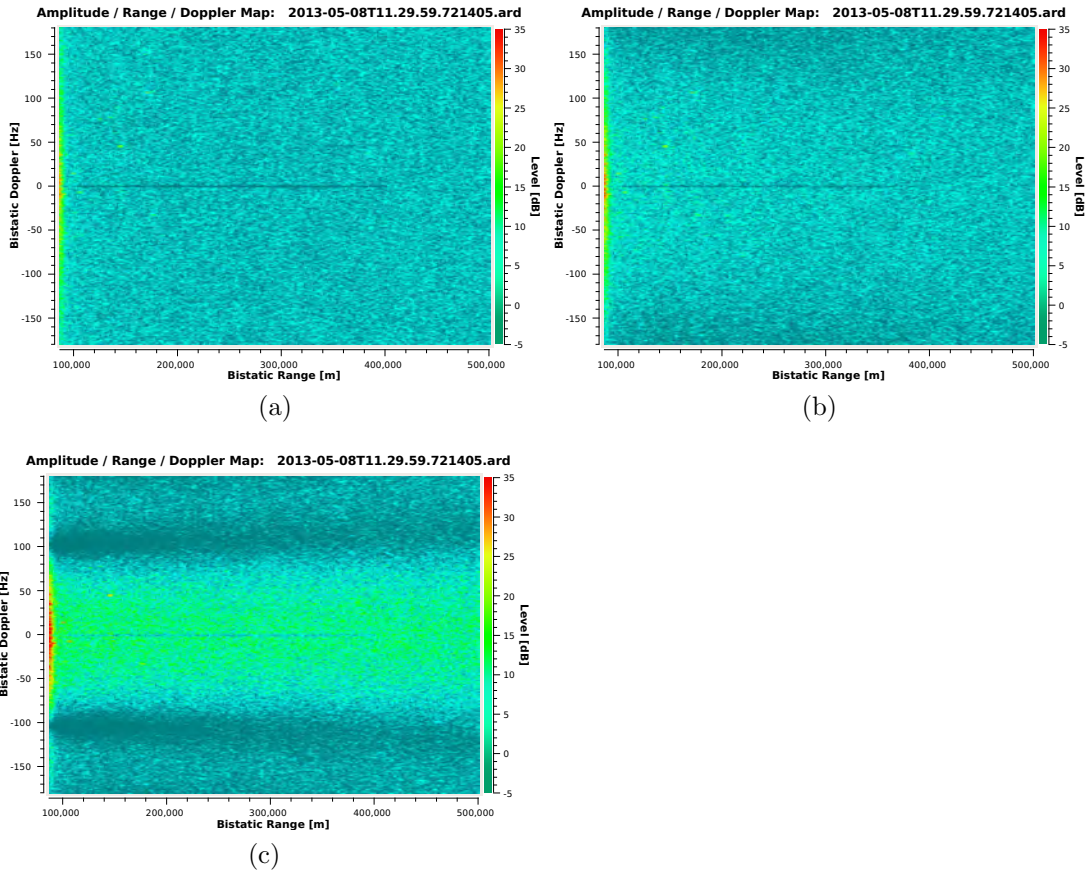


Figure 3.11: Comparison of the ARD maps produced from the XF CAF algorithm (a) vs the Batches CAF algorithm for a short batch length (b) and the Batches CAF algorithm for longer batch lengths. The Batches algorithm applied to a shorter batch length shows an ARD surface similar to that of the ideal XF algorithm but when the batch length is increased (c) losses at high Doppler become visible. The maps shown here were produced using a 4 s CPI of FM broadcast data captured at 98 MHz at a sample rate of 204.8 kSps.

3.3. PROCESSING DESIGN

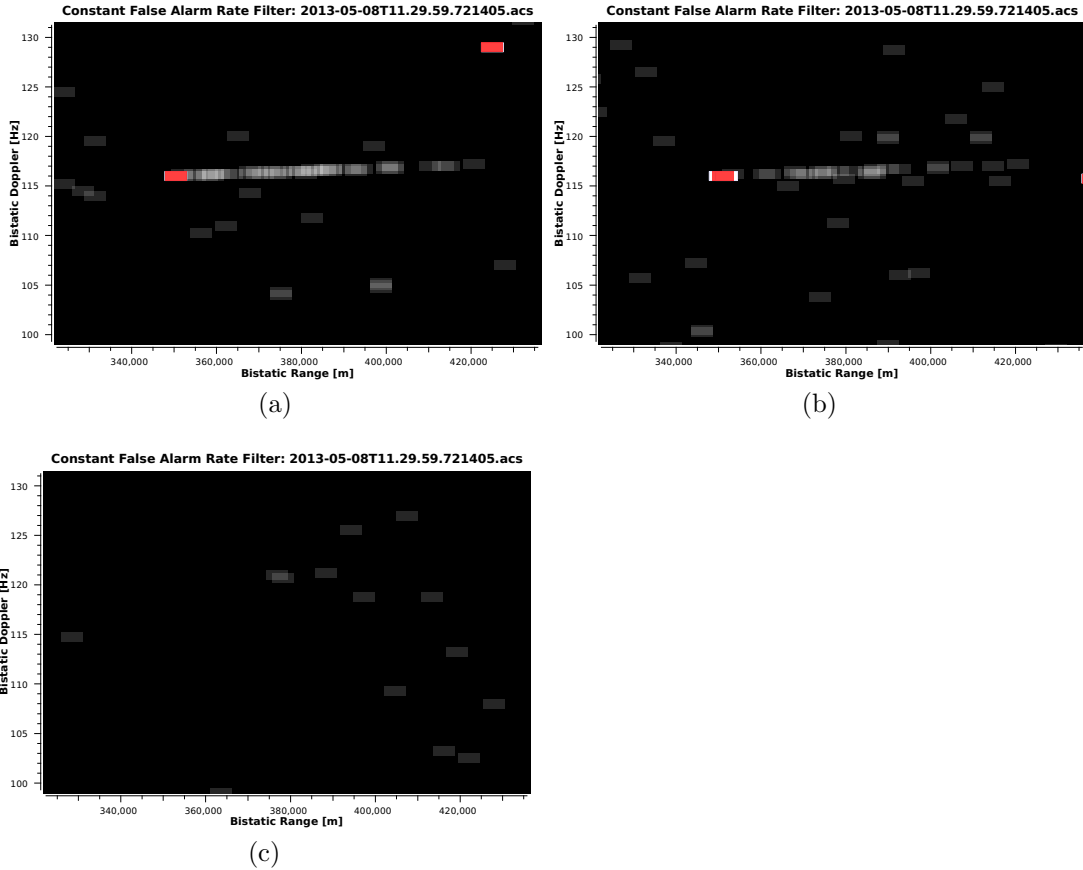


Figure 3.12: Comparison of CFAR data from the ARD maps shown in Figure 3.11. The maps shown here are a zoomed in section at high Doppler with a detection occurring at 250 km, 116 Hz. The CFAR algorithm was GOCA-CFAR operating in the Doppler dimension with $P_{fa} = 10^{-5}$. White cells indicate detected cells in the current CPI, red cells indicate the centroid of multiple adjacent cells detected in the current CPI and transparent-white cells are cells detected within 20 previous CPIs. As in Figure 3.11, (a) is data from the XF algorithm, (b) from the Batches algorithm with a shorter batch length and (c) Batches algorithm with a longer batch length. The shorter batch length displays a slightly sparser trail when compared to XF which suggests a partial decorrelation at high Doppler. The longer batch length shows that the target is not detected at all and therefore that large decorrelation has occurred at high Doppler.

$$s_{in} = \mathbf{s}[N_s] \text{ be the incoming sample} \quad (3.16)$$

Then the update energy value for each bin is:

$$F_{update}[k] = \left(F_{current}[k] + \frac{s_{in} - s_{out}}{N_s} \right) e^{j2\pi \frac{k}{N_s}} \quad (3.17)$$

Where N_s is the effective **DFT** size or integration time in number of samples, k is the discrete frequency bin and $F_{current}$ is the current frequency bin value. Typically all $F_{current}$ are initialised to zero and then after N_s samples are added the output will represent the equivalent bin values of an N_s length **DFT** signal from $\mathbf{s}[0]$ to $\mathbf{s}[N_s]$ and will continue to be representative of the **DFT** after each single sample thereafter i.e. $\mathbf{s}[n]$ to $\mathbf{s}[n + N_s]$ for $n > N_s$.

The following are apparent from the above description.

- Calculation of each frequency bin is independent and therefore only the frequency bins of interest need to be calculated, unlike **FFT** based methods.
- Updates could potentially be done in batches of samples accumulating several of the $(s_{in} - s_{out})$ part of Equation 3.17 before evaluating the rest. This would reduce the update rate of the spectrum but decrease the computation requirement.
- Whether using the batching described in the previous point or not, the updates must be performed for 100% duty cycle of samples to maintain a meaningful spectrum at all times. Dropping a block of samples will require a N_s sample update before a correct spectral representation will be achieved again. There is an equivalent requirement after resetting all frequency bins to zero.
- This algorithm could be integrated into the ‘F’ part of the **XF** algorithm which would allow for arbitrarily high update rates assuming a continuous stream of input samples.

- Given the recursive nature of the algorithm it is important to note that it is likely to having diverging arithmetic error especially when using floating point arithmetic.

The [RDFT](#) was integrated in the [XF CAF](#) algorithm and implemented on a Geforce GTX480. After memory access optimisation, 72000 [CAF](#) cells (any combination of range and Doppler cells) can be calculated in real-time when blocks of more than 12800 samples are loaded at a time (for 204.8 kSps FM data). The 12800 sample block is sufficiently long to hide memory latencies in the device and therefore allows for optimal use of shared memory techniques. Increasing this block size further improves the processing-time to block-time ratio. This does, however, occupy the device 100% of the time which makes integration into the current processing chain difficult given that all samples must be processed in continuous time as per the [RDFT](#) algorithm (blocks of input samples cannot be discarded). Furthermore the divergence of the error in floating arithmetic which [GPUs](#) are suited to is also of some concern.

At present the implementation is not viable for use with the prototype system however, it is noteworthy in that it is embarrassingly parallel, has a much lower memory footprint than either the [XF](#) or [FX](#) methods because only the exact frequency bins and range of interest need to be calculated. This may make it well suited to [FPGA](#) architectures which can also apply suitably high bit depths in fixed point. This is of particular note as Van Der Byl demonstrates that the arithmetic error can be made to converge using suitable fixed point error correction [169].

Further details of the [GPU](#) implementation as well as an [FPGA](#) based design are discussed by Van der Byl et al. [169, 69].

3.3.2.5 Choice of Algorithm

Selection between [XF](#) and [FX](#) algorithms comes down to the dimension of the [ARD](#) map that is generated from the [CAF](#). To illustrate practically, [UCT](#)'s [FM](#)-based prototype system makes use of long integration times (~ 4 s) to achieve

high Doppler resolution as it is intended to be exploited for tracking based on Doppler information as far as possible. These long integration times are possible in hardware due to the low bandwidth of the FM signal (digitised at 204.8 kSps). This low bandwidth translates to a low range resolution, accordingly 250 range bins cover the radar's typical detection range (~ 300 km bistatic). Commercial airliners rarely exceed speeds of 300 ms^{-1} which at FM broadcast frequencies translates to a maximum bistatic Doppler shift in the order of 180 Hz. The 4 s integration time results in a Doppler resolution of 0.25 Hz which means we need to calculate 1441 Doppler bins. The ARD map therefore spans 250 range by 1441 Doppler bins. It is therefore logical to use the XF method as we can specify the number of range bins which is the lower dimension and have the larger Doppler dimension be covered by the implicit calculation of all Doppler frequencies up to $\pm f_s/2$ (in this case ± 102.4 kHz).

If a DVB-T based system is considered, the typical channel bandwidth is in the order of 7.6 MHz and so it is likely to be complex-sampled at around 8 MSps. This translates to a range resolution in the order of 38 m. To achieve a bistatic detection range of 300 km, we now need ~ 7900 range bins. Practically DVB-T will be unlikely to illuminate targets at this range due to both elevation patterns of the radiation [54] and propagation at the higher carrier frequency. So for argument sake 4000 range bins need to be calculated. To prevent range walk of targets with velocities of 300 m/s the CPI is limited to 127 ms assuming conventional matched filtering and anti-range walk processing [24] is not being used. This time-bandwidth product translates to a slightly higher (25% more) number of samples to the FM case. For UHF carriers around 600 MHz maximum Doppler shift will be in the order of 1 kHz. The Doppler resolution for a CPI of 127 ms is 8 Hz so only 251 Doppler bins are required. The ARD map is now 4000 range by 127 Doppler bins so opting for the FX algorithm where we can choose the exact number of Doppler bins to process and have the range bins be covered by the implicit range calculation up to the number of samples in the CPI is therefore likely to be a more fitting approach.

The Batches algorithm allows for large speed-ups (approximately 100 times) compared to XF and FX algorithms, however, the processing dimensions required

extra tuning parameters which can cause unacceptable losses when they are not optimal. Given that **XF** algorithm can be executed in real-time along with the cancellation stages on the hardware available for the prototype system as is described in Section 3.3.2.6, the **XF** algorithm is preferred to guarantee optimal system detection capability. The Batches algorithm does, however remain a noteworthy tool for the future that it will allow for increased update rates, the processing of more **FM** channels or processing on less capable hardware such as a typical **CPUs**. **CPU** only based implementation results using the batches algorithm are presented later in this chapter.

3.3.2.6 Implementation

As described in Section 3.3.2.5, the **XF** algorithm for **CAF** calculation is preferential for the **FM** broadcast signals that the prototype radar exploits. NVIDIA's Compute Unified Device Architecture (**CUDA**) **API** provides a **FFT** library [170] which has functions for doing a batch of **FFTs** along a dimension of a matrix. This is ideally suited to the **XF** algorithm if one envisions a matrix where the columns are a point-wise multiplication between the reference and conjugate of the surveillance signal for each delay and columns, left to right, represent increasing delays (i.e. range bins). **FFTs** are then performed using each column as both the input array and output array of the respective **FFT** operation. An advantage of the **CUDA FFT** library is that it provides functions for optimally allocating the memory of the data input/output matrix as well as queuing batch **FFT** execution. This guarantees optimal execution and memory access due to correct coalescing.

A similar class structure is used to that of the cancellation. The code is organised into a worker class called "cCudaARDMaker" that derives a base class "cARDMakerBase". Again this ensures that all ARDMaker implementations share a common calling interface.

cARDMakerBase base provides interfaces to operations that any ARDMaker implementation would have. These include inputting and storing of a **CPI** of sample data, storing and outputting **ARD** data and populating a member array

3.3. PROCESSING DESIGN

which holds a windowing function used before applying **FFTs**. **cCudaARDMaker** extends the base class with **CUDA** functionality. As with the cancellation stage, the **CUDA** version of the worker class includes device (**GPU**) memory structures and device functions as well as functionality to clear all device memory, backup sections of memory to **CPU** memory and then also to recreate the device memory and restore any backed up sections. This allows the device to be used for other operations such as **DPI** and clutter suppression between **CAF** processing jobs.

For the data dimensions described for **FM** broadcast data in Section 3.3.2.5, that is, 8 million samples over the 4 seconds **CPI** and 250 range bins, the **ARD** processing takes in the order of 0.2 s on a Geforce GTX480. **CUDA**'s **FFT** library creates a **FFT** plan which creates a working space for the **FFT** algorithm. For batch **FFTs** this plan tends to be quite large and is typically similar to the size of the input matrix which is to be **FFT**ed. This does however allow for the **FFTs** to be performed in-place from the point of view of the calling code. That is, the input matrix is used as the output matrix. The result of this is that the 250 ranges need to be split up into 3 sequentially executed sections to fit into the 1.5 GB of memory on the GTX480. All calculations are performed in single precision complex floating point numbers.

The execution is as follows. To begin execution, in **CPU** context, a pointer to a block of 1 **CPI**'s worth of reference and surveillance signal are passed to the "cCudaARDMakerClass". Once all subsections of the **CPI** are flagged as being ready (i.e. **DPI** and clutter suppression are completed on the entire **CPI**) the "run" member function is called. The **DPI** and cancellation device memory structures are backed up to host (**CPU**) memory and removed from the device (**GPU**) and the **ARD** device memory structures are restored. Note that this is done on the first available device if there is more than 1. The number of delays (range bins) that can be calculated given the memory size is determined and the calculation of the **CAF** surface then proceeds. This process is illustrated in Algorithm 2. Note that although lines 8, 9 and 11 are described by for-loops, the **CUDA** framework will execute this section in parallel as far as possible given the **GPU** hardware.

Algorithm 2: The XF CAF algorithm on GP-GPU

Data: Time domain sample data for reference surveillance channels with interference suppressed.

Result: ARD data for the required range and Doppler.

```

1 Allocate device memory for reference, surveillance and window arrays;
2 Copy reference, surveillance and window arrays to the device;
3 Declare 2D FFTInput matrix FFTInput for as many range bins as can fit into
  memory;
4 Create Batch FFTPlan;
5 NRangeBinsComputed  $\leftarrow$  0;
6 while NRangeBinsComputed < NRangeBins do
7   NRangeBinsPossible  $\leftarrow$  Number of range bins left or that will fit into
  GPU memory;
8   for i  $\leftarrow$  NRangeBinsComputed to
  NRangeBinsComputed + NRangeBinsPossible - 1 do
9     for j  $\leftarrow$  0 to NSamplesInCPI - 1 - i do
10      FFTInput[i]  $\leftarrow$  Ref[j] * conj(Surv[j + RangeBinNo]) * Window[j];
11      //Point-wise conjugate multiplication and windowing at given
  //correlation shift.
12     for j  $\leftarrow$  NSamplesInCPI - i to NSamplesInCPI - 1 do
13      FFTInput[i]  $\leftarrow$  0;
14      //Zeroing of non-overlapping edge values in correlation shift.
15   Execute Batch FFT plan;
16   Calculate magnitudes of ARD cells for all range bins in memory and for
  Doppler bins of interest;
17   Copy these magnitude values to host memory;
18   NRangeBinsComputed  $\leftarrow$ 
  NRangeBinsComputed + NRangeBinsPossible;
19 Destroy Batch FFT plan;
20 Free remaining device memory;

```

CUDA provides a mechanism for processing 1D, 2D and 3D data structures. Algorithm 2 is well suited to 2D processing where the 1st dimension is the number of samples in the **CPI** and the 2nd is the delay (or correlation shift or range bin) number. When the **CUDA** kernel is then executed the device will work its way across the 2D grid in tiles, which are subsections of the grid and the dimensions of which can be specified according to device capability and grid size. The “run” function of the **cCudaARDMaker** class blocks until all processing is completed. Returning from the “run” function indicates to the calling thread that a new **ARD** object is ready to be copied from the **cCudaARDMaker** object instance.

3.3.3 Detection

There are several established techniques in which the **CUT** is compared to its surrounding cells and so different flavours of **CFAR** filter exist. The properties of these filters are extensively documented in literature [171, 144, 172, 158, 157, 173] and will not be discussed in detail here.

For the **ARD** maps of **FM** based commensal radar, the “greater of, cell averaging” **CFAR** (**GOCA-CFAR**) filter has proven to be most optimal as it is able to reject clutter edges which are common as a result of the mountainous topography which occurs in the Western Cape of South Africa. This clutter rejection capability of the **GOCA-CFAR** is consistent with what is described in literature [158, Ch 5.7], [157, Ch 16.6.1], [171, 173]. **GOCA-CFAR** achieves clutter edge rejection behaviour by averaging the reference cells on either side of the **CUT** separately and selecting the greater of the 2 averages to compare to the thresholded **CUT**. This also helps to reduce false alarms.

Due to the low signal bandwidth of **FM** broadcasts and the dependence of the instantaneous bandwidth on the signal content, it is problematic to run the **CFAR** filter in the range dimension. The fluctuation of a target’s length in range due to changes in instantaneous signal bandwidth make setting the number of guard cells of the filter challenging. Fortunately the long integrations times used in **FM** based commensal radar produce high Doppler resolution which make sharp

target edges if the **CFAR** is run in the Doppler dimension which results in an effective detection scheme.

CFAR filters can also be constructed to use a combination of the range and Doppler domains together but once again because of the fluctuation of the range dimension of the target it is difficult to weight the reference cells of the range and Doppler dimensions together effectively.

Due to the negligible computation requirements of the **CFAR** filter this stage of the processing chain was integrated directly in the **GUI** application used to visualise **ARD** maps. A separate thread calculates the **CFAR** output upon reception of **ARD** data and draws the output in the **CFAR** map widget. This allows each user to select the desired **CFAR** algorithm and configure the parameters of that algorithm on the fly while visualising the output. This **CFAR** tuning can therefore also be done independently at each network client receiving **ARD** data of which there can be several.

The preferred **CFAR** filtering implementation and configuration used for all **CFAR** results presented in this thesis (unless stated otherwise) are **GOCA-CFAR** running in the Doppler dimension. The **CFAR** runs on squared-law detected **ARD** map surface (i.e. the amplitude scale of the map is power) and as such the probability of false alarm is set at 10^{-5} against an exponential distribution. 4 guard cells and 5 reference cells are used on each side of the **CUT**.

Consideration needs to be given to the sidelobes of the **ARD** surface in the Doppler domain and how this will affect the performance of a **CFAR** detector applied in the Doppler dimension. To this end, a Blackman window is preferred in the “F” stage of the **XF** algorithm for **CAF** calculation to minimise sidelobe level at the expense of a slightly broader peak in Doppler extent. Furthermore, reviewing the discussion of the **FM** ambiguity function in Section 1.1.3 it was identified that the highest Doppler sidelobes sit offset in range, centred about the peak in the **ARD** surface. This is a useful characteristic as it results in detection of the target peak without influence of the sidelobes. Furthermore, the offset sidelobes rarely produce false alarms.

3.3.4 Pipelining the design

Figure 3.13 illustrates the data flow through the processing server application. The server implements a pipelined data flow using separate threads to perform processing at each stage of the pipeline. Some of these threads wrap calls to GPU kernels where appropriate. IQ data is received either via a socket connection from receiver equipment during live operation or from file on disk during off-line operation. The IQ data is packetised into CPI blocks for processing. The next stage is the GPU based processing which in itself has a sequential progression of cancellation and then range/Doppler processing. Both cancellation and range/Doppler processing are performed on GPU as described in Sections 3.3.1.2 and 3.3.2.6 respectively and these functions therefore have to share the available GPU hardware. There may be multiple GP-GPU capable processors available in the processing server and, as such, the data needs to be partitioned in a way that best exploits the available hardware. The CPI of the cancellation stage is typically a fraction of that of the range/Doppler processing and so cancellation is performed on several cancellation CPIs before the CAF calculation is done on a larger composite CAF CPI. The algorithm for splitting this work up is detailed in Algorithm 3. Each GPU device and corresponding context is wrapped in its own CPU thread to allow for CPU threading structures such as mutexes and condition variables to be used to control data access and flow.

The result of the pipelined design is that the first thread can packetise data while the available GPUs process the previously packetised CPI. This is achieved by a circular buffer for packed data. In the current implementation the buffer operates effectively with only 2 elements and so it functions very similarly to a double buffer. If there are multiple GPUs, while 1 performs the CAF calculation the others can go on to begin cancellation of the next CPI. This guarantees maximum throughput and optimal use of hardware. Furthermore if the continuous incoming data rate is large enough that the processing time is larger than the capture time of the CPI block, the packetising thread will automatically discard samples between CPIs to create block-mode processing. Alternatively if a fixed duty

3.3. PROCESSING DESIGN

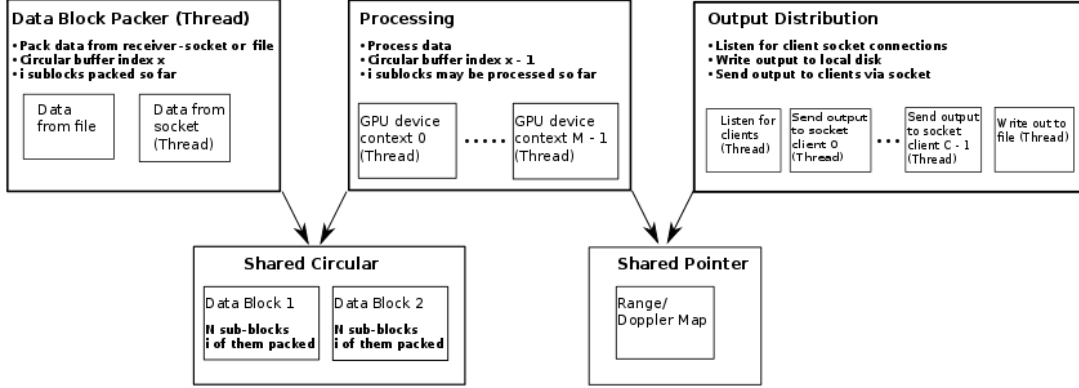


Figure 3.13: Data flow through the Processing Server. Each block shows a class object. Those appended with “(Thread)” run their own concurrent execution path.

Algorithm 3: Data access algorithm for each processing thread and corresponding GPU device in the processing server application

```

1 while AbortProcessingFlag == false do
2   if CancellationBlocks left to cancel in CPI == 0 then
3     Advance circular buffer read pointer;
4     Wait if this element of circular buffer is not yet available for access;
5     Continue;
6   if CancellationBlocks available to process == 0 then
7     Wait for a cancellation block to become available;
8   Get next available cancellation block for processing;
9   Perform CGLS cancellation on that block;
10  CancellationBlocks left to cancel in CPI -= 1;
11  if CancellationBlock was the last in the CPI then
12    //Some threads may be slower than others;
13    if CancellationBlocks left to cancel != 0 then
14      Wait for all cancellation blocks in CPI to be processed;
15    Perform CAF processing on the CPI;
16    Advance circular buffer read pointer;
17    Wait if this element of circular buffer is not yet available for access;

```

3.3. PROCESSING DESIGN

cycle is required the packetising thread can either discard a fixed number of incoming samples or interpret block-mode data from the receiver, that is blocks of data where the receiver digital back-end discards fixed size blocks of samples subsequent the each [CPI](#) sample block.

Once the processing stage has created an [ARD](#) object it is passed on to the [ARD](#) distribution stage. Here a socket server accepts incoming connections from data visualisation clients. Each socket connection is maintained by a thread which has a “send” queue of [ARD](#) maps for its specific client. Lastly a final thread can be started to write [ARD](#) data to local disk from the processing server application. The disk writing thread implements the same queue to act as buffer for potentially high-latency disk storage such as network mounts or externally attached disks.

The final stage of the processing chain takes place in a custom data visualisation client [GUI](#) application. This is the [CFAR](#) detection stage. Owing to the relatively low computation requirements of [CFAR](#) filtering, the [CFAR](#) algorithm can be performed just before displaying the data which allows the observer to tune the [CFAR](#) filter interactively while viewing the data. A screenshot of data visualisation [GUI](#) application called *ARDView* is shown in Figure 3.14. The data visualisation application also provides socket output to pass on [CFAR](#) data to subsequent processing stages such as tracking. These stages are currently under active development.

As an indication of the performance of the system as a whole, a large continuous data recording is fed into processing chain. Typically data fed from a receiver via socket connection will arrive at the packetising thread at approximately 2.5 MB/s for 204.8 KS/s data. When pre-recorded data is loaded into the processing chain from disk it can be supplied to the processing chain at 20 times the speed of live sample data from the receiver and this scenario therefore provides a good indication of the processing chain’s maximum throughput capability. The processing parameters are those typically used for commercial airliner detection with [FM](#) broadcast signals. That is, [CGLS](#) cancellation performed for 10 iterations on [CPIs](#) of 0.5 s (102400 samples) for 250 range bins at zero Doppler. For

3.3. PROCESSING DESIGN

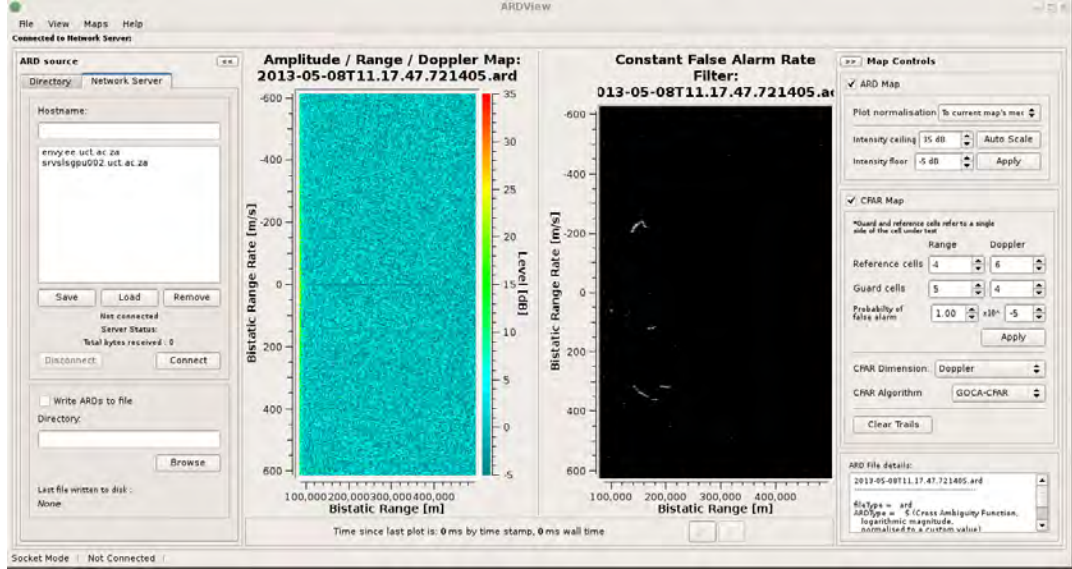


Figure 3.14: Screenshot of ARDView, the data visualisation GUI application which is able to receive ARD data from file or socket connection, draw the ARD map and CFAR of the ARD map on the fly.

the CAF calculation, 4 s CPIs of 819200 samples each and 280 range bins. The ARD map is then cropped to 1601 Doppler bins symmetric about 0 Doppler. CFAR detection is done using GOCA-CFAR with 4 guard cells and 6 reference cells per side of the CUT with a P_{fa} of 10^{-5} .

The ARDView GUI application provides an indication of the input rate of the ARD and CFAR maps that it receives. The data is available at a higher rate than what the processing chain can process. The processing chain therefore runs at maximum throughput. ARDView's update rate can therefore be used to gauge the throughput of the processing chain. When testing this setup using 1 and 2 Geforce GTX840s, the results show that each GPU can execute a CPI of data in approximately $\frac{1}{5}$ of the time it takes to capture the CPI data. This gives an indication of the efficiency of the processing scheme and the ability to expand the processing server to processing more channels (e.g. from multiple DDCs each provided a separate FM broadcast channel) on the same hardware.

The system load that is observed for the same scenarios show that again there is still capacity available on the processing hardware. The CPU hardware is

an AMD Phenom II X4 955 quad-core processor. Even with the application operating at maximum throughput with 2 GPUs only half of the CPUs total resources are used by the processing server application. Also noteworthy is that the system uses a negligible amount (1.3% of the available 16GB) of the systems RAM. This is because the majority of data expansion is performed in GPU memory.

3.4 A Minimalistic Solution

The solution presented above presents what are considered to be highly optimal results which minimise the latency of the throughput. This provides either a detection output soon after the end of the CPI or alternatively the ability to sequentially process multiple bistatic data sets received in parallel from multiple sources before the end of the CPI. As mentioned this might include data from different FM band channels or, possibly, multiple surveillance antennas to in turn allow for AoA techniques or even when there is suitable transmitter infrastructure to process data digitised from several transmitters to gain a multistatic configuration at a single receiver site. At the opposite end of this scale however, is to determine how simple the processing hardware can be for stages up to detection using only single FM band channel in a single bistatic triangle. To this end, 2 possibilities are presented, namely multicore CPU only and the NVIDIA Jetson TK1 [174] platform.

3.4.1 CPU only solution

The first is a CPU only solution. Given that the processing chain design makes use of standardised BLAS and FFT libraries it is straightforward to port to a CPU-only application using appropriate CPU libraries. In this case AMD's AMD Core Math Libraries [175] were selected due to portability and royalty-free license agreement. CPUs cannot easily match the throughput of GPUs when it comes to large matrix-based linear algebra due the massive parallelism of simple

processing elements provided by the GPU. This is clear when reviewing the results presented at the end of this chapter. Only when server-class CPUs are used, in this case a 16-core Intel Xeon, do the timings start to compare to that of the majority of the tested GPUs. This type of hardware is however far more costly and so a GPU solution is deemed to be preferable in all cases.

In all the results presented in the tables below the CPUs were run exploiting all of their available cores to achieve maximum throughput.

3.4.2 NVIDIA Jetson TK1

The NVIDIA Jetson TK1 development kit is a small form factor (12.7 x 12.7 mm) embedded development board equipped with a Kepler series GPU with 192 CUDA cores and a quad-core ARM Cortex A15 CPU in the same chip package. It also features all of the typical desktop style peripherals, most importantly to this application gigabit LAN for sending data to and from the board. The board runs an ARM build of Ubuntu Linux which appears to have most of the typical development packages that regular x86 Ubuntu provides. CUDA and Boost could therefore easily be installed and the processing chain software compiled with no source code modification required. An image of the Jetson is shown in Figure 3.15.

The throughputs of 4 s of sample data in ~ 4 s could be achieved, which will be acceptable in certain use cases. Implementation of the batches algorithm for the GPU could therefore make this platform quite effective albeit one would have to concede the limitations of the batches algorithm as described in Section 3.3.2.3. The timing results for this implementation are shown in more detail in Section 3.6.

The small form factor and lower power consumption of this solution could prove to be useful in applying commensal radar to space, weight and power limited use cases such as airborne platforms [42, 43] or hand-held applications. Chetty describes a through-wall motion detection system based on the exploitation of WiFi signals. The final system is envisioned to be used by law enforcement



Figure 3.15: NVIDIA Jetson TK1 development kit.

during hostage situations and therefore might take on such a hand-held form factor [78].

3.5 Non-coherent ARD Fusion

Near the time of completion of this research, industry partner Peralex Electronics designed and built a purpose specific **FM** band receiver called the “ComRad3” [72] to serve as a research tool for further development of commensal radar capability. An image and flow diagram are shown in Figure 3.16. This hardware is capable of direct sampling the entire **FM** broadcast band on 3 separate phase synchronous **ADCs** concurrently. The **FPGA** of the receiver provides 16 narrow band digital down converters (**DDCs**) which output at 200 kSps, and are available for extracting **FM** channels from the **ADC** data. If 2 **ADCs** are used (i.e. from 2 antennas) then 2 **DDCs** are assigned per **FM** channel. With the 16 **DDCs** this allows for up to 8 **FM** band channels to be extracted. Similarly if all 3 of the **ADCs** are use then 3 **DDCs** are required per **FM** channel. The 16 **DDCs** will then extract up to 5 **FM** channels. This uses 15 **DDCs**, leaving the remaining 1

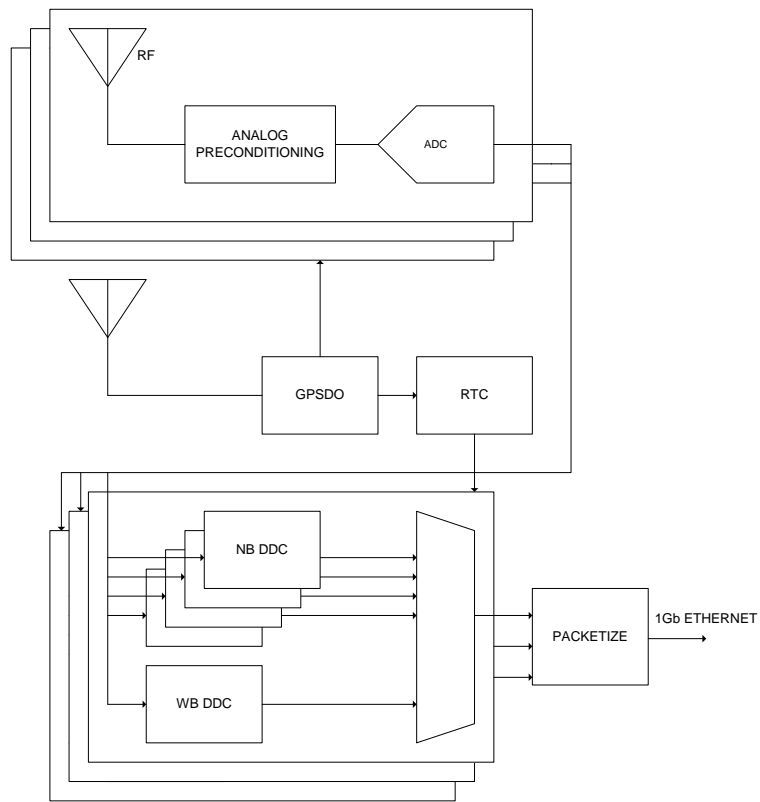
3.5. NON-COHERENT ARD FUSION

unused. Furthermore, a wideband [DDC](#) channelises the 88 - 108 MHz range in a best effort block capture mode to provide an overview of the spectrum of the full [FM](#) band.

3.5. NON-COHERENT ARD FUSION



(a)



(b)

Figure 3.16: Photo and block diagram of the ComRad3 receiver developed by Peralex Electronics. From the block diagram, RTC is realtime clock, NB and WB are narrow band and wide band respectively. Images courtesy of Peralex Electronics.

As demonstrated by Bongioanni [20] and later by Colone [31, 103], non-coherent fusion of data from multiple illuminating channels of the same bistatic geometry in the **ARD** domain can provide improved detection performance due to redundancy against both **FM** modulation bandwidth fluctuations and propagation nulls which will be different for different carrier frequencies. A field test was therefore conducted with the ComRad3 receiver to obtain some initial multi-**FM** channel data recordings to test the receiver capability. A software processing stage to fuse this data in the **ARD** domain was developed and this is presented here as a consideration for future integration for multi-**FM** channel support. The existing processing chain will have to be extended to be able to process several **FM** band streams concurrently and while the performance results suggest that this is possible on current hardware, the integration will require redesign of the data flow in the processing chain and is, as such, listed in the Future Work section (Section 5.1.1).

3.5.1 Algorithm

Fusing multiple **ARDs** non-coherently implies averaging the amplitude information from several **ARD** maps containing data from the same bistatic geometry but generated from sample data captured at different carrier frequencies. Before the averaging takes place each map is normalised to the median of the amplitude of all cells in the respective map. This is a good approximation of the noise floor and therefore ensures that all maps provide equally weighted contributions to the overall cell average. The median normalisation is used for the robust normalisation of the plot surface when viewing in **ARD** space. This is suitably robust when large, nearby targets create large returns in the receiver. Given that this algorithm implementation was already in place for the visualisation of **ARD** data, it is also used as the normalisation method for the non-coherent **ARD** fusion. This does of course require a partial sort of the **ARD** cells based on amplitude which is not necessarily the most computationally efficient way of normalising the data. Colone et al. [31] for example uses a the average piece of **ARD** map and high range/Doppler where targets are not expected to be found.

The median is thought to be a more robust method especially during periods of low signal bandwidth. The difference in execution time between these 2 methods is negligible at 10s of milliseconds.

Care must be taken to ensure that the range and Doppler scales line up. Given that the bistatic geometry is the same and that the ComRad3 receiver output all channels at 200 kSps, the range scales of all [ARD](#) maps will be identical, for the Doppler scale this is not the case as a given value of Doppler in Hertz implies a different bistatic range rate in metres per second for different carrier frequencies. Colone used [FFTs](#) sized proportionally to the respective carrier frequency in the [CAF](#) processing to give effectively equivalent bistatic range rate resolutions [31]. This is not ideal in the current real-time processing chain as this implies different size [CPIs](#) for different carrier frequencies. This complicates the data flow and setup of [GPU](#) memory structures which will need to be different sizes depending on the respective carrier frequency. Such an implementation would therefore require reallocation of memory or redundant space if the same [GPU](#) is used for all frequencies as batch [FFT](#) processing schemes typically expect the same fixed [FFT](#) sizes for all [FFTs](#). Another consideration is that varying the [FFT](#) size might not give the suitable integer on integer ratio to align the velocity bins.

In the signal processing context, changing the [FFT](#) size for the same sample rate, as is the case in this implementation, would change the integration time for different carrier frequencies. This would in turn change the integration gain as per the formula $G_{int} = T_{CPI} * Bw$ where G_{int} is the integration gain, T_{CPI} is the integration time i.e. coherent processing interval and Bw is the bandwidth of the signal. This implies that signals with higher carrier frequencies would have shorter [CPIs](#) to in turn lower the velocity resolution to match that of the signal with lower carrier frequencies and the processing for the higher frequencies would produce less gain proportional to the difference in carrier frequency. This would be detrimental to the averaging process used to merge the maps as those generated from higher carrier frequencies would have a lower [SNR](#). This is further reason why varying the [FFT](#) size is not the preferred way of matching velocity resolution for non-coherent [ARD](#) fusion, but rather nearest neighbour velocity matching with fixed [FFT](#) sizes across carrier frequencies.

Nearest neighbour interpolation allows for arbitrary resolutions to be combined even in the range domain. The interpolation algorithm requires a round-off operation and an array element lookup per [ARD](#) cell and is therefore of minimal computation cost. The nearest neighbour interpolation was also implemented in the range dimension as an optional function if data from different receivers (in the same bistatic geometry) is combined. Different receivers might have different sample rates and therefore require this interpolation. It would also hypothetically allow for the possibility of combining [ARD](#) data from multiple illuminating signal types. For example [FM](#) and [DVB-T](#) are often broadcast from the same tower. The behaviour of such fusion has however, not been tested and would require further investigation to determine if it could be beneficial.

The [ARD](#) fusion software was implemented in standard single threaded C++ code for easy integration into the processing pipeline in the future. It would be wrapped in a worker thread for a new pipeline stage in the real-time processing chain. As with the other stages of processing there is a worker class from which to create a worker object. This object has a member function to which a standard template library ([STL](#)) [176] container of [ARD](#) objects can be added. The worker object then combines these [ARDs](#) into a single output. The output [ARD](#) has the bistatic range rate resolution of the input [ARD](#) which was created from the highest carrier frequency and therefore retains the maximum range rate resolution out of the input [ARDs](#).

3.5.2 Timing and Test Results

[ARDs](#) of size 210 range by 1701 Doppler were combined using an AMD Phenom II X4 955 quad-core processor running in a single thread. Timing was triggered from when the component [ARDs](#) were passed to the worker object to when the resultant [ARD](#) is output in memory. Combination of 8 [ARDs](#) as per the ComRad3 receiver's maximum channel capability for 2 receiver channels active took in the order of ~ 0.45 s to run. 5 [ARDs](#) as per the receivers 3 receiver channel capability scale proportionally at ~ 0.3 seconds. It should be noted however than the 3 receiver channel application will likely involve [AoA](#) and so an extra

quantity in the [ARD](#) information will need to be averaged. This is currently not implemented in the software but it is likely to double the computational time as there will be twice as many single precision floating point numbers to average.

To illustrate the benefits of exploiting multiple [FM](#) channels in the same bistatic geometry, the results of [CFAR](#) filtering performed on a single [ARD](#) vs the output non-coherent [ARD](#) fusion of several [FM](#) channels is shown in [Figure 3.17](#). Specifically, the performance of a single [FM](#) channel is compared to that of a combination of 4 channels. Interesting to note is the averaging of the background noise which, given its exponential nature tends to its mean. This allows for the use of a relaxed threshold without experiencing an increase in the number of false alarms observed. Similar behaviour was reported by both [Bongioanni \[20\]](#) and [Colone \[31\]](#). It is clear that an improvement in detection performance is achievable when exploiting multiple [FM](#) channels in this way.

Based on the visual results and improved performance of the [CFAR](#) detector, the nearest neighbour approach appears to be an effective means of combining [ARD](#) maps with different resolutions. Further investigation into other interpolations such as bilinear interpolation might be considered for future work but this is likely to result in minimal benefit at the expense of increased computational complexity.

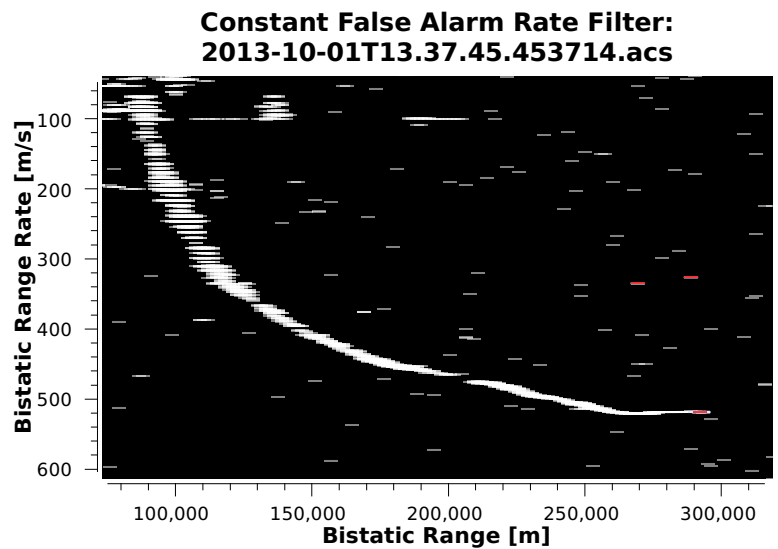
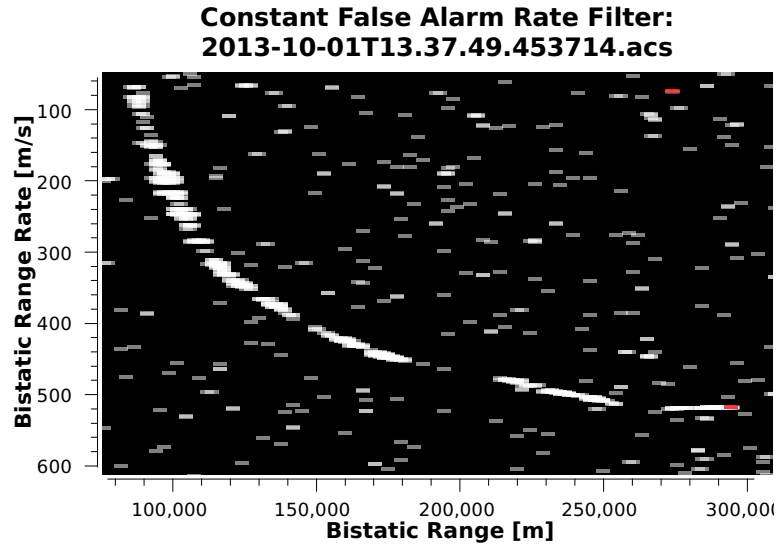


Figure 3.17: Comparison of CFAR outputs generated (a) from 1 FM broadcast channel with $P_{fa} = 10^{-5}$ and (b) from a combination of 4 FM broadcast channels with the detection threshold relaxed by 3 orders of magnitude against the same noise model. The multichannel combination provides better detection capability and less false alarms due to the averaging of the background noise. The extra detection seen at 150 km, 100 m/s in the multichannel data is a result of target ghosting (the effects of which, are described by Tong et al. [70]) caused by multipath that is more prominent at some of the combined frequencies. The results presented here are from real data collected in the field with UCT prototype radar system and the Peralex ComRad3 [72] receiver.

3.6 Summary of Timing Results

This section presents a summary of all the timing results of the processing chain design discussed in this chapter. Results for additional configurations of the processing hardware are also included for completeness and to give a more general idea of software performance on a variety of hardware configurations.

For individual timings of stages, results are presented on the processing pipeline as per the data flow order. This is followed by a section on the maximum achievable pipeline throughput.

3.6.1 DPI and Clutter Suppression

Table 3.6.1 shows timings for the DPI and clutter suppression stage using CUDA capable GPUs and libraries. The timings show processing from when a CPI of sample data is available in CPU memory to when it is completely processed by a single GPU and back in CPU memory. This test is done as a one-shot measurement of the complete 4 s CPI (819200 samples) which is sequentially processed in 8 equal sub-CPIs of 0.5 s (102400 samples) due to memory limitations and to generalise the Doppler resolution. The timings for the same processing parameters are also presented in a CPU-only build of the cancellation algorithm using AMD's AMD Core Math Libraries. This is shown in Table 3.6.1

In the complete processing chain implementation the data packetisation is pipelined with the DPI and clutter cancellation at a sub-CPI level which allows the first sub-CPI to be processed as soon as those 102400 samples have been received from the receiver. The sub-CPIs cancellation processing is also parallelised across GPUs given available hardware. This will therefore reduce the overall processing chain latency to less than the sum of the singular processing times presented in these tables. This is evident when reviewing the maximum throughput timings in Table 3.6.5. The latency is reduced by more or less a factor equal to the number of GPUs given similar GPU devices. Note that the Tegra K1 on the Jetson board has exactly half (192) of the GT640's 384 CUDA cores and that

3.6. SUMMARY OF TIMING RESULTS

the timing has approximately scaled accordingly.

A comparison of the equivalent **CPU** only implementation of the processing stage is shown in Table 3.6.1 which is built with AMD Core Math Libraries.

Table 3.1: Timing of **DPI** and clutter suppression on different **GPU** hardware using **CUDA** libraries for a single bistatic pair and single **FM** broadcast channel. Details of the processing scheme are included below the timings.

CPU	GPU	Execution time
Intel Core 2 Quad Q9400, quad-core 2.66 GHz	1x NVIDIA Geforce GT640	1769 ms
AMD Phenom II X4 955, quad-core 3.2 GHz	1x NVIDIA Geforce GTX480	575 ms
Intel I7 960, quad-core 3.2 GHz	1x NVIDIA Geforce GTX570	366 ms
Intel Xeon E5-2650, 16-core 2 GHz	1x NVIDIA Tesla M2090	410 ms
ARM Cortex A15 “r3” quad-core 2.3 GHz	1x NVIDIA Tegra K1	3059 ms

Operation	Parameters / Data dimensions / Details
Data input	Sample data in CPU memory
DPI and clutter suppression	CGLS algorithm, 10 iterations, 8x CPIs of 102400 samples, 210 range bins, 1 Doppler bins
Data output	Sample data with interference suppressed surveillance channel in CPU memory

3.6. SUMMARY OF TIMING RESULTS

Table 3.2: Timing of **DPI** and clutter suppression on different **CPU** only hardware using AMD Core Math Libraries for a single bistatic pair and single **FM** broadcast channel. Details of the processing scheme are included below the timings.

CPU	Execution time
AMD Turion 64 X2 Mobile TL-63, dual-core 2.1 GHz	18210 ms
Intel I5 760, quad-core 2.8 GHz	1780 ms
Intel Xeon E5-2470, 16-core 2.3 GHz	1630 ms

Operation	Parameters / Data dimensions / Details
Data input	Sample data in CPU memory
DPI and clutter suppression	CGLS algorithm, 10 iterations, 8x CPIs of 102400 samples, 210 range bins, 1 Doppler bins
Data output	Sample data with interference suppressed surveillance channel in CPU memory

3.6.2 CAF Processing

Table 3.6.2 shows the processing times for the CAF calculation to produce ARD maps using CUDA capable GPUs and libraries. Once again this is the processing time from when the full CPI of 4 s is in the CPU memory as sample data to when the ARD maps created by a single GPU and copied back to CPU memory. Notice that these times are consistently less than the DPI and clutter suppression stage. It is interesting to note here that the Tegra performance does follow the trend of being approximately double the time of the GT640. This suggests that the performance of the FFT modules are architecture-dependant.

The timings for the same processing parameters are also presented in a CPU only build of the CAF algorithm using AMD's AMD Core Math Libraries. This is shown in Table 3.6.2. As can be observed this processing time is often prohibitively long on these architectures and so the same dimensions are processed using the batches algorithm, the results of which are shown in Table 3.6.2. As can be observed the batches algorithm provides significant speed-ups over the XF algorithm.

3.6. SUMMARY OF TIMING RESULTS

Table 3.3: Timing of CAF calculation on different GPU hardware using CUDA libraries for a single bistatic pair and single FM broadcast channel. Details of the processing scheme are included below the timings.

CPU	GPU	Execution time
Intel Core 2 Quad Q9400, quad-core 2.66 GHz	1x NVIDIA Geforce GT640	544 ms
AMD Phenom II X4 955, quad-core 3.2 GHz	1x NVIDIA Geforce GTX480	220 ms
Intel I7 960, quad-core 3.2 GHz	1x NVIDIA Geforce GTX570	157 ms
Intel Xeon E5-2650, 16-core 2 GHz	1x NVIDIA Tesla M2090	191 ms
ARM Cortex A15 “r3” quad-core 2.3 GHz	1x NVIDIA Tegra K1	1420 ms

Operation	Parameters / Data dimensions / Details
Data input	Sample data in CPU memory
CAF calculation	XF algorithm, CPI of 819200 samples, 280 range bins, cropped to 1601 Doppler bins
Data output	ARD map magnitude data in CPU memory

3.6. SUMMARY OF TIMING RESULTS

Table 3.4: Timing of CAF calculation on different CPU only hardware using the XF CAF algorithm and AMD Core Math Libraries for a single bistatic pair and single FM broadcast channel. Details of the processing scheme are included below the timings.

CPU	Execution time
AMD Turion 64 X2 Mobile TL-63, dual-core 2.1 GHz	20360 ms
Intel I5 760, quad-core 2.8 GHz	4100 ms
Intel I7 960, quad-core 3.2 GHz	3980 ms
Intel Xeon E5-2470, 16-core 2.3 GHz	1150 ms

Operation	Parameters / Data dimensions / Details
Data input	Sample data in CPU memory
CAF calculation	XF algorithm, CPI of 819200 samples, 280 range bins, cropped to 1601 Doppler bins
Data output	ARD map magnitude data in CPU memory

3.6. SUMMARY OF TIMING RESULTS

Table 3.5: Timing of CAF calculation on different CPU only hardware using the batches CAF algorithm and AMD Core Math Libraries for a single bistatic pair and single FM broadcast channel. Details of the processing scheme are included below the timings.

CPU	Execution time
AMD Turion 64 X2 Mobile TL-63, dual-core 2.1 GHz	208 ms
Intel I5 760, quad-core 2.8 GHz	47 ms
Intel I7 960, quad-core 3.2 GHz	45 ms
Intel Xeon E5-2470, 16-core 2.3 GHz	20 ms

Operation	Parameters / Data dimensions / Details
Data input	Sample data in CPU memory
CAF calculation	Batches algorithm, batch length 280, CPI of 819200 samples, 280 range bins, cropped to 1601 Doppler bins
Data output	ARD map magnitude data in CPU memory

3.6.3 CFAR Filtering

Table 3.6.3 shows the execution times of the CFAR processing using the greater-of-cell averaging CFAR filter. This processing is performing by the data visualisation GUI due to its relatively low execution time for the provision of quick interactive tunability and is therefore run on desktop or laptop computing hardware. An example of a typical desktop and a laptop are presented. As indicated this process takes only several milliseconds and, therefore largely negligible in the context of the larger processing chain. It is however executed in a single thread and given that the algorithm is highly parallel the processing time could be further reduced proportionally to the number of available CPU cores. Ordered statistic based CFAR tends to be more computationally demanding as it requires a partial sort of the background cells. It does however remain an embarrassingly parallel algorithm. These results are presented in Table 3.6.3 for completeness.

Table 3.6: Timing of CFAR calculation of the GOCA-CFAR on different hardware for a single bistatic pair and single FM broadcast channel. Details of the processing scheme are included below the timings.

CPU	Execution time
AMD Turion 64 X2 Mobile TL-63, dual-core 2.1 GHz	13 ms
Intel I5 760, quad-core 2.8 GHz, quad-core 2.66 GHz	8 ms

Operation	Parameters / Data dimensions / Details
Data input	ARD map in CPU memory, 280 range bins, 1601 Doppler bins
CFAR Algorithm	GOCA-CFAR, 4 guard cells, 6 reference cells (per side of CUT), $P_{fa} = 10^{-5}$
Number of parallel threads	1
Data output	Vector of CFAR detection co-ordinates in CPU memory

3.6. SUMMARY OF TIMING RESULTS

Table 3.7: Timing of OS-CFAR calculation on different hardware for a single bistatic pair and single FM broadcast channel. Details of the processing scheme are included below the timings.

CPU	Execution time
AMD Turion 64 X2 Mobile TL-63, dual-core 2.1 GHz	118 ms
Intel I5 760, quad-core 2.8 GHz, quad-core 2.66 GHz	64 ms

Operation	Parameters / Data dimensions / Details
Data input	ARD map in CPU memory, 280 range bins, 1601 Doppler bins
CFAR Algorithm	OS-CFAR, order 4, 4 guard cells, 6 reference cells (per side of CUT), $P_{fa} = 10^{-5}$
Number of parallel threads	1
Data output	Vector of CFAR detection co-ordinates in CPU memory

3.6.4 Non-coherent ARD Fusion

Table 3.6.4 shows the execution times of the non-coherent ARD fusion. This stage is not currently implemented in the complete processing chain, however, this capability is intended to be implemented in the near future. The processing is envisioned to be performed in a CPU thread of the processing server (which also does the GPU processing for the DPI and clutter suppression and CAF processing) and the timing was therefore measured on appropriate hardware. This algorithm is also highly parallel and the processing time could therefore, as with the CFAR stage, be reduced proportional to number of available CPU cores. Implementation on GPU might also be considered.

3.6. SUMMARY OF TIMING RESULTS

Table 3.8: Timing of non-coherent [ARD](#) fusion on different hardware for a single bistatic pair and several [FM](#) broadcast channels. Details of the processing scheme are included below the timings.

CPU	Number of ARDs	Execution time
AMD Phenom II X4 955, quad-core 3.2 GHz	8	450 ms
AMD Phenom II X4 955, quad-core 3.2 GHz	5	295 ms
Intel I7 960, quad-core 3.2 GHz	8	380 ms
Intel I7 960, quad-core 3.2 GHz	5	275 ms

Operation	Parameters / Data dimensions / Details
Data input	ARD map magnitude data in CPU memory
ARD size	1701 range bins, 210 Doppler bins
Interpolation	Range: none, Doppler: nearest neighbour
Number of parallel threads	1
Data output	Fused ARD map magnitude data in CPU memory

3.6.5 Maximum Throughput

Table 3.6.5 shows the maximum throughput that can be achieved when data is loaded from hard disk at maximum speed. It is shown that the processing pipeline can produce an output of **ARD** and **CFAR** map pairs every ~ 190 ms using 3 high-end but previous generation NVIDIA Geforce **GPU**s. Better performance was achieved on a cluster machine boasting 4 NVIDIA Tesla M2090 which allows the cancellation stage to use an extra channel of parallelism. The maximum update rate of output data appears to be largely equal to the processing time taken for a single **GPU** divided by the number of **GPU** devices (assuming each **GPU** is similar). This scaling will however taper off as the number of devices nears the number of cancellation **CPI**s with the current scaling algorithm. The timings also show that it should be possible to process many concurrent channels of **FM** data on a single computer equipped with multiple **GPU**s.

Another notable result is that of the top entry in Table 3.6.5. The NVIDIA Geforce GT640 is a ~ 100 US Dollar, mid range **GPU** and, as indicated by timings, is quite capable of processing the 4 s **CPI**s in under 4 s. It can therefore provide output for 100% duty cycle of sample data for a single **FM** channel and single bistatic pair. The GT640 doesn't require a high capacity desktop power supply as all the other **GPU**s referred to in this thesis do. 350 W, which has been typical entry level power supply rating for desktop computers for some time, is adequate and the GT640 can therefore be used in most current or prior generation desktop computers to provide low cost commensal radar signal processing on the fly. The latency requirements for the greater system will, of course need to be considered, but during the research and development stages such as the work being undertaken at the University of Cape Town, it should prove to be adequate in stable and mild clutter environments.

Tables 3.6.5 and 3.6.5 show equivalent **CPU** only processing schemes implemented using AMD Core Math Libraries using the **XF** and **batches** algorithms for **CAF** calculation respectively. As can be seen even with the large speed-ups of the **batches** algorithm and when making use of server class hardware the **GPU** implementation still provides mostly better performance. Furthermore, the **GPU**

3.6. SUMMARY OF TIMING RESULTS

Table 3.9: Maximum throughput for off-line processing of complete processing chain on different GPU hardware using CUDA libraries for a single bistatic pair and single FM broadcast channel. The output interval indicates the amount of time between successive ARD and CFAR map pair outputs. Details of the processing scheme are included below the timings.

CPU	GPU	Output interval
Intel Core 2 Quad Q9400, quad-core 2.66 GHz	1x NVIDIA Geforce GT640	2547 ms
AMD Phenom II X4 955, quad-core 3.2 GHz	1x NVIDIA Geforce GTX480	810 ms
AMD Phenom II X4 955, quad-core 3.2 GHz	2x NVIDIA Geforce GTX480	410 ms
Intel I7 960, quad-core 3.2 GHz	1x NVIDIA Geforce GTX570	535 ms
Intel I7 960, quad-core 3.2 GHz	1x NVIDIA Geforce GTX570, 2x NVIDIA Geforce GTX480	175 ms
Intel Xeon E5-2650, 16-core 2 GHz	1x NVIDIA Tesla M2090	615 ms
Intel Xeon E5-2650, 16-core 2 GHz	2x NVIDIA Tesla M2090	307 ms
Intel Xeon E5-2650, 16-core 2 GHz	4x NVIDIA Tesla M2090	150 ms
ARM Cortex A15 “r3” quad-core 2.3 GHz	1x NVIDIA Tegra K1	4690 ms

Operation	Parameters / Data dimensions / Details
Data input	Local hard disk
DPI and clutter suppression	8x CPIs of 102400 samples, 210 range bins, 1 Doppler bins
CAF calculation	XF algorithm, CPI of 819200 samples, 280 range bins, cropped to 1601 Doppler bins
Data output from processing server	Gigabit Ethernet to client running ARDView
CFAR filtering	GOCA-CFAR, 4 guard cells, 6 reference cells (per side of CUT), $P_{fa} = 10^{-5}$ done on Intel Core 2 Quad Q9400, quad-core 2.66 GHz
Final data output	Display of data in ARDView

3.6. SUMMARY OF TIMING RESULTS

solution will come at a fraction of the cost and typically in a smaller form factor.

Table 3.10: Maximum throughput for off-line processing of complete processing chain on different CPU hardware using the XF CAF algorithm and AMD Math Core Libraries for a single bistatic pair and single FM broadcast channel. The output interval indicates the amount of time between successive ARD and CFAR map pair outputs. Details of the processing scheme are included below the timings.

CPU	Output interval
AMD Turion 64 X2 Mobile TL-63, dual-core 2.1 GHz	39520 ms
Intel I5 760, quad-core 2.8 GHz	7680 ms
Intel I7 960, quad-core 3.2 GHz	7380 ms
Intel Xeon E5-2470, 16-core 2.3 GHz	2761 ms

Operation	Parameters / Data dimensions / Details
Data input	Local hard disk
DPI and clutter suppression	8x CPIs of 102400 samples, 210 range bins, 1 Doppler bins
CAF calculation	XF algorithm, CPI of 819200 samples, 280 range bins, cropped to 1601 Doppler bins
Data output from processing server	Gigabit Ethernet to client running ARDView
CFAR filtering	GOCA-CFAR, 4 guard cells, 6 reference cells (per side of CUT), $P_{fa} = 10^{-5}$ done on Intel Core 2 Quad Q9400, quad-core 2.66 GHz
Final data output	Display of data in ARDView

3.6. SUMMARY OF TIMING RESULTS

Table 3.11: Maximum throughput for off-line processing of complete processing chain on different CPU hardware using the batches CAF algorithm and AMD Math Core Libraries for a single bistatic pair and single FM broadcast channel. The output interval indicates the amount of time between successive ARD and CFAR map pair outputs. Details of the processing scheme are included below the timings.

CPU	Output interval
AMD Turion 64 X2 Mobile TL-63, dual-core 2.1 GHz	19540 ms
Intel I5 760, quad-core 2.8 GHz	3280 ms
Intel I7 960, quad-core 3.2 GHz	3110 ms
Intel Xeon E5-2470, 16-core 2.3 GHz	1600 ms

Operation	Parameters / Data dimensions / Details
Data input	Local hard disk
DPI and clutter suppression	8x CPIs of 102400 samples, 210 range bins, 1 Doppler bins
CAF calculation	Batches algorithm, batch length of 280, CPI of 819200 samples, 280 range bins, cropped to 1601 Doppler bins
Data output from processing server	Gigabit Ethernet to client running ARDView
CFAR filtering	GOCA-CFAR, 4 guard cells, 6 reference cells (per side of CUT), $P_{fa} = 10^{-5}$ done on Intel Core 2 Quad Q9400, quad-core 2.66 GHz
Final data output	Display of data in ARDView

3.6.6 Comparison of Computation

Figure 3.18 shows the comparison of the processing time of each stage of the processing chain running in a single core of a CPU. AMD Core Math Libraries are used for the DPI and clutter suppression stages. The timing results are from running in a single thread on an Intel I5 760 quad-core 2.8 GHz CPU. This aims to give an indication of the relative amount of computation that is required for each stage. It is this break-down that indicates that using GPU hardware only for the DPI and clutter suppression stages is a more efficient approach as remaining stages are easily pipelined in CPU threads. The processing parameters used are the same as that shown in Tables 3.6.5 and 3.6.5.

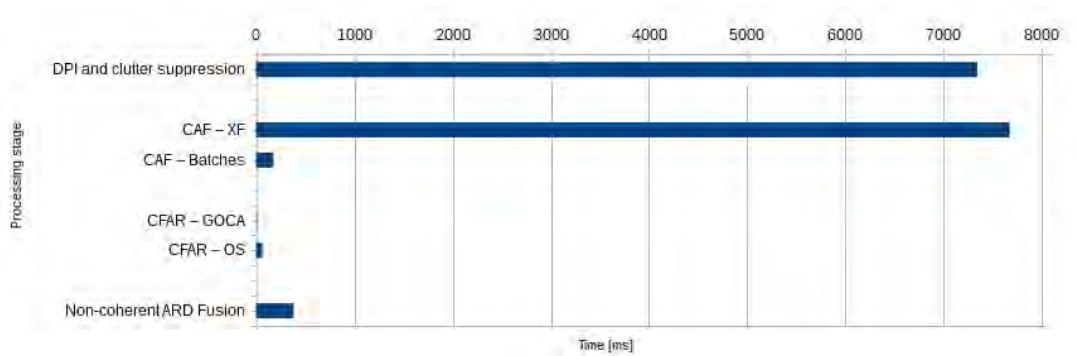


Figure 3.18: Comparison of execution time of various stages of the processing chain executed on a single thread of a CPU.

3.7 Conclusions

A complete design of a real-time processing chain for a commensal radar system is presented, making use of commercial off the shelf computing and GP-GPU capable GPU hardware. The processing chain includes stages of packetisation from the receiver, DPI and clutter suppression (cancellation), range/Doppler processing and finally detection by CFAR filter. Algorithms for each stage are compared and an implementation is described for a processing chain where the CGLS algorithm is used for cancellation on GPU hardware due to the algorithms

3.7. CONCLUSIONS

lower memory footprint and iterative refinement approach, the [XF](#) algorithm for [CAF](#) calculation is chosen for its mathematical optimality as well as suitability to the dimensions of the typical [ARD](#) map of the [FM](#) broadcast band radar and is efficiently implemented on [GPU](#) exploiting the [CUDA FFT](#) library's batch mode. Lastly the [GOCA-CFAR](#) algorithm is implemented in the [GUI](#) display software to perform detection.

It is empirically shown that better than real-time throughput can be achieved using the described algorithms on several different variations of hardware consisting of multi-core [CPUs](#) as well as [GPUs](#) where the variations of [GPU](#) include previous generation (at the time of writing), high-end gaming hardware in the form of NVIDIA Geforce GTX480 and GTX570. Low-cost mid-level hardware in the form of NVIDIA Geforce GT640 and high-end [GP-GPU](#) specific [GPUs](#) in the form of NVIDIA Tesla M2090s. With limited data dimensions the NVIDIA Jetson TK1 embedded platform can achieve real-time throughput using the complete processing chain with optimal [XF CAF](#) algorithm. This is an interesting detail for space, size and weight limited use-cases such as airborne platforms [42, 43]. The presented processing chain scales automatically to these variations in hardware and also to multiple [GPU](#) devices requiring no alteration of source code.

Equivalent [CPU](#)-only solutions are presented but rely on non-optimal [CAF](#) calculation unless a server-class multicore [CPU](#) is used which is typically a high cost and non-portable platform.

A method for non-coherent combination of [ARDs](#) that are created from different frequencies in the same bistatic geometry is also presented which uses nearest neighbour interpolation to combine the [ARD](#) data which might exist at different resolutions over the same scale. It is shown that 8 [ARDs](#) of 210 by 1701 cells can be combined under 500 ms in the single thread on a current [CPU](#). This latency could be reduced by parallelising across more threads if necessary or the calculation could be moved to [GPU](#).

It is clear that a fully functional commensal radar system will require more than the processing of a single bistatic triangle and a single [FM](#) band channel and as such the high throughput capabilities of the [GPU](#) should be highly attractive to

the commensal radar system designer.

3.7.1 Future Work

The following aspects are intended to be investigated or implemented in the future.

Multi-FM Channel capability and angle of arrival

The most immediate improvement that is intended for this processing chain is to add capability for processing multiple [FM](#) channels for the same bistatic geometry and non-coherent combining to improve the detection performance of the system given that the newly developed ComRad3 receiver is capable of providing multiple [FM](#) channels concurrently. Furthermore, the ComRad3's ability to digitise from a third antenna feed provides the capability for [AoA](#) and this capability should also be included.

Integration of a Control GUI Client

The processing chain is currently configured by a configuration file. Initial framework exists for control by [GUI](#) based network client to make parameter changes easier. The final integration of this software needs to be completed. Integration for control of the ComRad3 receiver into the same [GUI](#) software is also intended, to streamline overall control of the radar system.

Development of a Tracking Scheme

Tracking is not discussed in this thesis in any great detail but in the context of a working radar system it will prove critical. Work has already been done at the University of Cape Town to investigate tracking for commensal radar systems [[30](#), [53](#)] and it is likely to require further innovation to make a sufficiently robust

tracking system that can extract the most out of the measurement information that the commensal radar processing chain can provide.

Compressive Sampling

Given that the modulation bandwidth fluctuations of the [FM](#) broadcast signal, the sample rate will often end being well beyond the Nyquist requirement. Compressive sample techniques might help to minimise this potentially inefficient behaviour. Furthermore, if one considers the [FM](#) channels broadcast from any [FM](#) transmitter site, the spectrum across the entire 88 to 108 MHz can be viewed as sparse for that transmitter site which also suggests the application of compressive sampling techniques.

Chapter 4

The Separated Reference Configuration

4.1 Introduction

This chapter presents a novel configuration for a multi-site, multistatic commensal radar system in which a single reference signal is recorded (per illuminating channel that is exploited) at an optimal site for recording the specific reference signal. Multiple surveillance receivers are then set up at various sites to record a diversity of surveillance data. Temporal coherency is maintained by the use of GNSS disciplined oscillators in all receiver nodes. Sample data is brought to a central processing node over a data network where the radar signal processing is performed. This configuration allows the reference antenna to be optimally placed at a site where there is a clear LoS to the transmitting antenna and furthermore, a site can be selected where multipath effects are minimal. The surveillance antennas can be placed where they have optimal aspect of the surveillance region of interest and also where DPI and clutter are at a minimum. This configuration of radar receiver nodes is termed the *separated reference* configuration as shown in Figure 4.1. The data flow of the system is illustrated in Figure 4.2

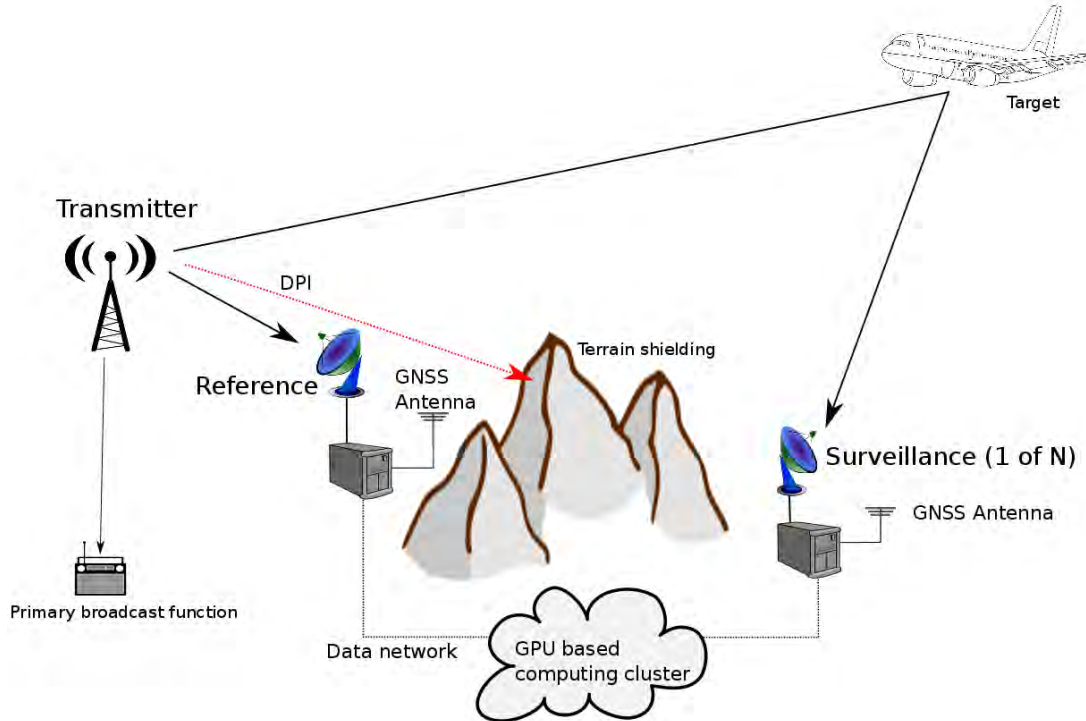


Figure 4.1: The separated reference configuration allows optimal placement of both the reference and surveillance antennas.

The concept of splitting the receiver channels to separate receivers was first demonstrated for the Manastash Ridge Radar [57][6, Ch. 7] which was a bistatic system developed for atmospheric monitoring. This concept is now extended to a multistatic case for the purpose of detecting aircraft. This chapter presents some initial results of field testing this configuration which is believed to be novel in a multistatic, multi-site (3 or more nodes) commensal radar configuration for the purpose of aircraft detection. It is practically demonstrated that equal if not better performance can be achieved with the separated reference configuration over the traditional co-located architecture while adding the simplicity to the receiver site selection because each receiver needs only to perform a single function which would be either reference or surveillance signal capture.

The obvious limitation of the separated reference configuration is that a suitable data network is required between the receiver nodes to transport the sample data to a central processing node but where this infrastructure exists the benefits of

4.2. FIELD TESTS AND RESULTS

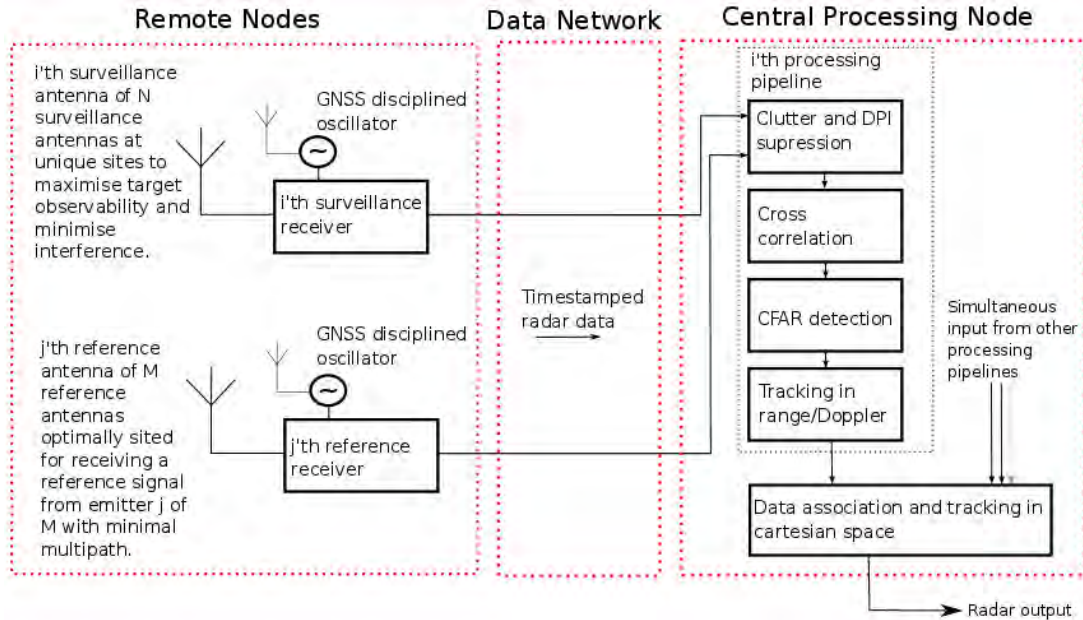


Figure 4.2: Flow diagram of a complete commensal radar system making use of the the separated reference configuration.

the configuration can be exploited. For example, many academic and research institutions in South Africa are connected to a high speed fibre network called the South African National Research Network (SANReN) [177] and so the campuses of these institutions could be evaluated as potential radar receiver sites. Similarly many cellular base stations are connected together by fibre network for their back-hauls. Further networking considerations are discussed in Section 4.5.2

4.2 Field Tests and Results

This sections details field tests done to prove the separated reference configuration concept in multi-site deployment. FM broadcast signals were used for the purpose of detecting commercial airliner aircraft.

4.2.1 Deployment

To test the separated reference configuration in a practical environment, 3 GPSDO equipped receivers were deployed around the Western Cape of South Africa to detect air traffic to and from Cape Town International Airport (see Figure 4.3). The receivers each provide 2 receiver channels so co-located reference and surveillance antennas were deployed at each site. This would allow for a variety of comparisons to be made using the recorded data. Reference channels from any of the sites can be combined with surveillance channels from any of the other sites and compared to the co-located cases. Given the absence of a suitable data network during this deployment all data was recorded to disk at each respective receiver site for later off-line processing.

4.2.2 Reduction of Multipath

The Tygerberg receiver site as shown in Figure 4.3 has good aspect over the predominant flight path in and out of Cape Town International Airport, and as good a terrain shielding as one could hope for in a co-located deployment by being located just over the edge of a steep hill from the transmitter to be exploited. The site does however, have a disadvantage in that it is subject to large multipath reflections from several large terrain structures all lying at the same bistatic range of ~ 60 km. This geometry is illustrated in Figure 4.4.

The multipath caused by the terrain structures shown in Figure 4.4 is so severe that it causes a large secondary peak in correlation processing at a delay equivalent to 60 km of bistatic range. The effects of this are shown in Figure 4.5 where a target moves from 60 km, -160 ms^{-1} to 15 km, -90 ms^{-1} and a ghost target can be observed at ~ 49 km greater bistatic range for the duration of the target motion. This ghost distance corresponds to the 60 km terrain structures minus the 11 km bistatic baseline.

In a co-located configuration this multipath would be impingent on both the reference and surveillance antennas. For the surveillance channel this multi-

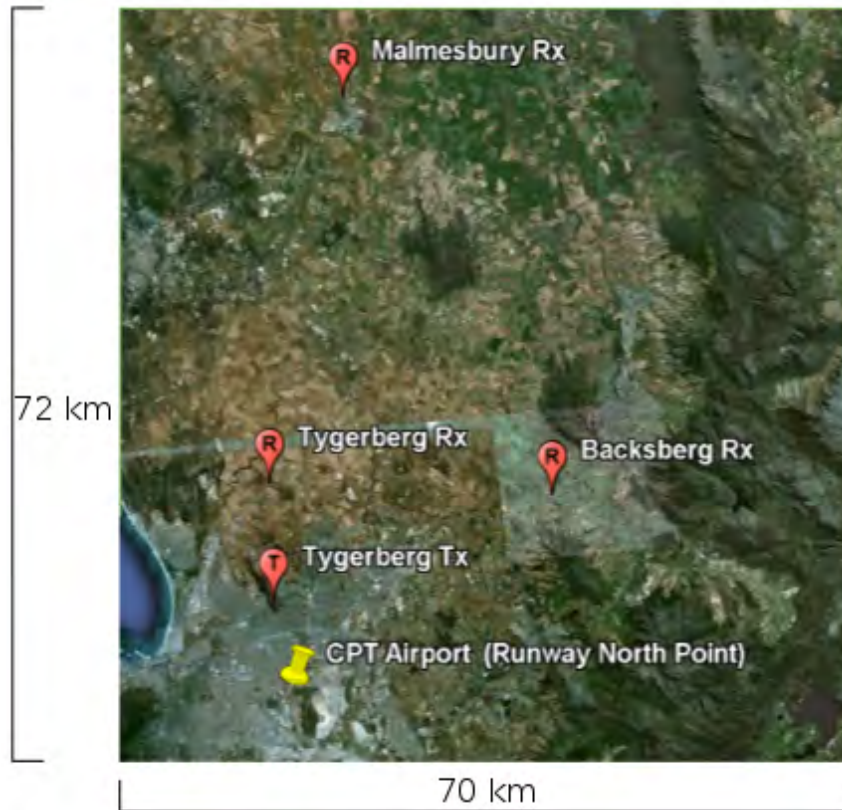


Figure 4.3: Locations of the receiver nodes marked by ‘R’s and the transmitter with was exploited marked by the ‘T’. The Cape Town International Airport is shown by the thumbtack. The predominant air traffic comes from the North-East.

path would present itself as clutter in the model represented by Equation 3.2 in Chapter 3 and can therefore be suppressed to a large degree by a DPI and clutter suppression algorithm such the CGLS implementation described in Section 3.3.1.2. In the case of the reference channel the effects are more problematic. These multipath returns change the form of the digitised reference signal compared to the transmitted signal which is incident on, and reflected by targets of interest. This directly degrades the performance of the matched filter and also the DPI and clutter suppression stage where the reference signal is used in the construction of the A matrix (see Equation 3.2) which models the interference. When the A matrix contains multipath contributions, it corrupts the clutter model which will then not be well representative of the DPI and clutter in the

4.2. FIELD TESTS AND RESULTS



Figure 4.4: The Tygerberg receive site has good aspect of the predominant flight path to the North-East but it suffers from severe multipath effects at 60 km bistatic range due to many large terrain structures lying at this range as shown by the red ellipse and thumbtacks.

surveillance channel. The [DPI](#) and clutter suppression algorithm will therefore not suppress the interference correctly and also possibly corrupt skin echoes in the surveillance signal when the [DPI](#) and clutter subtraction is applied. This could in turn result in further losses in the matched filter processing.

Colone et al. propose a cleaning algorithm for the reference channel before it is used for the [DPI](#) and clutter suppression and matched filter stages of the processing chain [89]. This can be a complicated process for a complex multipath environment and if the space-time technique is to be exploited an antenna array and multichannel receiver is necessary for capturing the reference channel which can raise equipment cost and complexity significantly.

Given that the site for the reference antenna need only have clear LoS to the transmitting antenna, a site optimisation can be performed with relative ease

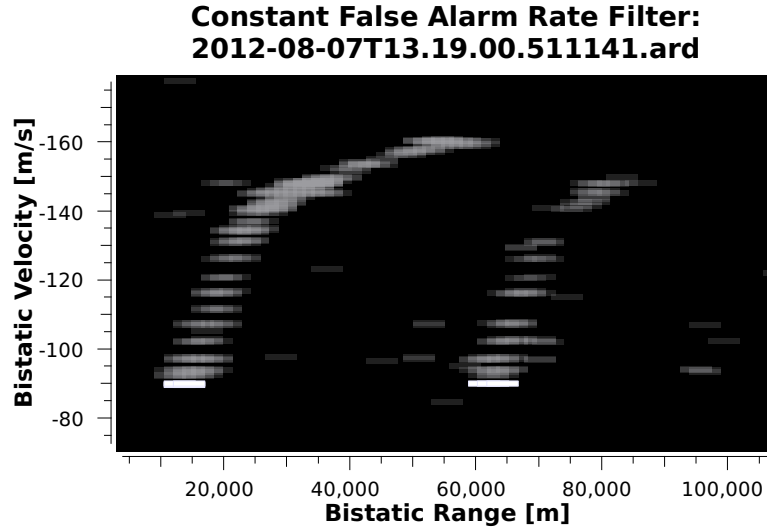


Figure 4.5: **CFAR** detections with the co-located configuration show target ghosting created by the large multipath returns at 60 km bistatic range at the Tygerberg receiver site.

when using the separated reference configuration. To illustrate, Figure 4.6 shows simple propagation modelling of the reference signal from the Tygerberg transmitter using Radio Mobile software [178] and terrain elevation data of the region. Once a suitable minimal signal level has been determined based on the receiver sensitivity and the antenna to be used, several sites with suitable reference signal level can be tested until one with minimal multipath is found. The level of multipath can be determined by mapping an **ARD** of the auto ambiguity function (**AAF**) of the reference signal which is essentially the **CAF** of the reference signal with itself.

To demonstrate that the separated reference can be used to remove the effects of multipath, the 2 other receiver sites from the deployment shown in Figure 4.3 were examined to determine if either of them could offer a significantly cleaner reference signal. The **AAF ARD** maps of the reference signals for all 3 sites are shown in Figure 4.7. The Tygerberg site contains maximum multipath at 14.8 dB below the 0 delay peak at 60 km bistatic range as per the terrain structures described in Figure 4.4. The Backsberg site, 11.8 dB below the 0 delay peak. This is as a result of the close proximity (28 km) to Paarl mountain, the location

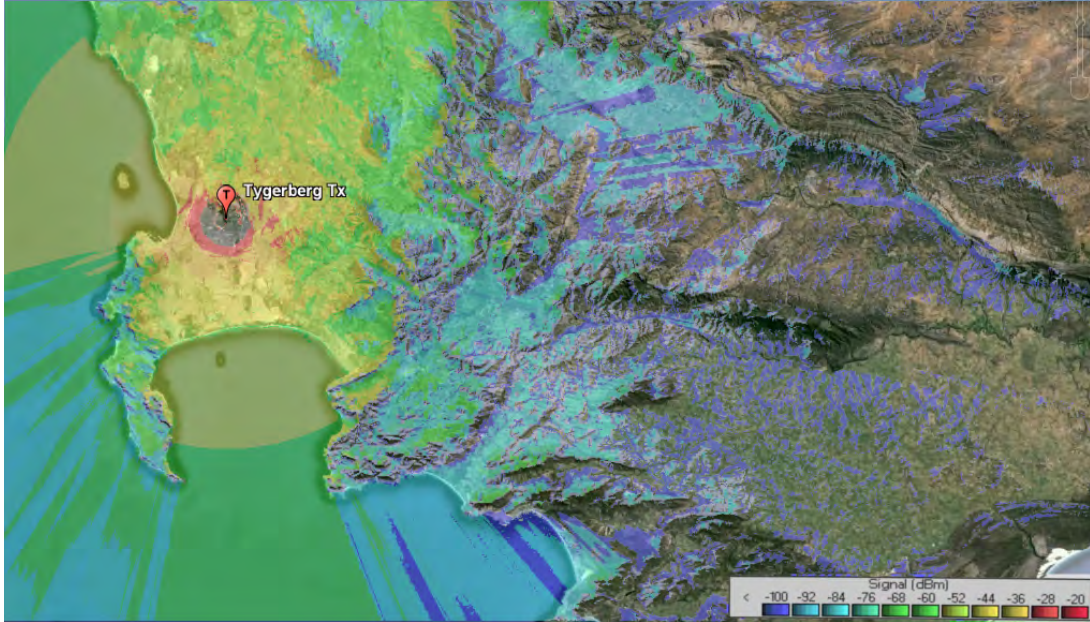


Figure 4.6: Modelling of signal strength at ground level for transmissions from the 1.3 kW 88.2 MHz FM broadcast channel on the Tygerberg transmitter in the Western Cape of South Africa. This data was generated with Radio Mobile software [179] and 30 m digital terrain elevation and overlaid in Google Earth. Figure courtesy of Francois Maasdorp, Council for Scientific and Industrial Research, DPSS Unit

of which is also shown in Figure 4.4. Finally the Malmesbury site is furthest from most of the large terrain structures and therefore has multipath with a maximum of 29.2 dB below the 0 delay peak and therefore provides a ~ 15 and ~ 18 dB reduction in multipath compared to the reference signals recorded at Tygerberg and Backsberg respectively.

Figure 4.8 shows the CFAR map which was generated using the same surveillance data recorded at the Tygerberg site as shown in Figure 4.5. Here instead of using both surveillance and reference data from the Tygerberg site, the time corresponding reference data from Malmesbury was used to feed an identical processing chain of DPI and clutter suppression, CAF calculation and CFAR filtering. As can be observed the target ghost is totally removed while the true target is detected as before.

4.2. FIELD TESTS AND RESULTS

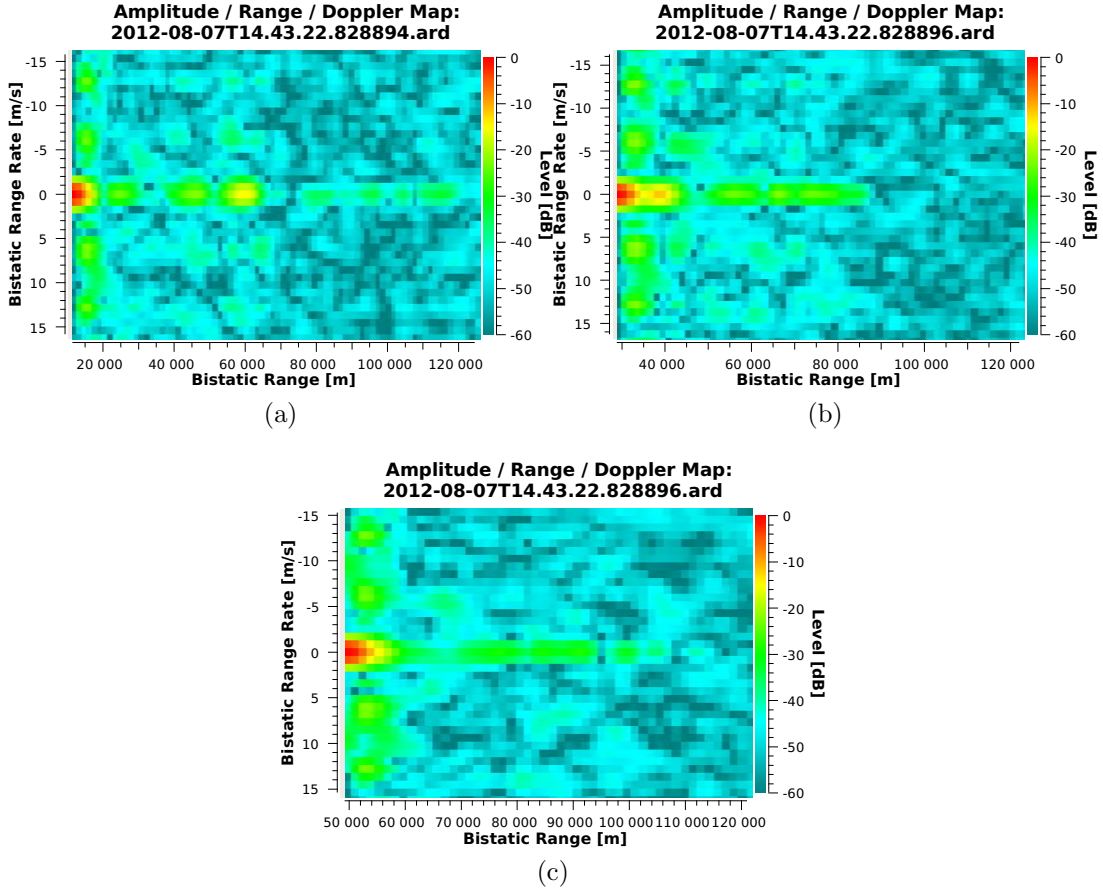


Figure 4.7: Comparison of ARD maps of the AAFs of the reference signals for the receiver sites shown in Figure 4.3. (a) shows the Tygerberg site, (b) the Backsberg site and (c) the Malmesbury site which has the cleanest reference signal.

4.2.3 Detection Performance

To determine if there is significant correlation loss when using the reference signal from a difference receiver, long range detections are compared where SNR is expected to be at a minimum. Figure 4.9 shows a long range detection using co-located data from the Tygerberg receiver site. Figure 4.10 shows the same surveillance data but used reference data from the Malmesbury site. As can be seen, the separated reference provides detections in subsequent range bins indicating an improved SINR resulting from the reference channel with lower

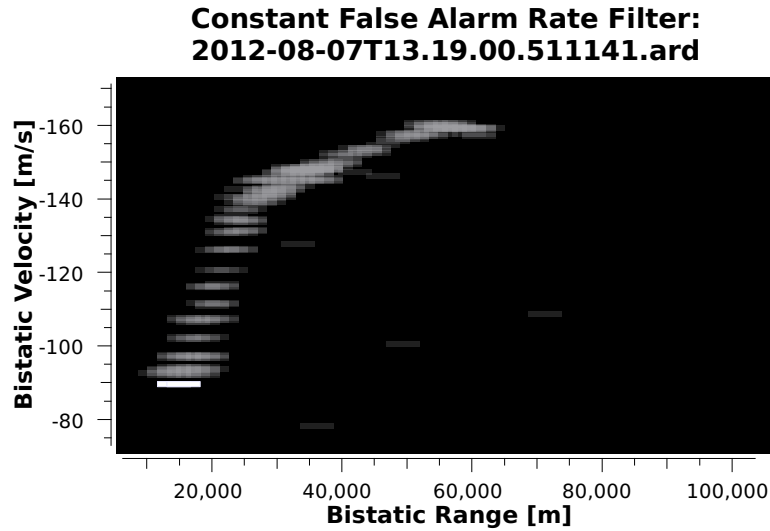


Figure 4.8: Removal of the target ghosting effect with the separated reference configuration. Using the same surveillance data as in Figure 4.5 but with a cleaner reference signal from Malmesbury site, the CFAR detections show that target ghosting effect is totally removed.

interference.

Given the bistatic baseline of the Malmesbury receive site is in the order of 50 km while that of the Tygerberg receiver site is approximately 10 km and, that a clean LoS path is available from the respective reference antennas to the transmitter, the Malmesbury site should receive the reference signal with a proportionally degraded SNR. The improved performance obtained from using the reference signal from Malmesbury can therefore be attributed to the decrease in multipath in the reference signal and, as such, a more favourable interference environment.

4.2. FIELD TESTS AND RESULTS

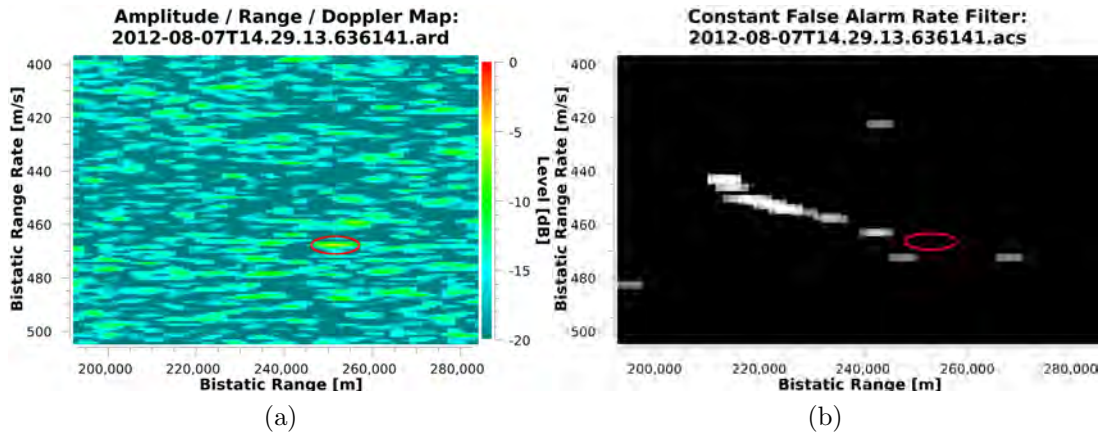


Figure 4.9: Detections of a target at its furthest detectable range using the colocated configuration. Figure (a) shows the ARD and gives an indication of the poor SINR. Figure (b) shows the corresponding CFAR. All detections shown are from previous CPIs and detection in the current CPI should be within the red ellipse. The SINR is however too poor for the CFAR detector to detect.

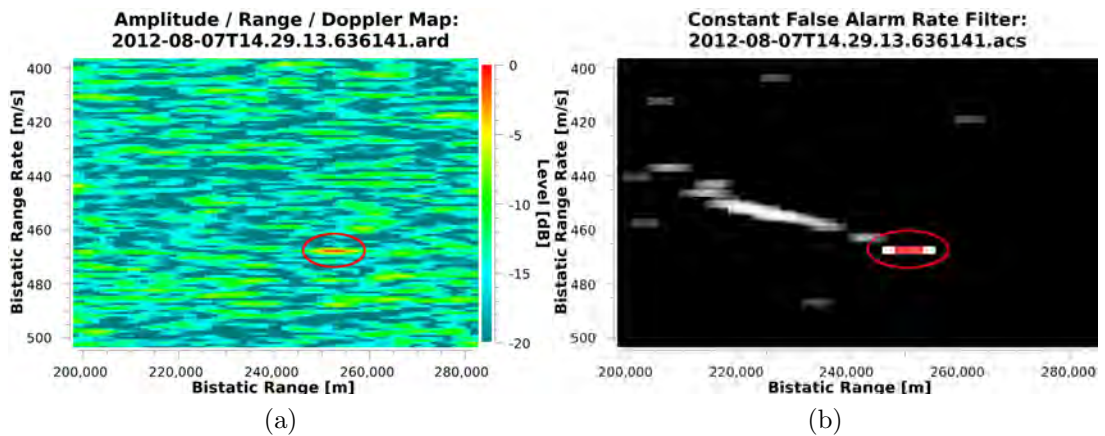


Figure 4.10: Detection ranges with the separated reference. Using the same surveillance channel as in Figure 4.9 with a cleaner reference signal yields similar detection performance. The maximum range is actually increased which can be attributed to improved SINR as shown in Figure (a). Figure (b) now shows a detection in current CPI as indicated within the red ellipse.

The cleanest reference signal, namely that from the Malmesbury receiver site could therefore be used with each surveillance signal to do the radar processing for each surveillance site.

A more complete investigation of correlation losses would require a more controlled environment where factors such as multipath are not present. This is to be the subject of future work.

4.3 Oscillators Performance Considerations

During the deployment, experiments were also conducted with 2 different types of receivers which are actually spectrum monitoring products. The first is a rackmount unit which is equipped with [GPS](#) disciplined oven controlled crystal oscillators ([OCXOs](#)) which provided relative high frequency stability. The second receiver type is a mobile unit and therefore due to power and size constraints is fitted with [GPS](#) disciplined temperature compensated crystal oscillators ([TCXOs](#)) which show relatively lower frequency stability which is to be expected from this type of oscillator. The [TCXO](#) equipped receivers were seen to have up to 0.25 Hz of offset between data streams from different receivers. [Figure 4.11](#) shows an [ARD](#) map of separated reference data created with 2 of the [TCXO](#) equipped receivers. Both were located at the same site for testing purposes so the geometry is in fact co-located. As can be observed in [Figure 4.11](#) there are lobing effects present which is spread throughout the Doppler scale as a result of the frequency error between the receivers. A target is present at 45 km, -120 ms^{-1} , however as can be observed from the amplitude level, it could disappear behind the grating lobes at certain positions in the range/Doppler map. As such, all the successful results as reported previously in [Section 4.2](#) of this chapter were done with the [OCXO](#) equipped receivers.

Furthermore, it was observed that when using the better performing oven controlled oscillators, the combination of a reference channel from any of the 3 deployment sites could be combined with a surveillance channel of any of the sites to perform radar signal processing. The detection performance was very

similar to the co-located case, notwithstanding the effects of using a reference channel with a greater multipath content.

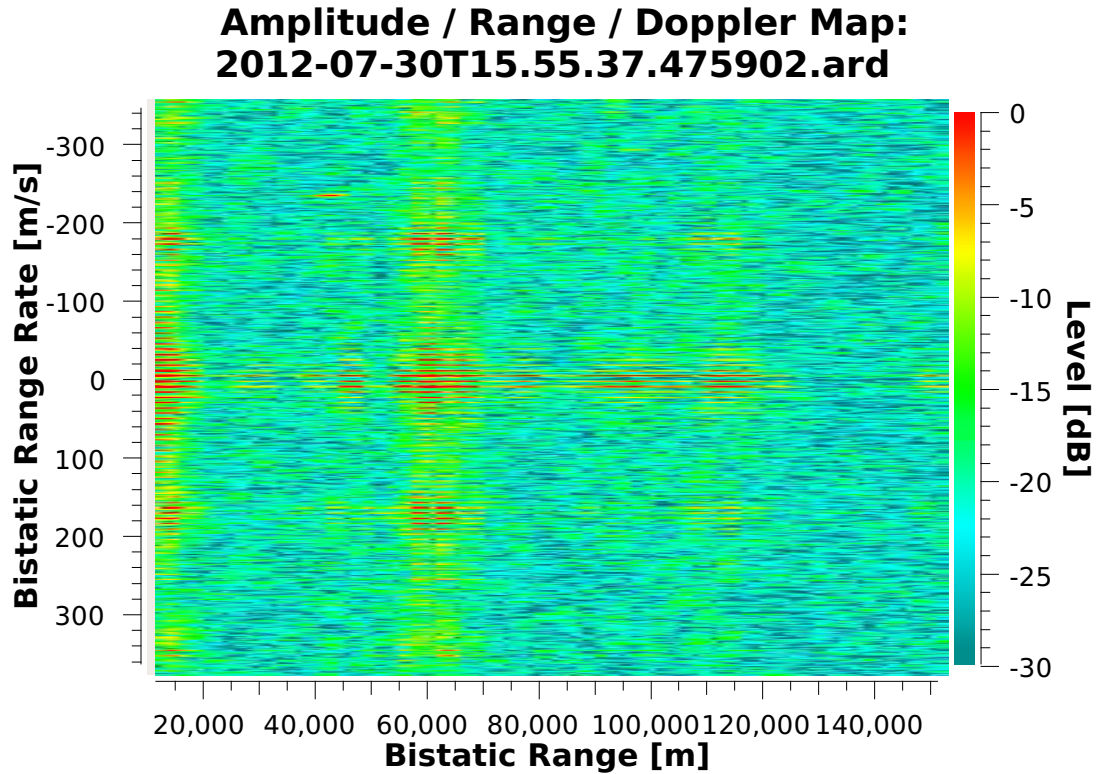


Figure 4.11: ARD map of separated reference data where receivers with lower quality temperature compensated oscillators were used. Lobing effects originating from the clutter are observable right across the Doppler dimension which will negatively effect target detection.

Figure 4.12 shows the phase drift between the surveillance and reference channels for co-located channels on the same receiver (in this case the OCXO equipped ones), on separate receivers with OCXOs and separate receivers equipped with TCXOs. Inspecting Figure 4.12 it can be seen that the phase is, on average, constant for the co-located channels. Phase wrapping occurs approximately every 24 s between the receivers equipped with OCXOs and every 3.3 s for the receivers equipped with TCXO's. The 3.3 s is a particular concern as it indicates that the phase will wrap within the 4 s integration time typically used by the prototype commensal radar system under development at UCT. This is likely to be responsible for the poor performance experienced with these receivers as

shown in Figure 4.11.

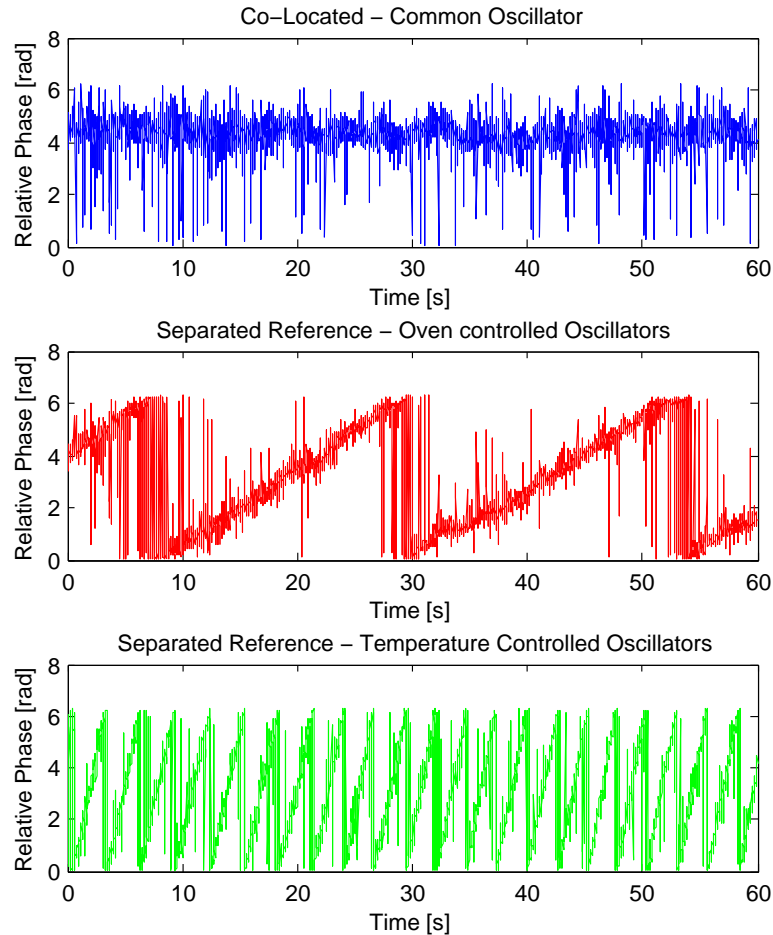


Figure 4.12: Comparison of phase drift between channels on the same receiver, on separate **OCXO** equipped receivers and on separate **TCXOs** equipped receivers.

4.4 Frequency Offset Correction

This section discusses correction of the frequency offset by means of signal processing. While it is not trivially possible to recover from higher order phase noise effects that occur at different receivers, inspecting Figure 4.12 suggests that the main difference between the common oscillator digitisation, the **OCXO**-based digitisation and the **TCXO**-based digitisation is a varying amount of fixed

frequency offset between local oscillators within the radar receivers.

The NetRad networked pulse radar system also made use of [GPS](#) disciplined oscillators to maintain synchronicity between remote receiver nodes [[129](#), [130](#), [77](#), [180](#)]. When analysing the data collected using NetRad, Al-Ashwal reported similar lobing effects in the Doppler spectrum to those observed in [Figure 4.11](#) which he referred to as “tramlines” [[181](#)]. Using signal processing to correct the phase drift Al-Ashwal showed that the lobing effects could be suppressed. This was done by monitoring the phase advance from pulse-to-pulse stationary targets or that of the direct break through of the transmitter to the bistatic receiver nodes within the radar network.

When using a pseudo-continuous wave transmitter such as that of [FM](#) broadcast transmitters the detection of stationary targets is normally not possible due to the large clutter returns that are obtained, nor is there a leading pulse edge to examine the phase of. Given, however, that [DPI](#) tends to be the dominating energy in the surveillance channel in most practical deployments, one can compare the phase progression between the reference and surveillance channels as shown in [Figure 4.12](#) and thereby estimate the fixed frequency offset that typically occurs between crystal oscillators. This technique was used by Heunis [[9](#)] to remove the frequency offset between the separate local oscillators of the 2 [TV](#) tuner based daughterboards that were used with the [USRP SDR](#) platform.

This technique was applied to the data collected with [GPS](#) disciplined [TCXO](#) equipped receivers. The data used to produce the [ARD](#) map shown in [Figure 4.11](#) and the bottom relative phase plot in [Figure 4.12](#). The 4 s, 204800 sample [CPI](#) of baseband [IQ](#) data are divided up into 2048 sample blocks which were [FFT](#)ed. The relative phase between reference and surveillance channels at the 0 Hz bin of each [FFT](#) are then put in a vector and unwrapped relative to 2π . A straight line is fitted to the data using least squares to get the average phase advance rate between the reference and surveillance channels for the duration of the [CPI](#). This phase advance rate is equivalent to a frequency offset which is then subtracted from the surveillance channel by mixing with an equivalent complex exponential in the time domain. The upper plot in [Figure 4.13](#) shows the unwrapped phase

4.4. FREQUENCY OFFSET CORRECTION

difference before correction. This is plotted against sample number of the original 4 s CPI. The lower plot then shows the unwrapped phase difference after the frequency offset corrected for.

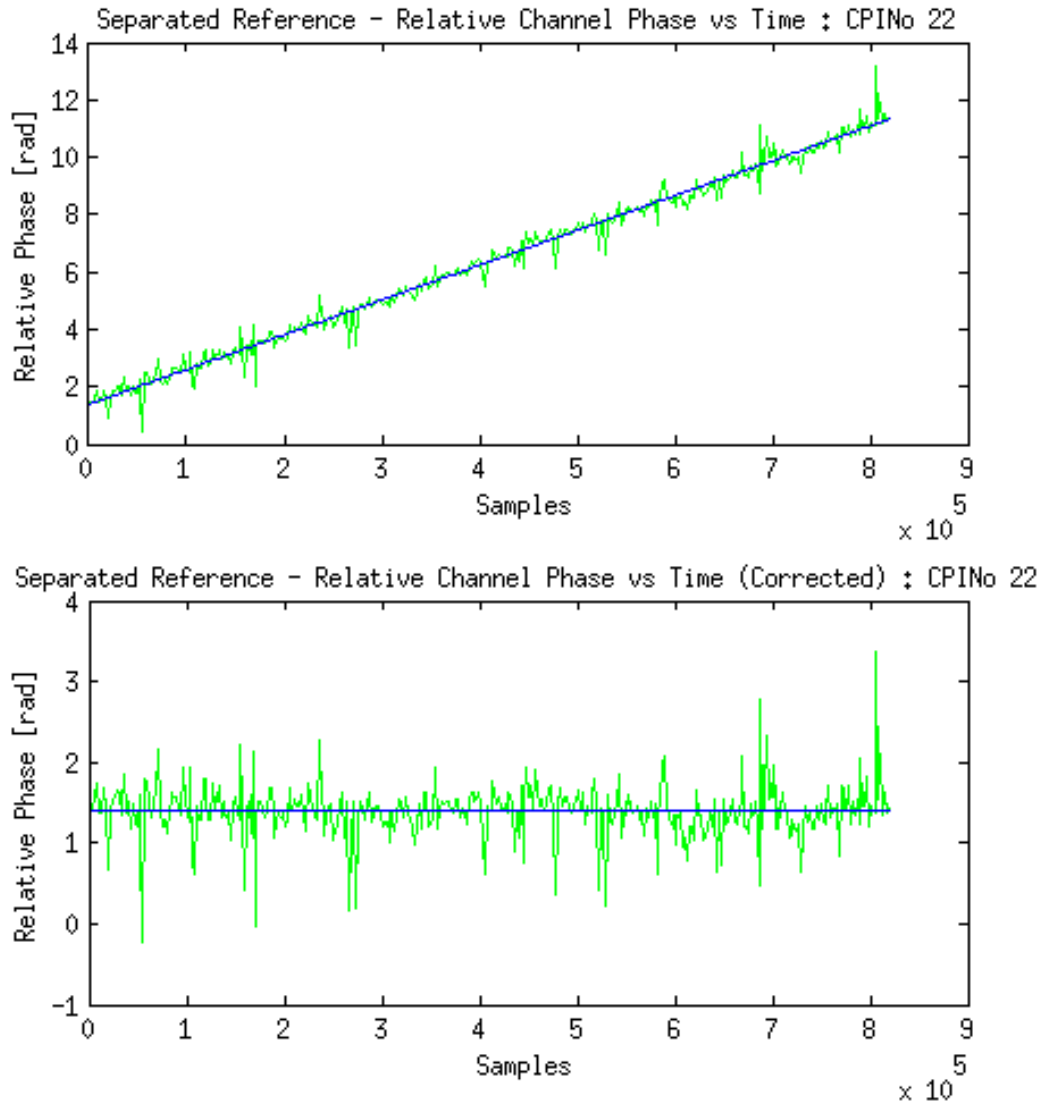


Figure 4.13: Fitting a curve to phase advance between the reference and surveillance channels. The phase advance and fitted curve for the ARD map in Figure 4.12 is shown in the upper plot, the phase and fitted curve is after correction and for the ARD map shown in Figure 4.14 is shown in lower plot.

Figure 4.14 shows the resultant ARD map using the same signal processing chain

after the frequency offset correction has been performed. Several improvements are immediately noticeable over Figure 4.11. Firstly the lobes in Doppler have been suppressed which is important as they would likely create many false alarms. Secondly the target signal to noise ratio is about 10 dB higher. Both Figures 4.11 and 4.14 are normalised to the target at 45 km, -235 ms^{-1} as the different in noise floor is prohibitively large for any other logical comparison. It should also be noted that the target level is raised by 34 dB after the frequency offset correction. An additional target located at 96 km, -294 ms^{-1} is now also clearly visible. A further point of interest is that the cancellation filter appears to achieve improved suppression, successfully reducing DPI and clutter below the background noise. This is to be expected as the DPI and clutter model generated from the reference signal should now be correctly aligned with the actual recorded response in Doppler.

Figure 4.15 shows an enlarged region of the ARD maps around the targets before and after the frequency offset correction respectively for a better indication of the SINR.

Higher order curves such as polynomials could be fitted to determine the frequency offset as it might not be a linear trend depending on the phase lock loop time constant. In fact, in the case of the equipment used, the linear approximation does fail in CPIs where the phased lock loop makes adjustments to correct the frequency. While this technique does prove that signal process can be used to make up for hardware timing limitations it should be noted that this might not be the case where the surveillance site does receive a clean copy of the transmitted signal which is after all a large motivation for using the separated reference configuration in the first place.

4.5 Further Considerations

This section discussed some other relevant details about the separated reference configuration. These are, using the separated reference configuration to combat in-band interference from third party illuminators as well as some points about

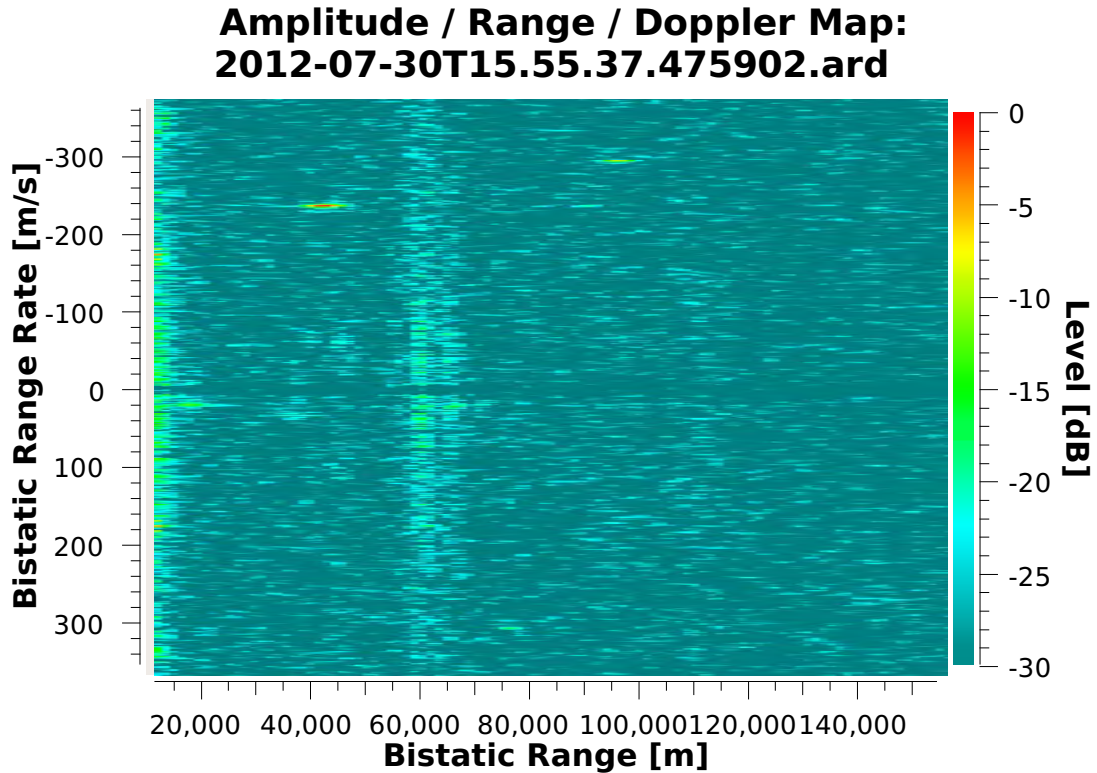


Figure 4.14: ARD map of separated reference data where receivers with lower quality oscillators where the frequency offset has been corrected for in signal processing.

the network architecture used to connect the receiver nodes of the commensal radar system.

4.5.1 Combating In-Band Interference

A further advantage of the separated reference configuration is that site selection no longer requires a compromise between optimisation of conditions for reference and surveillance antennas at the same site. The site selection process can therefore better cater for other factors such as in-band interference from 3rd party sources. Lombardo et al. describe reduced capability of DPI and clutter suppression processing due to in-band interference from other transmitters [182]. Suppression of this type of interference can be achieved by using available ter-

rain and man made structures to screen from these signals in the same way as the surveillance antenna is screened from the exploited transmitter. When no screening is available the antennas can simply be moved as far away as possible from potential interferers, while still maintaining adequate primary functionality, thereby exploiting the R_{IntTx}^2 factor of the one way Friis transmission [183] equation along with $(R_{Tx-Target}^2 \cdot R_{Target-Rx}^2)$ of the bistatic radar equation [68, Ch 7.2.1] to maximise SIR, where R_{IntTx} is the range to interfering transmitter and $R_{Tx-Target}$ and $R_{Target-Rx}$ are the ranges from transmitter-to-target and target-to-receiver respectively. While these quantities are not totally independent, it should be possible to increase the distance to the interfering transmitter without significantly increasing the distance of the skin echo path.

4.5.2 Network Infrastructure

The design of the network infrastructure for a networked commensal radar system is beyond the scope of this thesis but the following comments are presented for consideration.

A single FM broadcast radio channel can be reliably digitised at 200 kSps. If complex short samples (32 bits per IQ sample pair) are used, a single channel of data will require a continuous throughput of 1.6 MBps. Assuming each node digitised a single reference or surveillance channel at its site then a network connection of 1.6 MBps will be required to each node.

The ideal situation would be a fibre optic connections between each node as this technology provides massive amounts of throughput typically far greater than the required 1.6 MBps. Mobile phone (cellular) network base-stations are typically connected together by fibre-optic cables in urban and semi urban areas so this would be a useful infrastructure on which to piggy-back a commensal radar as it provides power, communications, and suitable elevation for antenna mounting and furthermore the cellular basestations are a common occurrence even in the 3rd world.

Looking to other communication options WiFi links are capable of providing the

required throughput over 10s of kilometres but will suffer performance loss if there are other networks operating in the same area. It would not be desirable for an essential service such as [ATC](#) to operate on a band shared by public unlicensed users as contention for the band could cause the system to not meet its throughput requirements.

Last mile consumer connections such as high-speed downlink packet access ([HS-DPA](#)), and asymmetric digital subscriber line ([ADSL](#)) are, as their names suggest, geared towards high download throughput but limited in their upload capacity. High-end versions of these technologies will be able to offer the required throughput in their downlinks but this would require a deviation from the architecture as described in Section [4.1](#). To make use of the high-speed downlink the reference signal would have to be sent to each surveillance node so that they can exploit their download channels. This means that processing hardware (and power to support it) will need to be available at every surveillance node site. Detection data, which is orders of magnitude smaller per time interval, can then be sent back across the network to a central node for combining.

White space communications, an emerging technology which operates in the licensed frequency bands such as that of television in the [UHF](#) band, operate at low power as to not interfere with the licensed services. This technology may be able to provide another solution to the networking problem. IEEE 802.22 [[184](#)] defines a standard for using white spaces in the television frequency spectrum. Networks using this standard are referred to as wireless regional area networks ([WRANs](#)) The [VHF](#) and lower [UHF](#) bands such as those used for both analogue and digital television provide an attractive trade-off between propagation distance and throughput for telecommunications links and may therefore be well suited to the separated reference configuration networking requirements. Langman et al. [[185](#)] propose a platform intended to provide both commensal radar and white space communications concurrently and, furthermore, to use the communication signals as the illumination source of opportunity. This will, however, be far lower power than [FM](#) broadcast radio or [DVB-T](#) and detection capability would scale accordingly. In-band interference could also negatively impact the [SIR](#) depending on the distance to television transmitters operating on the

selected channel.

A final consideration around the use of wireless links as a means communicating between the nodes of a commensal radar system. Given that the analogue “radar” waveforms (albeit they are non-co-operative) are always sampled at greater than critical Nyquist sample rates, this information will therefore require more spectrum to transmit over a wireless digital link in real-time than the spectral occupancy of the original analogue signal being exploited as the radar waveform. This means that the commensal radar system is, in fact, requiring more spectrum than what it is saving by piggy-backing off the illuminator of opportunity. This spectrum requirement might only be for a limited area but nonetheless it is contradictive to the main benefit of commensal radar which is spectrum efficiency in an age where spectrum is becoming an increasingly scarce resource. This does bring to light a potential limitation of the separated reference configuration if a suitable communications network is not available. In this case the co-located architecture might prove to be preferable despite its relative deployment disadvantages with regard to interference.

4.6 Conclusions

This chapter describes a demonstration of the separated reference configuration for networked commensal radar where receivers equipped with GNSS disciplined oscillators are used to record exclusively either reference or surveillance signals at separate sites. It is shown that given suitably stable oscillators a single reference channel can be combined with multiple surveillance channels all recorded at different sites to provide multistatic radar detections of aircraft.

Furthermore, given that the reference receiver node can be positioned purely for the purpose of recording the reference signal, a better quality reference signal recording can be obtained versus that which might be captured at a suitable surveillance receiver site. Radar performance can be improved for example as demonstrated in Section 4.2.2 by reducing multipath in the reference channel and as demonstrated in the case of the Manastash Ridge Radar [57][6, Ch. 7],

the separated reference configuration can also be used to suppress [DPI](#) in the surveillance channel. It should therefore also be possible to optimise the receiver positions to minimise effects such as in-band interference from transmitters not being exploited for radar purposes.

It is demonstrated that a fixed frequency offset between local oscillators that results in corruption of the range/Doppler output can be corrected for by using simple mixing. It is also, however noted that this requires suitable reception of the transmitted signal in the surveillance channel which is converse to the motivation for using the separated reference channel.

Finally it is acknowledged that network infrastructure required to operate such a system in real-time could be extremely costly as it will likely require fibre optic physical media to provide both the coverage range and throughput needed. It might however be possible to piggy-back off existing infrastructures such as academic and research networks or the back-haul networks for cellular providers.

4.6.1 Future Work

This chapter presents only a practical and empirical investigation into the multi-site separated reference configuration. There is as such a vast amount of investigation that need to be performed to better quantify and predict the performance of such system configurations. The following lists some possible ideas.

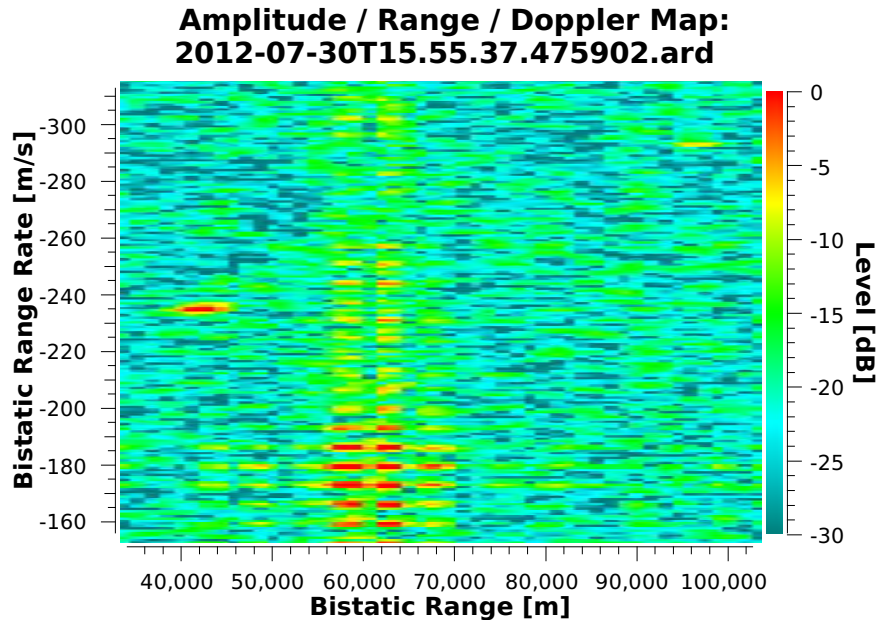
- Detailed investigation into the temporal stability requirements and associated coherency of the receiver oscillators. A measure of how phase noise or jitter will impact on [SNR](#) will be very useful.
- Further experimentation with long baselines (100s of km) between receivers. Cancellation algorithms may then not be necessary at all. This will then also allow for the use of the [RDFT](#) based range/Doppler processing as presented in Section [3.3.2.4](#) with the benefit of the associated high time resolution. Very long baselines may result in the view of different [GNSS](#)

4.6. CONCLUSIONS

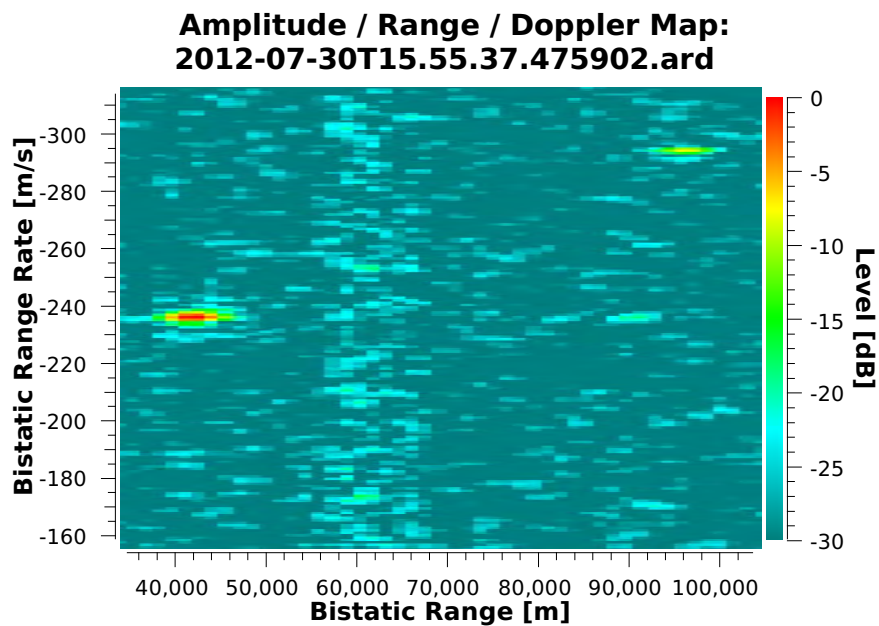
satellites. It needs to be determined how will this effect GNSS disciplined oscillator performance.

- The degree to which frequency offsets can be corrected for in software and how this is affected by the front end architecture e.g. mixing stages also needs to be quantised.

4.6. CONCLUSIONS



(a)



(b)

Figure 4.15: Comparison of target signal to noise ratio after frequency offset correction. An improvement in the order of 10 dB is clearly visible in addition to the reduction of lobes in Doppler spectrum. The scales are normalised to the level of the 45 km, -235 ms^{-1} target. This target peak was 34 dB higher after frequency offset correction.

Chapter 5

Conclusions

Conclusions and the future work are presented individually for the Processing Chain chapter (Chapter 3) and the Separated Reference chapter (Chapter 4) respectively.

5.1 Processing Design

A complete design of a real-time processing chain for a commensal radar system is presented, making use of commercial of the shelf computing and GP-GPU capable GPU hardware. The processing chain includes stages of packetisation from the receiver, DPI and clutter suppression (cancellation), range/Doppler processing and finally detection by CFAR filter. Algorithms for each stage are compared and an implementation is described for an optimal processing chain where the CGLS algorithm is used for cancellation on GPU hardware due to the algorithm's lower memory footprint and iterative refinement approach, the XF algorithm for CAF calculation is efficiently implemented on GPU exploiting the CUDA FFT library's batch mode and lastly the GOCA-CFAR algorithm is implemented in the GUI display software to perform detection.

It is empirically shown that better than real-time throughput can be achieved using the described algorithms on several different variations of hardware con-

sisting of multi-core CPUs as well as GPUs where the variations of GPU include previous generation (at the time of writing), high-end gaming hardware in the form of NVIDIA Geforce GTX480 and GTX570. Low-cost mid-level hardware in the form of NVIDIA Geforce GT640 and high-end GP-GPU specific GPUs in the form of NVIDIA Tesla M2090s . The proposed processing chain scales automatically to these variations in hardware and also to multiple GPU devices requiring no alteration or recompilation of code.

Using an NVIDIA Jetson TK1 embedded development board, the throughputs of 4 s of sample data in ~ 4 s could be achieved, which will be acceptable in certain use cases. Implementation of the batches algorithm for the GPU could therefore make this platform quite effective albeit one would have to concede the batch length limitations of the batches algorithm as described in Section 3.3.2.3. The time results for this implementation are shown in more detail in Section 3.6. The small form factor and lower power consumption of this solution could prove to be highly useful in applying commensal radar to space, weight and power limited use cases such as airborne platforms [42, 43] or hand held applications. Chetty describes a through-wall system which might take on such a form factor [78].

AMD's AMD Core Math Libraries [175] were used to develop multicore CPU only version of the equivalent processing chain. CPUs cannot easily match the throughput of GPUs when it comes to linear algebra due the massive parallelism provided by the GPUs. This is clear when reviewing the results presented at the end of this chapter. Only when server class CPUs are used, in this case a 16 core Intel Xeon, do the timings start to compare to that of the majority of the tested GPUs. This type of hardware is however far more costly and so a GPU solution is deemed to be preferable in all cases.

A method for non-coherent combination of ARDs that are created from different frequencies in the same bistatic geometry is also presented. This implementation uses nearest neighbour interpolation to combine the ARD data which might exist at different resolutions over the same scale. It is shown that 8 ARDs of 210 by 1701 cells can be combined under 500 ms in the single thread on a current CPU. This latency could be reduced by parallelising across more threads if necessary

or the calculation could be moved to GPU.

This capability further solidifies the low cost attribute of commensal radar. As general purpose computing hardware is fractional in cost in comparison to the purpose built processing subsystems found on typical active radars.

5.1.1 Future Work

At the time of completion of this thesis a receiver with 3 analogue to digital channels and 16 DDCs in total was developed by an industry partner Peralex Electronics specifically for the purpose of investigation of FM broadcast band based commensal radar. This allows for both AoA and the combination of 5 FM frequencies (each digitised by all 3 of analogue to digital channels coherently). The integration of this capability into the real-time processing chain is therefore the immediate focus of future work.

As described in the performance results of the processing chain in Section 3.3 there is capacity on the current hardware to expand the throughput on the GPU by approximately 10 times when using the CGLS cancellation algorithm and the XF range/Doppler processing algorithm (on 2 NVIDIA Geforce GTX480 cards). It was also shown that at maximum possible GPU throughput only half the resources of a quad-core CPU are utilised. Handling the data throughput from the new receiver on the current processing hardware is likely to be borderline possible then. The new receiver provides narrowband sample data at 200 kSps as opposed to 204.8 kSps of the previous hardware which will relieve the processing overhead slightly. The current throughput capability may be adequate to allow processing of all data from the receiver on the current processing hardware with 2 NVIDIA Geforce GTX480 cards, otherwise less intensive algorithms such as the batches algorithm or the decimation between stages of the XF algorithm for range/Doppler processing might be considered to realise the processing and also to provide ARD updates at more regular intervals than 4 seconds by means of a sliding window. The number of iterations run for the CGLS DPI and clutter suppression algorithm could also potentially be reduced in certain low clutter

environments.

Tracking is not discussed in this thesis in any great detail by in the context of a working radar system it will prove critical. Work has already been done at the University of Cape Town to investigate tracking for commensal radar systems [30, 53] and it is likely to require further innovation to make a sufficiently robust tracking system that can extract the most out of the measurement information that the commensal radar processing chain can provide.

The processing chain is currently configured by a configuration file. Initial framework exists for control by the GUI based network client to make parameter changes easier. The final integration of this software needs to be completed. Integration for control of the ComRad3 receiver into the same GUI software is also intended, to streamline overall control of the radar system.

Given that the modulation bandwidth fluctuations of the FM broadcast signal, the sample rate will often end being well beyond the Nyquist requirement. Compressive sample techniques might help to minimise this potentially inefficient behaviour. Furthermore, if one considers the FM channels broadcast from any FM transmitter site, the spectrum across the entire 88 to 108 MHz can be viewed as sparse for that transmitter site which also suggests the application of compressive sampling techniques.

5.2 Separated Reference Configuration

This chapter describes a demonstration of the separated reference configuration for networked commensal radar where receivers equipped with GNSS disciplined oscillators are use to record exclusively either reference or surveillance signals at separate sites. It is shown that given suitably stable oscillators a single reference channel can be combined with multiple surveillance channels all recorded at different sites to provide multistatic radar detections of aircraft. Furthermore where there exists a fixed frequency offset between oscillators which results in lobed in the Doppler spectra, it is shown that mixing out this frequency offset

can suppress the sidelobes and also improve the performance of the [DPI](#) and clutter filter.

Furthermore, given that the reference receiver node can be positioned purely for the purpose of recording the reference signal, a better quality reference signal recording can be obtained versus that which might be captured at a suitable surveillance receiver site. Radar performance can be improved for example as demonstrated in [Section 4.2.2](#) by reducing multipath in the reference channel and as demonstrated in the case of the Manastash Ridge Radar [[57](#)][[6](#), Ch. 7], the separated reference configuration can also be used to suppress [DPI](#) in the surveillance channel. It should therefore also be possible to optimise the receiver positions to minimise effects such as in-band interference from transmitters not being exploited for radar purposes.

Finally it is acknowledged that network infrastructure required to operate such a system in real-time could be extremely costly as it will likely require fibre optic physical media to provide both the coverage range and throughput needed. It might however be possible to piggy-back off existing infrastructures such as academic and research networks or the back-haul networks for cellular providers.

5.2.1 Future Work

There is much scope for further work into the separated reference configuration and the following are presented for consideration.

- Detailed investigation into the temporal stability requirements and associated coherency of the receiver oscillators. A measure of how phase noise or jitter will impact on [SNR](#) will be very useful.
- Further experimentation with long baselines (100s of km) between receivers. Cancellation algorithms may then not be necessary at all. This will then also allow for the use of the [RDFT](#) based range/Doppler processing as presented in [Section 3.3.2.4](#) with the benefit of the associated high time resolution. Very long baselines may result in the view of different [GNSS](#)

5.2. SEPARATED REFERENCE CONFIGURATION

satellites. It needs to be determined how will this effect GNSS disciplined oscillator performance.

- The degree to which frequency offsets can be corrected for in software and how this is affected by the front end architecture e.g. mixing stages also needs to be quantised.

Bibliography

- [1] “UCT high performance computing cluster.” <http://hpc.uct.ac.za/>, 2014. Accessed: 2014/02/11. [vii](#)
- [2] F. Colone, D. O’Hagan, P. Lombardo, and C. Baker, “A multistage processing algorithm for disturbance removal and target detection in passive bistatic radar,” *Aerospace and Electronic Systems, IEEE Transactions on*, vol. 45, pp. 698 –722, Apr 2009. [xx](#), [3](#), [12](#), [47](#), [57](#), [64](#), [76](#), [82](#)
- [3] M. J. Brooker, *The Design and Implementation of a Simulator for Multistatic Radar Systems*. Doctoral thesis, University of Cape Town - RRSg, Jun 2008. [xx](#), [57](#)
- [4] M. Brooker and M. Inggs, “A signal level simulator for multistatic and netted radar systems,” *Aerospace and Electronic Systems, IEEE Transactions on*, vol. 47, pp. 178 –186, Jan 2011. [xx](#), [57](#)
- [5] M. Brooker, “The Flexible Extensible Radar Simulator (FERS).” <http://sourceforge.net/projects/fers/>. Accessed: 2013/10/11. [xx](#), [92](#)
- [6] N. J. Willis and H. D. Griffiths, *Advances in Bistatic Radar*. Scitech Publishing, 2007. [1](#), [15](#), [24](#), [35](#), [62](#), [78](#), [143](#), [162](#), [170](#)
- [7] P. Howland, D. Maksimiuk, and G. Reitsma, “FM radio based bistatic radar,” *Radar, Sonar and Navigation, IEE Proceedings -*, vol. 152, pp. 107 – 115, Jun 2005. [2](#), [4](#), [9](#), [10](#), [22](#), [45](#), [50](#), [64](#), [65](#), [82](#), [97](#)

BIBLIOGRAPHY

- [8] D. W. O'Hagan, *Passive Bistatic Radar Performance Characterisation Using FM Radio Illuminators of Opportunity*. PhD thesis, University College London, 2009. [2](#), [15](#), [42](#), [83](#)
- [9] F. S. Heunis, "Passive coherent location radar using software-defined radio techniques," Master's thesis, University of Cape Town, Private Bag, Rondebosch, 7701, South Africa, May 2010. [2](#), [11](#), [57](#), [83](#), [156](#)
- [10] K. Szumski, M. Malanowski, J. Kulpa, W. Porczyk, and K. Kulpa, "Real-time software implementation of passive radar," in *Radar Conference, 2009. EuRAD 2009. European*, pp. 33–36, 2009. [3](#), [55](#), [64](#)
- [11] M. Bernaschi, A. Di Lallo, A. Farina, R. Fulcoli, E. Gallo, and L. Timmoneri, "Use of a graphics processing unit for passive radar signal and data processing," *Aerospace and Electronic Systems Magazine, IEEE*, vol. 27, no. 10, pp. 52–59, 2012. [3](#)
- [12] F. Colone, R. Cardinali, and P. Lombardo, "Cancellation of clutter and multipath in passive radar using a sequential approach," in *Radar, 2006 IEEE Conference on*, pp. 7 pp.–, April. [3](#), [45](#), [64](#), [82](#)
- [13] M. Malanowski, "Comparison of adaptive methods for clutter removal in PCL radar," in *Radar Symposium, 2006. IRS 2006. International*, pp. 1–4, 2006. [3](#), [54](#), [82](#)
- [14] R. Cardinali, F. Colone, C. Ferretti, and P. Lombardo, "Comparison of clutter and multipath cancellation techniques for passive radar," in *Radar Conference, 2007 IEEE*, pp. 469–474, 2007. [3](#), [46](#), [82](#)
- [15] J. Palmer and S. Searle, "Evaluation of adaptive filter algorithms for clutter cancellation in passive bistatic radar," in *Radar Conference (RADAR), 2012 IEEE*, pp. 0493–0498, May. [3](#), [61](#), [64](#), [73](#), [82](#), [86](#)
- [16] M. Inggs and C. Tong, "Commensal radar using separated reference and surveillance channel configuration," *Electronics Letters*, vol. 48, no. 18, pp. 1158–1160, 30. [4](#), [15](#), [27](#), [43](#), [71](#), [99](#)

BIBLIOGRAPHY

- [17] C. Tong, M. Inggs, and G. Lange, “Processing design of a networked passive coherent location system,” in *Radar Conference (RADAR), 2011 IEEE*, pp. 692–697, May 2011. [4](#), [27](#), [83](#)
- [18] C. Tong, M. Inggs, and A. Mishra, “Towards a MIMO radar based on commensal use of FM broadcast transmitters of opportunity,” in *Synthetic Aperture Radar, 2012. EUSAR. 9th European Conference on*, pp. 283–286, April. [4](#), [27](#), [68](#)
- [19] M. Malanowski, K. Kulpa, P. Samczynski, J. Misiurewicz, and J. Kulpa, “Long range FM-based passive radar,” in *Radar Systems (Radar 2012), IET International Conference on*, pp. 1–4, 2012. [4](#), [10](#), [18](#), [56](#), [65](#), [69](#)
- [20] C. Bongioanni, F. Colone, and P. Lombardo, “Performance analysis of a multi-frequency FM based passive bistatic radar,” in *Radar Conference, 2008. RADAR '08. IEEE*, pp. 1–6, 2008. [4](#), [46](#), [50](#), [119](#), [122](#)
- [21] D. W. O’Hagan, F. Colone, C. Baker, and H. Griffiths, “Passive bistatic radar (PBR) demonstrator,” in *Radar Systems, 2007 IET International Conference on*, pp. 1–5, 2007. [4](#)
- [22] M. Edrich, A. Schroeder, and V. Winkler, “Design and performance evaluation of a FM / DAB / DVB-T multi-illuminator passive radar system,” in *Radar Systems (Radar 2012), IET International Conference on*, pp. 1–6, 2012. [4](#)
- [23] D. Petri, A. Capria, M. Conti, F. Berizzi, M. Martorella, and E. Dalle Mese, “High range resolution multichannel DVB-T passive radar: Aerial target detection,” in *Digital Communications - Enhanced Surveillance of Aircraft and Vehicles (TIWDC/ESAV), 2011 Tyrrhenian International Workshop on*, pp. 129–132, 2011. [4](#), [10](#), [53](#)
- [24] M. Malanowski, K. Kulpa, and K. Olsen, “Extending the integration time in DVB-T-based passive radar,” in *Radar Conference (EuRAD), 2011 European*, pp. 190–193, 2011. [4](#), [10](#), [55](#), [104](#)

BIBLIOGRAPHY

- [25] J. Palmer, H. Harms, S. Searle, and L. Davis, “DVB-T passive radar signal processing,” *Signal Processing, IEEE Transactions on*, vol. 61, no. 8, pp. 2116–2126, 2013. [4](#)
- [26] M. Jackson, “The geometry of bistatic radar systems,” *Communications, Radar and Signal Processing, IEE Proceedings F*, vol. 133, no. 7, pp. 604–612, 1986. [5](#)
- [27] W. Melvin and J. Scheer, *Principles of modern radar: Advanced Techniques*. No. v. 2 in Principles of Modern Radar, SciTech Publishing, Incorporated, 2010. [6](#), [79](#)
- [28] M. Malanowski and K. Kulpa, “Two methods for target localization in multistatic passive radar,” *Aerospace and Electronic Systems, IEEE Transactions on*, vol. 48, pp. 572–580, Jan 2012. [8](#), [56](#)
- [29] P. E. Howland, *Television Based Bistatic Radar*. PhD thesis, University of Birmingham, 1997. [9](#), [44](#)
- [30] N. Morrison, R. Lord, and M. Inggs, “The Gauss-Newton algorithm in passive aircraft tracking using Doppler and bearings,” in *Radar Systems, 2007 IET International Conference on*, pp. 1–5, Oct 2007. [9](#), [38](#), [57](#), [140](#), [169](#)
- [31] F. Colone, G. De Leo, P. Paglione, C. Bongioanni, and P. Lombardo, “Direction of arrival estimation for multi-frequency FM-based passive bistatic radar,” in *Radar Conference (RADAR), 2011 IEEE*, pp. 441–446, May 2011. [9](#), [10](#), [50](#), [65](#), [119](#), [120](#), [122](#)
- [32] D. Langellotti, M. Sedehi, F. Colone, and P. Lombardo, “Experimental results for passive bistatic radar based on DVB-T signals,” in *Radar Symposium (IRS), 2013 14th International*, vol. 1, pp. 178–183, 2013. [10](#), [52](#)
- [33] D. W. O’Hagan, H. Kuschel, M. Ummenhofer, J. Heckenbach, and J. Schell, “A multi-frequency hybrid passive radar concept for medium range air surveillance,” *Aerospace and Electronic Systems Magazine, IEEE*, vol. 27, no. 10, pp. 6–15, 2012. [10](#), [59](#), [63](#), [69](#)

BIBLIOGRAPHY

- [34] A. Schroeder and M. Edrich, “Cassidian multiband mobile passive radar system,” in *Radar Symposium (IRS), 2011 Proceedings International*, pp. 286–291, 2011. [10](#), [59](#)
- [35] H. Griffiths and N. Long, “Television-based bistatic radar,” *Communications, Radar and Signal Processing, IEE Proceedings F*, vol. 133, pp. 649–657, Dec 1986. [10](#), [41](#)
- [36] D. Tan, H. Sun, Y. Lu, and W. Liu, “Feasibility analysis of GSM signal for passive radar,” in *Radar Conference, 2003. Proceedings of the 2003 IEEE*, pp. 425 – 430, May 2003. [10](#), [61](#)
- [37] D. K. P. Tan, H. Sun, and Y. Lu, “Sea and air moving target measurements using a GSM based passive radar,” in *Radar Conference, 2005 IEEE International*, pp. 783–786, 2005. [10](#), [62](#)
- [38] K. Chetty, G. Smith, H. Guo, and K. Woodbridge, “Target detection in high clutter using passive bistatic WiFi radar,” in *Radar Conference, 2009 IEEE*, pp. 1–5, 2009. [10](#), [42](#)
- [39] P. Falcone, F. Colone, C. Bongioanni, and P. Lombardo, “Experimental results for OFDM WiFi-based passive bistatic radar,” in *Radar Conference, 2010 IEEE*, pp. 516–521, 2010. [10](#), [19](#), [48](#)
- [40] K. Chetty, K. Woodbridge, H. Guo, and G. Smith, “Passive bistatic WiMAX radar for marine surveillance,” in *Radar Conference, 2010 IEEE*, pp. 188–193, 2010. [10](#), [43](#)
- [41] F. Colone, P. Falcone, and P. Lombardo, “Ambiguity function analysis of WiMAX transmissions for passive radar,” in *Radar Conference, 2010 IEEE*, pp. 689–694, 2010. [10](#), [19](#), [48](#)
- [42] J. Brown, K. Woodbridge, A. Stove, and S. Watts, “Air target detection using airborne passive bistatic radar,” *Electronics Letters*, vol. 46, no. 20, pp. 1396–1397, 2010. [10](#), [43](#), [115](#), [139](#), [167](#)

BIBLIOGRAPHY

- [43] K. Kulpa, M. Malanowski, P. Samczynski, and B. Dawidowicz, “The concept of airborne passive radar,” in *Microwaves, Radar and Remote Sensing Symposium (MRRS), 2011*, pp. 267–270, Aug 2011. [10](#), [55](#), [115](#), [139](#), [167](#)
- [44] B. Dawidowicz, P. Samczynski, M. Malanowski, J. Misiurewicz, and K. Kulpa, “Detection of moving targets with multichannel airborne passive radar,” *Aerospace and Electronic Systems Magazine, IEEE*, vol. 27, no. 11, pp. 42–49, 2012. [10](#), [56](#)
- [45] B. Dawidowicz, K. Kulpa, M. Malanowski, J. Misiurewicz, P. Samczynski, and M. Smolarczyk, “DPCA detection of moving targets in airborne passive radar,” *Aerospace and Electronic Systems, IEEE Transactions on*, vol. 48, no. 2, pp. 1347–1357, 2012. [10](#), [56](#)
- [46] C. Clemente and J. Soraghan, “Passive bistatic radar for helicopters classification: A feasibility study,” in *Radar Conference (RADAR), 2012 IEEE*, pp. 0946–0949, 2012. [10](#)
- [47] J. Palmer, S. Palumbo, A. Summers, D. Merrett, and S. Howard, “DSTO’s experimental geosynchronous satellite based PBR,” in *Radar Conference - Surveillance for a Safer World, 2009. RADAR. International*, pp. 1–6, 2009. [10](#), [60](#)
- [48] H. Griffiths, C. Baker, J. Baubert, N. Kitchen, and M. Treagust, “Bistatic radar using satellite-borne illuminators,” in *RADAR 2002*, pp. 1–5, Oct 2002. [10](#), [41](#)
- [49] N. Willis, *Bistatic Radar, Second Edition*. Institution of Engineering and Technology, 2005. [10](#)
- [50] S. Searle, S. Howard, and J. Palmer, “Remodulation of DVB-T signals for use in passive bistatic radar,” in *Signals, Systems and Computers (ASILOMAR), 2010 Conference Record of the Forty Fourth Asilomar Conference on*, pp. 1112–1116, 2010. [11](#), [61](#)

BIBLIOGRAPHY

- [51] M. Radmard, M. Bastani, F. Behnia, and M. Nayebi, “Cross ambiguity function analysis of the ‘8k-mode’ DVB-T for passive radar application,” in *Radar Symposium (IRS), 2010 11th International*, pp. 1–4, 2010. [11](#)
- [52] R. Saini and M. Cherniakov, “DTV signal ambiguity function analysis for radar application,” *Radar, Sonar and Navigation, IEE Proceedings -*, vol. 152, no. 3, pp. 133–142, 2005. [11](#), [19](#), [45](#), [47](#)
- [53] R. Nadjiasngar, S. Middleton, and M. Inggs, “Doppler-only tracking with the recursive Gauss-Newton filter,” in *Radar Systems (Radar 2012), IET International Conference on*, pp. 1–5, 2012. [11](#), [12](#), [29](#), [38](#), [58](#), [68](#), [140](#), [169](#)
- [54] M. Klein and N. Millet, “Multireceiver passive radar tracking,” *Aerospace and Electronic Systems Magazine, IEEE*, vol. 27, pp. 26–36, Oct 2012. [11](#), [104](#)
- [55] C. Baker, H. Griffiths, and I. Papoutsis, “Passive coherent location radar systems. part 2: waveform properties,” *Radar, Sonar and Navigation, IEE Proceedings -*, vol. 152, no. 3, pp. 160–168, 2005. [14](#), [42](#), [98](#)
- [56] A. Lauri, F. Colone, R. Cardinali, C. Bongioanni, and P. Lombardo, “Analysis and emulation of FM radio signals for passive radar,” in *Aerospace Conference, 2007 IEEE*, pp. 1–10, 2007. [14](#), [46](#)
- [57] J. D. Sahr and F. D. Lind, “The Manastash ridge radar: a passive bistatic radar for upper atmospheric radio science,” *Radio Science*, vol. 32, pp. 2345–2358, Nov 1997. [15](#), [35](#), [143](#), [162](#), [170](#)
- [58] H. Griffiths, “Where has all the spectrum gone?,” in *Radar, 2013 International Conference on*, 2013. [17](#), [18](#), [20](#)
- [59] V. Chernyak, *Fundamentals of Multisite Radar Systems: Multistatic Radars and Multistatic Radar Systems*. Taylor & Francis, 1998. [18](#)
- [60] H. Kuschel, J. Heckenbach, S. Muller, and R. Appel, “Countering stealth with passive, multi-static, low frequency radars,” *Aerospace and Electronic Systems Magazine, IEEE*, vol. 25, no. 9, pp. 11–17, 2010. [18](#)

BIBLIOGRAPHY

- [61] F. Colone, P. Falcone, and P. Lombardo, “Passive bistatic radar based on mixed DSSS and OFDM WiFi transmissions,” in *Radar Conference (EuRAD), 2011 European*, pp. 154–157, 2011. [19](#), [49](#)
- [62] H. Harms, L. Davis, and J. Palmer, “Understanding the signal structure in DVB-T signals for passive radar detection,” in *Radar Conference, 2010 IEEE*, pp. 532 –537, May 2010. [19](#), [60](#)
- [63] C. Bongioanni, F. Colone, D. Langellotti, P. Lombardo, and T. Bucciarelli, “A new approach for DVB-T cross-ambiguity function evaluation,” in *Radar Conference, 2009. EuRAD 2009. European*, pp. 37–40, 2009. [19](#), [47](#)
- [64] M. Conti, F. Berizzi, D. Petri, A. Capria, and M. Martorella, “High range resolution DVB-T passive radar,” in *Radar Conference (EuRAD), 2010 European*, pp. 109 –112, Oct 2010. [19](#), [31](#), [53](#)
- [65] H. Kuschel, “Approaching 80 years of passive radar,” in *Radar, 2013 International Conference on*, 2013. [20](#), [40](#)
- [66] M. Inggs, C. Tong, A. Mishra, and F. Maasdorp, “Modelling and simulation in commensal radar system design,” in *Radar Systems (Radar 2012), IET International Conference on*, pp. 1–5, 2012. [21](#), [27](#), [58](#)
- [67] H. Griffiths and C. Baker, “The signal and interference environment in passive bistatic radar,” in *Information, Decision and Control, 2007. IDC '07*, pp. 1–10, 2007. [21](#), [42](#)
- [68] M. Cherniakov, ed., *Bistatic Radars: Emerging Technology*. John Wiley & Sons, Feb 2008. [21](#), [24](#), [94](#), [98](#), [160](#)
- [69] M. R. Inggs, A. Van der Byl, and C. Tong, “Commensal radar: Range-Doppler processing using a recursive DFT,” in *International Conference on Radar*, pp. 1 – 6, Sep 2013. Submitted. [27](#), [94](#), [103](#)
- [70] C. Tong, F. Maasdorp, and M. R. Inggs, “Performance improvements using the separated reference configuration in a multi-site commensal radar

BIBLIOGRAPHY

- system,” in *International Conference on Radar*, pp. 1 – 6, Sep 2013. [27](#), [71](#), [123](#)
- [71] F. Maasdorp, J. Cilliers, M. Inggs, and C. Tong, “Simulation and measurement of propeller modulation using FM broadcast band commensal radar,” *Electronics Letters*, vol. 49, pp. 1481–1482, Nov 2013. [28](#), [78](#)
- [72] C. Tong, M. Inggs, and C. Van Dyk, “ComRad3, a multichannel direct conversion receiver for FM broadcast band radar,” in *Radar Conference (RADAR), 2014 IEEE (Accepted)*, May 2014. [28](#), [116](#), [123](#)
- [73] M. Inggs, C. Tong, R. Nadjiasngar, G. Lange, A. Mishra, and F. Maasdorp, “Planning and design phases of a commensal radar system in the FM broadcast band,” *Aerospace and Electronic Systems Magazine, IEEE*, vol. 29, pp. 50–63, July 2014. [28](#)
- [74] H. Griffiths and C. Baker, “Passive coherent location radar systems. part 1: performance prediction,” *Radar, Sonar and Navigation, IEE Proceedings* -, vol. 152, no. 3, pp. 153–159, 2005. [41](#)
- [75] H. Guo, S. Coetzee, D. Mason, K. Woodbridge, and C. Baker, “Passive radar detection using wireless networks,” in *Radar Systems, 2007 IET International Conference on*, pp. 1–4, 2007. [42](#)
- [76] H. Guo, K. Woodbridge, and C. Baker, “Evaluation of WiFi beacon transmissions for wireless based passive radar,” in *Radar Conference, 2008. RADAR '08. IEEE*, pp. 1–6, 2008. [42](#)
- [77] M. Inggs, G. Inggs, S. Sandenbergh, W. Al-Ashwal, K. Woodbridge, and H. Griffiths, “Multistatic networked radar for sea clutter measurements,” in *Geoscience and Remote Sensing Symposium (IGARSS), 2011 IEEE International*, pp. 4449–4452, Jul 2011. [42](#), [156](#)
- [78] K. Chetty, G. Smith, and K. Woodbridge, “Through-the-wall sensing of personnel using passive bistatic WiFi radar at standoff distances,” *Geoscience and Remote Sensing, IEEE Transactions on*, vol. 50, no. 4, pp. 1218–1226, 2012. [43](#), [116](#), [167](#)

BIBLIOGRAPHY

- [79] K. E. Olsen, *Investigation of Bandwidth Utilisation Methods to Optimise Performance in Passive Bistatic Radar*. PhD thesis, University College London, Dec 2011. [43](#), [53](#)
- [80] K. Olsen and C. Baker, “FM-based passive bistatic radar as a function of available bandwidth,” in *Radar Conference, 2008. RADAR '08. IEEE*, pp. 1–8, 2008. [43](#)
- [81] K. Olsen and K. Woodbridge, “FM based passive bistatic radar range resolution improvement,” in *Radar Symposium (IRS), 2011 Proceedings International*, pp. 327–332, 2011. [43](#)
- [82] K. Olsen, K. Woodbridge, and I. Andersen, “FM based passive bistatic radar target range improvement - part ii,” in *Radar Symposium (IRS), 2010 11th International*, pp. 1–8, 2010. [44](#)
- [83] K. Olsen and K. Woodbridge, “Performance of a multiband passive bistatic radar processing scheme; part I,” *Aerospace and Electronic Systems Magazine, IEEE*, vol. 27, no. 10, pp. 16–25, 2012. [44](#), [53](#)
- [84] K. Olsen and K. Woodbridge, “Performance of a multiband passive bistatic radar processing scheme-part II,” *Aerospace and Electronic Systems Magazine, IEEE*, vol. 27, no. 11, pp. 4–14, 2012. [44](#), [53](#)
- [85] P. E. Howland, “Passive tracking of airborne targets using only Dppler and DOA information,” *IEE Colloquium on Algorithms for Target Tracking*, 1995. [44](#)
- [86] P. E. Howland, “Target tracking using television-based bistatic radar,” in *IEE Proceedings on Radar, Sonar and Navigation*, vol. 146, pp. 166–174, Institute of Electrical Engineers (United Kingdom), Jun 1999. [44](#)
- [87] R. Saini, M. Cherniakov, and V. Lenive, “Direct path interference suppression in bistatic system: DTV based radar,” in *Radar Conference, 2003. Proceedings of the International*, pp. 309–314, 2003. [45](#), [64](#), [82](#)

BIBLIOGRAPHY

- [88] A. Lauri, R. Cardinali, F. Colone, P. Lombardo, and T. Bucciarelli, “A geometrically based multipath channel model for passive radar,” in *Radar Systems, 2007 IET International Conference on*, pp. 1–5, 2007. [46](#)
- [89] F. Colone, R. Cardinali, P. Lombardo, O. Crognale, A. Cosmi, A. Lauri, and T. Bucciarelli, “Space-time constant modulus algorithm for multipath removal on the reference signal exploited by passive bistatic radar,” *Radar, Sonar Navigation, IET*, vol. 3, pp. 253–264, Jun 2009. [47](#), [147](#)
- [90] P. Falcone, F. Colone, P. Lombardo, and T. Bucciarelli, “Range sidelobe reduction filters for WiFi-based passive bistatic radar,” in *Radar Conference, 2009. EuRAD 2009. European*, pp. 133–136, 2009. [47](#), [48](#)
- [91] C. Bongioanni, F. Colone, T. Martelli, R. D’Angeli, and P. Lombardo, “Exploiting polarimetric diversity to mitigate the effect of interferences in FM-based passive radar,” in *Radar Symposium (IRS), 2010 11th International*, pp. 1–4, 2010. [48](#)
- [92] F. Gumiero, C. Nucciarone, V. Anastasio, P. Lombardo, and F. Colone, “Multistatic passive radar geometry optimization for target 3D positioning accuracy,” in *Radar Conference (EuRAD), 2010 European*, pp. 467–470, 2010. [48](#)
- [93] F. Gumiero, S. Santarelli, C. Bongioanni, F. Colone, and P. Lombardo, “Using real data for the implementation of multistatic passive radar geometry optimization procedure,” in *Radar Conference (EuRAD), 2011 European*, pp. 93–96, 2011. [49](#)
- [94] F. Colone, K. Woodbridge, H. Guo, D. Mason, and C. Baker, “Ambiguity function analysis of wireless lan transmissions for passive radar,” *Aerospace and Electronic Systems, IEEE Transactions on*, vol. 47, no. 1, pp. 240–264, 2011. [49](#)
- [95] P. Falcone, F. Colone, and P. Lombardo, “Doppler frequency sidelobe level control for WiFi-based passive bistatic radar,” in *Radar Conference (RADAR), 2011 IEEE*, pp. 435–440, 2011. [49](#)

BIBLIOGRAPHY

- [96] F. Colone, P. Falcone, A. Macera, and P. Lombardo, “High resolution cross-range profiling with passive radar via ISAR processing,” in *Radar Symposium (IRS), 2011 Proceedings International*, pp. 301–306, 2011. [49](#)
- [97] F. Colone, P. Falcone, C. Bongioanni, and P. Lombardo, “WiFi-based passive bistatic radar: Data processing schemes and experimental results,” *Aerospace and Electronic Systems, IEEE Transactions on*, vol. 48, no. 2, pp. 1061–1079, 2012. [50](#)
- [98] P. Falcone, F. Colone, A. Macera, D. Pastina, and P. Lombardo, “Advances in ISAR processing for high resolution cross-range profiling with passive radar,” in *Radar Symposium (IRS), 2012 13th International*, pp. 421–425, 2012. [50](#)
- [99] P. Falcone, F. Colone, and P. Lombardo, “Localization of moving targets with a passive radar system based on WiFi transmissions,” in *Radar Systems (Radar 2012), IET International Conference on*, pp. 1–6, 2012. [51](#)
- [100] P. Falcone, F. Colone, and P. Lombardo, “Potentialities and challenges of WiFi-based passive radar,” *Aerospace and Electronic Systems Magazine, IEEE*, vol. 27, no. 11, pp. 15–26, 2012. [51](#)
- [101] A. Macera, M. Caruso, C. Bongioanni, F. Colone, P. Lombardo, E. Anniballi, and R. Cardinali, “Civil air traffic surveillance with passive radar for anti-terrorism,” in *Advances in Radar and Remote Sensing (TyWRRS), 2012 Tyrrhenian Workshop on*, pp. 296–303, 2012. [52](#)
- [102] A. Macera, C. Bongioanni, F. Colone, and P. Lombardo, “Receiver architecture for multi-standard based passive bistatic radar,” in *Radar Conference (RADAR), 2013 IEEE*, pp. 1–5, 2013. [52](#)
- [103] F. Colone, C. Bongioanni, and P. Lombardo, “Multifrequency integration in FM radio-based passive bistatic radar. part I: Target detection,” *Aerospace and Electronic Systems Magazine, IEEE*, vol. 28, no. 4, pp. 28–39, 2013. [52](#), [119](#)

BIBLIOGRAPHY

- [104] F. Colone, C. Bongioanni, and P. Lombardo, “Multifrequency integration in FM radio-based passive bistatic radar. part II: Direction of arrival estimation,” *Aerospace and Electronic Systems Magazine, IEEE*, vol. 28, no. 4, pp. 40–47, 2013. [52](#)
- [105] D. Petri, A. Capria, M. Martorella, and F. Berizzi, “Ambiguity function study for UMTS passive radar,” in *Radar Conference, 2009. EuRAD 2009. European*, pp. 41–44, Sept 2009. [52](#)
- [106] F. Berizzi, M. Martorella, D. Petri, M. Conti, and A. Capria, “USRP technology for multiband passive radar,” in *Radar Conference, 2010 IEEE*, pp. 225–229, 2010. [53](#)
- [107] D. Olivadese, M. Martorella, E. Giusti, D. Petri, and F. Berizzi, “Passive ISAR with DVB-T signal,” in *Synthetic Aperture Radar, 2012. EUSAR. 9th European Conference on*, pp. 287–290, April 2012. [53](#)
- [108] D. Olivadese, E. Giusti, D. Petri, M. Martorella, A. Capria, F. Berizzi, and R. Soleti, “Passive ISAR imaging of ships by using DVB-T signals,” in *Radar Systems (Radar 2012), IET International Conference on*, pp. 1–4, Oct 2012. [53](#)
- [109] D. Petri, C. Moscardini, M. Martorella, M. Conti, A. Capria, and F. Berizzi, “Performance analysis of the batches algorithm for range-Doppler map formation in passive bistatic radar,” in *Radar Systems (Radar 2012), IET International Conference on*, pp. 1–4, 2012. [54](#), [94](#), [98](#)
- [110] D. Olivadese, E. Giusti, D. Petri, M. Martorella, A. Capria, and F. Berizzi, “Passive ISAR with DVB-T signals,” *Geoscience and Remote Sensing, IEEE Transactions on*, vol. 51, pp. 4508–4517, Aug 2013. [54](#)
- [111] K. Kulpa and J. Misiurewicz, “Stretch processing for long integration time passive covert radar,” in *Radar, 2006. CIE '06. International Conference on*, pp. 1–4, Oct 2006. [54](#), [69](#)

BIBLIOGRAPHY

- [112] M. Malanowski and K. Kulpa, “Analysis of integration gain in passive radar,” in *Radar, 2008 International Conference on*, pp. 323–328, Sept 2008. [55](#), [69](#)
- [113] P. Krysik, K. Kulpa, M. Baczyk, L. Maslikowski, and P. Samczynski, “Ground moving vehicles velocity monitoring using a GSM based passive bistatic radar,” in *Radar (Radar), 2011 IEEE CIE International Conference on*, vol. 1, pp. 781–784, 2011. [55](#)
- [114] P. Krysik, P. Samczynski, M. Malanowski, L. Maslikowski, and K. Kulpa, “Detection of fast maneuvering air targets using GSM based passive radar,” in *Radar Symposium (IRS), 2012 13th International*, pp. 69–72, 2012. [56](#)
- [115] M. Malanowski, K. Kulpa, P. Samczynski, J. Misiurewicz, J. Kulpa, P. Roszkowski, P. Dzwonkowski, D. Gromek, L. Maslikowski, M. Misiurewicz, and L. Podkalicki, “Experimental results of the PaRaDe passive radar field trials,” in *Radar Symposium (IRS), 2012 13th International*, pp. 65–68, May 2012. [56](#), [64](#)
- [116] J. Kulpa, M. Bączyk, A. Kurowska, and S. Rzewuski, “Wind farm interferences in passive coherent location,” in *Radar, 2013 International Conference on*, 2013. [56](#)
- [117] Y. Paichard and M. Inggs, “Multistatic passive coherent location radar systems,” in *Radar Conference, 2009. EuRAD 2009. European*, pp. 45–48, Sept 2009. [57](#)
- [118] M. Inggs, Y. Paichard, and G. Lange, “Passive coherent location system planning tool,” in *Radar Conference - Surveillance for a Safer World, 2009. RADAR. International*, pp. 1–5, Oct 2009. [57](#)
- [119] G. E. Lange, “Performance prediction and improvement of a bistatic passive coherent location radar,” Master’s thesis, University of Cape Town, Dec. 2009. Under Review. [57](#)

BIBLIOGRAPHY

- [120] S. Heunis, Y. Paichard, and M. Inggs, “Passive radar using a software-defined radio platform and opensource software tools,” in *Radar Conference (RADAR), 2011 IEEE*, pp. 879–884, May 2011. [57](#)
- [121] M. Inggs, “Passive coherent location as cognitive radar,” *Aerospace and Electronic Systems Magazine, IEEE*, vol. 25, pp. 12–17, May 2010. [57](#)
- [122] M. Inggs, G. Lange, and Y. Paichard, “Autonomic subsystems for cognition in passive coherent location,” in *Radar Conference, 2010 IEEE*, pp. 1317–1321, May 2010. [57](#)
- [123] P.-H. Tsai, K. Ebrahim, G. Lange, Y. Paichard, and M. Inggs, “Null placement in a circular antenna array for passive coherent location systems,” in *Radar Conference, 2010 IEEE*, pp. 1140–1143, May 2010. [57](#)
- [124] J. Han and M. Inggs, “Detection performance of MIMO passive radar systems based on FM signals,” in *Radar (Radar), 2011 IEEE CIE International Conference on*, vol. 1, pp. 161–164, Oct 2011. [57](#)
- [125] J. Han and M. R. Inggs, “Cumulative detection probability of moving targets by MIMO radar systems,” in *Proceedings of the 2011 IEEE Radar Conference*, (Piscataway, NJ, USA), Institute of Electrical and Electronic Engineers, Apr. 2011. [57](#)
- [126] J. Han, “Study on the detection performance of MIMO radar systems,” Master’s thesis, University of Cape Town, Private Bag, Rondebosch, 7701, South Africa., Aug. 2011. [57](#)
- [127] M. Inggs and M. Brooker, “Extensible simulator for waveform diversity testing,” in *Waveform Diversity and Design Conference, 2009 International*, pp. 273–277, Feb 2009. [57](#)
- [128] Y. Paichard, M. Brooker, and M. Inggs, “Signal level simulator for netted text radar waveforms evaluation,” *Aerospace and Electronic Systems Magazine, IEEE*, vol. 25, pp. 27–29, March 2010. [57](#)

BIBLIOGRAPHY

- [129] J. Sandenbergh and M. Inggs, “A common view GPSDO to synchronize netted radar,” in *Radar Systems, 2007 IET International Conference on*, pp. 1–5, Oct 2007. [57](#), [156](#)
- [130] J. Sandenbergh, M. Inggs, and W. Al-Ashwal, “Evaluation of coherent netted radar carrier stability while synchronised with GPS-disciplined oscillators,” in *Radar Conference (RADAR), 2011 IEEE*, pp. 1100–1105, May 2011. [57](#), [156](#)
- [131] R. Nadjiasngar, M. Inggs, Y. Paichard, and N. Morrison, “A new probabilistic data association filter based on composite expanding and fading memory polynomial filters,” in *Radar Conference (RADAR), 2011 IEEE*, pp. 152–156, May 2011. [58](#)
- [132] R. Nadjiasngar and M. Inggs, “Gauss-Newton filtering incorporating Levenberg-Marquardt methods for radar tracking,” *arXiv preprint arXiv:1110.5207*, 2011. [58](#)
- [133] R. Nadjiasngar and M. Inggs, “The recursive Gauss-Newton filter,” *arXiv preprint arXiv:1110.5212*, 2011. [58](#)
- [134] J. Pisane, S. Azarian, M. Lesturgie, and J. Verly, “Automatic real-time collection of RCS of airplanes in a real bistatic low-frequency configuration using a software defined passive radar based on illuminators of opportunity,” in *Radar Conference (RADAR), 2012 IEEE*, pp. 0950–0955, May 2012. [58](#)
- [135] J. Pisane, *Automatic target recognition using passive bistatic radar signals*. PhD thesis, University of Liège and SUPELEC, 2013. [58](#)
- [136] V. Anastasio, F. Colone, and P. Lombardo, “A procedure for effective receiver positioning in multistatic passive radar,” in *Radar Conference, 2009. EuRAD 2009. European*, pp. 493–496, 2009. [58](#)
- [137] V. Anastasio, F. Colone, A. Di Lallo, A. Farina, F. Gumiero, and P. Lombardo, “Optimization of multistatic passive radar geometry based on CRLB

BIBLIOGRAPHY

- with uncertain observations,” in *Radar Conference (EuRAD), 2010 European*, pp. 340–343, 2010. [58](#)
- [138] H. Kuschel, J. Heckenbach, D. O’Hagan, and M. Ummenhofer, “A hybrid multi-frequency passive radar concept for medium range air surveillance,” in *Microwaves, Radar and Remote Sensing Symposium (MRRS), 2011*, pp. 275–279, 2011. [58](#)
- [139] A. Schroeder, M. Edrich, and F. Wolschendorf, “Multiband experimental PCL system: Concept and measurement results,” in *Radar Symposium (IRS), 2010 11th International*, pp. 1–4, 2010. [59](#)
- [140] A. Schroeder, M. Edrich, and V. Winkler, “Multi-illuminator passive radar performance evaluation,” in *Radar Symposium (IRS), 2012 13th International*, pp. 61–64, 2012. [59](#)
- [141] M. Edrich, A. Schroeder, and V. Winkler, “Design and performance evaluation of a FM / DAB / DVB-T multi-illuminator passive radar system,” in *Radar Systems (Radar 2012), IET International Conference on*, pp. 1–6, 2012. [59](#)
- [142] M. Edrich and A. Schroeder, “Multiband multistatic passive radar system for airspace surveillance: A step towards mature PCL implementations,” in *Radar, 2013 International Conference on*, 2013. [59](#)
- [143] A. Schroeder, M. Edrich, and V. Winkler, “Stationary Cassidian FM passive radar demonstrator for 24/7 operation and sensor cluster measurements,” in *Radar Symposium (IRS), 2013 14th International*, vol. 1, pp. 161–166, 2013. [60](#)
- [144] T.-T. Van Cao, “A CFAR thresholding approach based on test cell statistics,” in *Radar Conference, 2004. Proceedings of the IEEE*, pp. 349–354, 2004. [60](#), [108](#)
- [145] G. Fabrizio, F. Colone, P. Lombardo, and A. Farina, “Passive radar in the high frequency band,” in *Radar Conference, 2008. RADAR ’08. IEEE*, pp. 1–6, 2008. [60](#)

BIBLIOGRAPHY

- [146] G. Fabrizio, F. Colone, P. Lombardo, and A. Farina, “Adaptive beam-forming for high-frequency over-the-horizon passive radar,” *Radar, Sonar Navigation, IET*, vol. 3, no. 4, pp. 384–405, 2009. 60
- [147] H. Sun, D. Tan, and Y. Lu, “Design and implementation of an experimental GSM based passive radar,” in *Radar Conference, 2003. Proceedings of the International*, pp. 418 – 422, Sep 2003. 62
- [148] Y. Lu, D. K. P. Tan, and H. Sun, “Air target detection and tracking using a multi-channel GSM based passive radar,” in *Waveform Diversity and Design Conference, 2007. International*, pp. 122–126, 2007. 62
- [149] “HA100 passive radar from thales.” <https://www.thalesgroup.com/en/content/ha100-passive-radar-thales-play-role-protecting-flypast-14th-july-paris>, 2010. Accessed: 2014/02/15. 62
- [150] M. John and M. R. Ingg, “Real time processing of networked passive coherent location radar system,” *INTL Journal of Electronics and Telecommunication*, vol. 57, pp. 363–368, Jul 2011. 64
- [151] “CUDA Parallel Computing Platform.” http://www.nvidia.com/object/cuda_home_new.html, 2014. Accessed: 2014/09/14. 67
- [152] “APP SDK A Complete Development Platform.” <http://developer.amd.com/tools-and-sdks/opencv-zone/amd-accelerated-parallel-processing-app-sdk/>, 2014. Accessed: 2014/09/14. 67
- [153] “Intel Xeon Phi Product Family.” <http://www.intel.co.za/content/www/za/en/processors/xeon/xeon-phi-detail.html>, 2014. Accessed: 2014/09/14. 67
- [154] “The open standard for parallel programming of heterogeneous systems.” <https://www.khronos.org/opencv/>, 2014. Accessed: 2014/09/14. 67
- [155] R. Nath, “Modified generalized autocorrelation based estimator for time delays in multipath environment -a tradeoff in estimator performance and number of multipath,” *Computers and Electrical Engineering*, vol. 37, no. 3, pp. 241 – 252, 2011. 72

BIBLIOGRAPHY

- [156] V. Madisettu, *The Digital Signal Processing Handbook*. Electrical Engineering Handbook, Taylor & Francis, 1997. [76](#), [82](#), [94](#)
- [157] M. Richards, J. Scheer, and W. Holm, *Principles of modern radar: Basic Principles*. No. v. 1 in Principles of Modern Radar, SciTech Publishing, Incorporated, 2010. [78](#), [81](#), [108](#)
- [158] *Introduction to Radar Systems*. McGraw-Hill Education (India) Pvt Limited, 2003. [81](#), [108](#)
- [159] T.-T. Van Cao, “Ground clutter suppression in noise radar,” in *International Conference on Radar Systems*, p. 236, 2004. [82](#)
- [160] “TESLA.” <http://www.nvidia.com/object/why-choose-tesla.html>, 2014. Accessed: 2014/02/07. [84](#)
- [161] F. Bazn, “CGLS-GCV: A hybrid algorithm for low-rank-deficient problems,” *Applied Numerical Mathematics*, vol. 47, no. 2, pp. 91 – 108, 2003. Second International Workshop on Numerical Linear Algebra - Numerical Methods for Partial Differential Equations and Optimization. [86](#), [87](#)
- [162] G. Boray and M. Srinath, “Conjugate gradient techniques for adaptive filtering,” *Circuits and Systems I: Fundamental Theory and Applications, IEEE Transactions on*, vol. 39, no. 1, pp. 1–10, 1992. [86](#)
- [163] P. S. Chang and J. Willson, A.N., “Analysis of conjugate gradient algorithms for adaptive filtering,” *Signal Processing, IEEE Transactions on*, vol. 48, no. 2, pp. 409–418, 2000. [86](#)
- [164] “Basic linear algebra subprograms technical (BLAST) forum standard,” Aug 2001. [86](#)
- [165] NVIDIA, *CUBLAS LIBRARY*, Oct 2012. v5.0. [88](#)
- [166] P. McMahan, A. Langman, D. Werthimer, D. Backer, T. Filiba, J. R. Manley, A. Parsons, and A. Siemion, “Packetized FX correlator architectures.” CASPER Memo, 2007. [94](#)

BIBLIOGRAPHY

- [167] W. Stanley, *Digital signal processing*. Reston Pub. Co., 1975. 97
- [168] G. M. Dillard, “Recursive computation of the discrete fourier transform, with applications to a pulse-doppler radar system,” *Computers and Electrical Engineering*, vol. 1, no. 1, pp. 143 – 152, 1973. 99
- [169] A. Van der Byl, *A Parallel Processing Framework for Spectral Based Computations*. PhD thesis, University of Cape Town, Dec 2012. 99, 103
- [170] NVIDIA, *CUFFT LIBRARY*, Oct 2012. v5.0. 105
- [171] T. T. V. Cao, J. Palmer, and P. Berry, “False alarm control of CFAR algorithms with experimental bistatic radar data,” in *Radar Conference, 2010 IEEE*, pp. 156–161, 2010. 108
- [172] H. Rohling, “Radar CFAR thresholding in clutter and multiple target situations,” *Aerospace and Electronic Systems, IEEE Transactions on*, vol. AES-19, no. 4, pp. 608–621, 1983. 108
- [173] V. Hansen and J. Sawyers, “Detectability loss due to “greatest of” selection in a cell-averaging CFAR,” *Aerospace and Electronic Systems, IEEE Transactions on*, vol. AES-16, no. 1, pp. 115–118, 1980. 108
- [174] “Buy Jetson TK1 Development Kit.” <https://developer.nvidia.com/jetson-tk1>, 2014. Accessed: 2014/09/16. 114
- [175] “ACML - AMD Core Math Library.” <http://developer.amd.com/tools-and-sdks/cpu-development/amd-core-math-library-acml/>, 2014. Accessed: 2014/09/16. 114, 167
- [176] “C++ standard template library.” <http://www.cplusplus.com/reference/stl/>, 2014. Accessed: 2014/02/09. 121
- [177] “The South African Nation Research Network (SANReN).” <http://www.sanren.ac.za/>, 2014. Accessed: 2014/02/13. 144
- [178] R. Coudé, “Radio Mobile.” <http://www.cplus.org/rmw/english1.html>. Accessed: 2013/10/09. 148

BIBLIOGRAPHY

- [179] “Radio Mobile Web Site.” <http://www.cplus.org/rmw/english1.html>, 2014. Accessed: 2014/09/23. 149
- [180] W. A. Al-Ashwal, A. Balleri, H. Griffiths, W. J. Miceli, K. Woodbridge, C. Baker, R. Harmanny, M. Inggs, J. S. Sandenbergh, M. A. Ritchie, A. G. Stove, S. Watts, R. J. A. Tough, and K. D. Ward, “Measurements of bistatic radar sea clutter,” in *Radar Conference (RADAR), 2011 IEEE*, pp. 217–221, May 2011. 156
- [181] W. A. M. Al-Ashwal, *Measurement and modelling of bistatic sea clutter*. PhD thesis, University College London, 2011. 156
- [182] P. Lombardo, F. Colone, C. Bongioanni, A. Lauri, and T. Bucciarelli, “PBR activity at INFOCOM: Adaptive processing techniques and experimental results,” in *Radar Conference, 2008. RADAR '08. IEEE*, pp. 1–6, May 2008. 159
- [183] H. Friis, “A note on a simple transmission formula,” *Proceedings of the IRE*, vol. 34, pp. 254–256, May 1946. 160
- [184] “IEEE standard for information technology: Telecommunications and information exchange between systems wireless regional area networks (WRAN): Specific requirements,.” <http://www.ieee802.org/22/>, 2011. Accessed: 2013/10/11. 161
- [185] A. Langman, O. Hazarika, A. Mishra, and M. Inggs, “White RHINO: A low cost whitespace communications and radar hardware platform,” in *Radioelektronika (RADIOELEKTRONIKA), 2013 23rd International Conference*, pp. 240–244, 2013. 161